

Aromatic And Aliphatic Carbon Contents  
of Coals and Oil Shales by  $^{13}\text{C}$  NMR

Gary E. Maciel and Victor J. Bartuska  
Department of Chemistry, Colorado State University  
Fort Collins, Colorado U.S.A. 80523

and

Francis P. Miknis, Laramie Energy Research Center  
U.S. Department of Energy  
Laramie, Wyoming 82070

For many types of samples in the field of fossil fuels, e.g., oil shales and typical coals, only a small fraction of the organic substances can be extracted from a solid under mild conditions that would be expected to retain the primary structural integrity of the organic compounds. Hence, the constraint of analytical techniques to liquid samples has been very restrictive. This constraint has been shared by nuclear magnetic resonance (nmr), for which high-resolution analytical applications have been limited to liquid samples until very recently. The "standard"  $^{13}\text{C}$  nmr techniques, including pulse Fourier transform (FT) approaches<sup>1</sup> have not been generally useful for solid samples because of (a) the excessive line broadening due to dipole-dipole interactions between  $^{13}\text{C}$  and  $^1\text{H}$  magnetic dipoles, (b) chemical shift anisotropies (different shielding values for the many different orientations of the molecules in an amorphous state with respect to the magnetic field direction), and (c) long  $^{13}\text{C}$  spin-lattice relaxation times ( $T_1$ ).<sup>2</sup> All of these problems are eliminated in liquids (or in the case of long  $T_1$  values, at least greatly reduced) by the normal tumbling motions occurring randomly in the liquid state.

This paper is concerned with the refinement and application of recently introduced  $^{13}\text{C}$  nmr techniques for obtaining high resolution spectra of solid samples. Dipolar line broadening in the  $^{13}\text{C}$  spectra, due to protons, is eliminated by high-power proton decoupling; when this is carried out under the Hartmann-Hahn condition,  $^{13}\text{C}$ - $^1\text{H}$  cross polarization occurs, which enhances the  $^{13}\text{C}$  signal intensity and largely overcomes the problem of long  $^{13}\text{C}$  relaxation times.<sup>3</sup> The primary line-broadening effect that would remain, chemical shift anisotropy, is eliminated by rapid spinning (2.2 to 2.6 kHz) of the solid sample about an axis tilted at  $54^\circ 44'$  (the magic angle) relative to the direction of the static magnetic field of the instrument.<sup>4-7</sup> Under rapid magic-angle-spinning conditions, the  $^{13}\text{C}$  resonance lines that are obtained are essentially what one would expect of a corresponding nonviscous liquid sample. Examples of the type of spectra one might expect for a pure (chemically homogeneous) sample are shown in Figures 1 and 2. For a complex chemical mixture, such as coal or oil shale, one may still expect to obtain broad resonance peaks, as is usually found to be the case in experimental results (Figures 3 and 4). The reason for the broad peaks is the presence of a large number of chemically similar species present in the sample, for which the (isotropic) chemical shifts and resonance positions are close together and cannot be resolved even under conditions of reasonably high resolution. The typical result for a coal or oil shale sample is a broad peak due to aromatic and olefinic carbons and another broad peak due to aliphatic carbons (Figures 3 and 4).

The specific experimental approach that we have employed in this work is a single-contact technique based on the more general experiment originally described by Pines, Gibby and Waugh.<sup>3</sup> A  $90^\circ$   $^1\text{H}$  pulse is applied, followed by a  $90^\circ$  phase shift, after which the  $^1\text{H}$  rf power is maintained during the  $^1\text{H}$ - $^{13}\text{C}$  cross polarization and for  $^1\text{H}$  decoupling during  $^{13}\text{C}$  data acquisition. Radiofrequency power at the  $^{13}\text{C}$  resonance frequency (at a level determined by the Hartmann-Hahn condition) is applied during the contact period (1-8 msec), then turned off during the period in which the  $^{13}\text{C}$  free induction decay (FID) is observed.

Our experiments were carried out at 15.1 MHz on a home-built spectrometer, based upon a 14-kgauss Varian 12-in magnet and a JEOL EC-100 Fourier transform data system. The Hartmann-Hahn condition was achieved with a 40 gauss  $H_1$  field for  $^{13}\text{C}$  and a 10-gauss  $H_1$  field for  $^1\text{H}$ . The spinning rates of 2.2- to 2.6 kHz were achieved with a spinner of the general Andrew-type,<sup>3</sup> using 14 lb/in<sup>2</sup> pressure from a "house" air supply. Higher spinning speeds could be achieved with higher pressures and/or helium. The spinner contained about 1.1 cm<sup>3</sup> of sample.

As can be seen in Figures 1-4, a great deal of structural detail is available in the spectra of solid pure substance, while for coal and oil shale, only broad bands are obtained. In some cases these bands contain "hints" of fine structure (e.g., bumps and shoulders), which should become more distinct in a high-field spectrometer. Even in the 14-kgauss spectra of the type shown in Figures 3 and 4, clear separations between the aromatic/olefinic and aliphatic resonances are achieved. This is in contrast with the overlapping resonance bands of spectra obtained without magic-angle spinning, in which chemical shift anisotropies cause overlapping of the resonances from these different structural classes of carbons.<sup>7,9,11</sup>

From  $^{13}\text{C}$  nmr spectra of the type shown in Figures 3 and 4, one can hope to make quantitative determinations of aromatic/olefinic and aliphatic carbon contents. However, many questions must be raised to determine the reliability of the above-mentioned approach for quantitative analytical purposes. These questions revolve largely about the dynamics of the experiment, i.e., the characteristic relaxation times of the pertinent processes ( $^1\text{H}$  and  $^{13}\text{C}$  relaxation in the rotating frame,  $^{13}\text{C}$ - $^1\text{H}$  cross polarization,  $^1\text{H}$  and  $^{13}\text{C}$  spin-lattice relaxation). The essential question is: can experimental conditions and corrections be found so that all organic carbon types are "counted" equally in the  $^{13}\text{C}$  experiment? Many experiments have been carried out to characterize the conditions for typical coals and oil shales, so that optimized experiments could be designed. Comparisons with experiments carried out with high-power  $^1\text{H}$  decoupling, but without  $^{13}\text{C}$ - $^1\text{H}$  cross polarization, are essential for assessing the efficiency and deviations from uniformity of the cross polarization process. Success in optimizing the experimental conditions for determining aromatic/olefinic and aliphatic carbon contents determines the scope and accuracy of the approach. One key feature of calibrating the  $^{13}\text{C}$  approach so that absolute aromatic/olefinic or aliphatic carbon contents can be determined is an external  $^{13}\text{C}$  standard. The requirements for an external standard involve both the chemical shift (to avoid critical peak overlaps) and relaxation times (to avoid intensity distortions).

With a method capable of determining aromatic/olefinic and aliphatic carbon contents, various comparisons and correlations are possible. These include comparisons among related samples (e.g., oil shale and shale oil; coal and solvent-refined coal or hydrogenated coal), and correlations with pertinent fuel parameters, e.g., gal/ton obtained from oil shale or BTu/ton for coal or oil shale.

#### Acknowledgement

The authors gratefully acknowledge support of this research by the U.S. Energy Research and Development Administration, Laramie Energy Research Center.

## References

1. T.C. Farrar and E.D. Becker, "Pulse and Fourier Transform NMR," Academic Press, New York, 1971.
2. J.A. Pople, W. G. Schneider and H.J. Bernstein, "High-resolution Nuclear Magnetic Resonance," Ch. 3, McGraw-Hill, New York, 1959.
- 3a. A. Pines, M.G. Gibby and J.S. Waugh, 1972, J. Chem. Phys., 56, 1776.  
b. A. Pines, M.G. Gibby and J.S. Waugh, 1973, ibid., 59, 569.
4. I.J. Lowe, 1959, Phys. Rev. Letters, 2, 285.
5. H. Kessemeier and R.E. Norberg, 1967, Phys. Rev., 155, 321.
6. E.R. Andrew, 1971, Progr. Nucl. Magn. Reson. Spectrosc., 8, 1.
7. V.J. Bartuska, G.E. Maciel, J. Schaefer and E.O. Stejskal, 1977, Fuel, 56, 354.
- 8a. J. Schaefer, S.H. Chin and S.I. Weissman, 1972, Macromol., 5, 798.  
b. E.O. Stejskal, J. Schaefer, J.M.S. Hemis and M.K. Tripodi, 1975, J. Chem. Phys., 61, 2352.
9. D.L. VanderHart, H.L. Retcofsky, Fuel, 1976, 55, 202.
- 10a. F.P. Miknis, A.W. Decora, and G.L. Cook, Pulsed Nuclear Magnetic Resonance Studies of Oil Shales - Estimation of Potential Oil Yields, U.S. Bureau of Mines, RI 7984 (1974).  
b. E.W. Cook, Fuel, 1974, 53, 16.
11. G.E. Maciel, V.J. Bartuska and F.P. Miknis, 1978, Fuel, 57, in press.

## Figure Captions

- Figure 1.  $^{13}\text{C}$  nmr spectrum of catechin, obtained at 15.1 MHz under conditions of high-power  $^1\text{H}$  decoupling,  $^1\text{H}$ - $^{13}\text{C}$  cross polarization and magic-angle spinning. Spectral width 530 ppm, higher shielding to the right.
- Figure 2.  $^{13}\text{C}$  nmr spectrum of polymethylmethacrylate, obtained at 15.1 MHz under conditions of high-power  $^1\text{H}$  decoupling,  $^1\text{H}$ - $^{13}\text{C}$  cross-polarization and Magic-angle spinning. Spectral width 530 ppm, higher shielding to the right.
- Figure 3.  $^{13}\text{C}$  nmr spectrum of coal (Indiana), obtained at 15.1 MHz under conditions of high-power  $^1\text{H}$  decoupling,  $^1\text{H}$ - $^{13}\text{C}$  cross polarization and magic-angle spinning. Spectral width 530 ppm, higher shielding to the right. Spinning sidebands are marked with arrows.
- Figure 4.  $^{13}\text{C}$  nmr spectrum of New Zealand shale, obtained at 15.1 MHz under conditions of high-power  $^1\text{H}$  decoupling,  $^1\text{H}$ - $^{13}\text{C}$  cross polarization and magic-angle spinning. Spectral width 530 ppm, higher shielding to the right.

Figure 1

D-CATECHIN  
500 scans

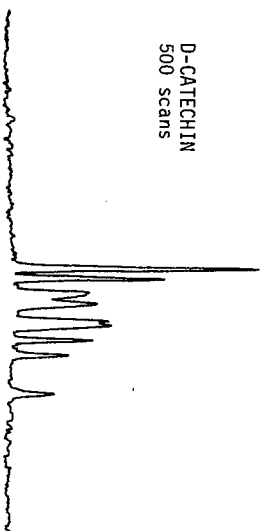


Figure 3

INDIANA BITUMINOUS  
COAL  
3000 scans

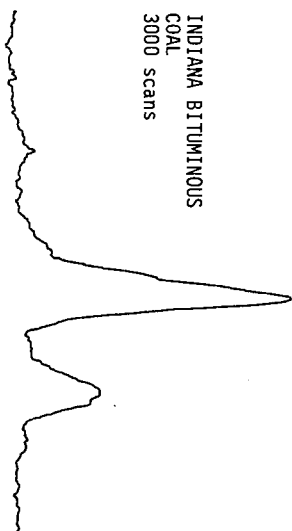


Figure 2  
POLY(METHYL METHACRYLATE)  
500 scans

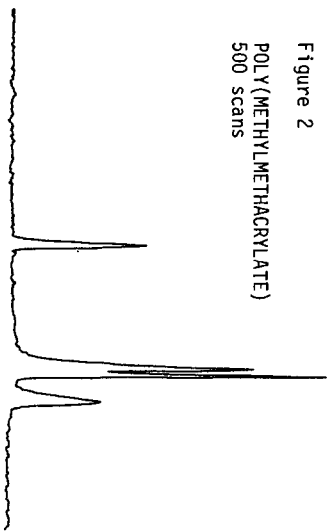
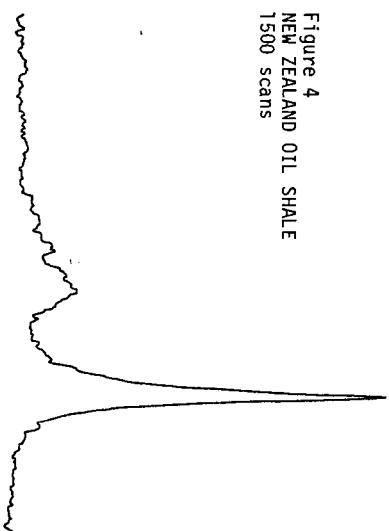


Figure 4  
NEW ZEALAND OIL SHALE  
1500 scans



8KHz (530 ppm)

## A Re-evaluation of Carbon Ring Structure in Coal

A.W. Scaroni and R.H. Essenhigh

Combustion Laboratory, The Pennsylvania State University, University Park, Pa. 16802

### INTRODUCTION

Working models of coal constitution are important because of their potential predictive capacity. A basic approach is to develop a qualitative structure of coal which can be given subsequent quantitative expression. Without a model we are faced, as at present, with the prospect of endless repeat of experiments on all coals of interest. With a working model, however, experimental results on certain coals under certain conditions can in principle be generalized to allow prediction of properties, both physical and chemical, of other coals or the same coals under untested conditions. This is an ultimate objective of developing a working model of coal constitution.

Traditional coal tests provide relatively little insight into structural configuration. Ultimate analysis will yield the elements and their proportions but nothing of their arrangement. The volatiles expelled during carbonization may not have been present as such in the raw coal. They can be formed *in situ* by primary or secondary reactions. The use of results from such methods for structural analysis, therefore, has always been indirect and inferential.

Direct information on structure, however, is obtainable from X-ray scattering from coals. During such experiments Hirsch (1), for example, found that up to 80% of the carbon is ordered and evidently exists as flat plates or lamellae made up of condensed aromatic rings. By measuring the diameters of the lamellae Hirsch estimated that the number of rings in each lamella was rank dependent varying from 4 or 5 in bituminous coals to 30 or more in anthracite. The remainder of the coal was amorphous to X-rays.

Van Krevelen and co-workers (2) predicted physical and chemical properties from the ultimate analysis. The equations were based on the general equation for alkanes. Ayre and Essenhigh (3) criticize this approach on two grounds: it gives no insight into the structure in coal and prediction of the number of rings in each of Hirsch's lamellae showed considerable discrepancy with experimental values. They, in turn proposed a qualitative model of the coal molecule based on the Hirsch structure and derived an equation relating the number of rings per lamella to the total carbon percentage in the coal. The quantitative expression was based on a relationship previously proposed by Essenhigh (4) between the weight percent oxygen and carbon in coal.

In this present paper the essential features of the Ayre and Essenhigh analysis are used but incorporating an improved relationship between the hydrogen/carbon and oxygen/carbon atomic ratios in coal.

### QUALITATIVE MODEL

The structure of coal proposed by Ayre and Essenhigh is an elaboration of that described by Hirsch. The basic unit is considered to be the crystallite which contains all the ordered carbon as condensed aromatic lamellae plus a fixed quantity of amorphous material situated around the edges of the lamellae. The lamella carbon is loosely identified as fixed carbon, and the amorphous material as volatile matter as measured by proximate analysis. Each crystallite may contain a single lamella or groups of two, three, or more lamellae stacked parallel with each other. The amorphous material which is weakly

bonded to the edges of the lamellae, possibly by double or triple bonds, provides for some cross linking between lamellae. A fraction of the amorphous material, however, is considered to be more closely associated with the lamellae than the rest and can be thought of as an integral part thereof, so each lamella contains some hydrogen, oxygen and nitrogen (and possibly sulfur). The coal molecule is thus based on the single lamella with a fixed quantity of associated volatile matter.

According to the X-ray results the percentage of ordered carbon, the number of rings per lamella and the degree of parallel stacking of the lamellae increase with rank. At low carbon percentages the coal is highly porous, the number of rings per lamella is low, and the lamellae are randomly ordered. As the carbon percentage rises the parallel packing of the lamellae improves and both the number of rings per lamella and the fraction of carbon in rings increase. At 89% C what Hirsch described as a perfect "liquid" structure is reached where the crystallite packing is an optimum but a large fraction of the internal pore volume is isolated. A further increase in rank leads to a more rapid increase in the number of rings per lamella and a greater fraction of ordered carbon. At 94% C the structure is almost perfectly graphitic. The changes with rank are illustrated in Figure 1. Coalification is the process of transforming the open structure into the anthracitic structure.

#### TWO-COMPONENT HYPOTHESIS

Clark and Wheeler (5) identify two main stages of volatile evolution when coal is heated: the constituents easily evolved on heating to 650°C (hydrocarbons, gases, vapors, tars); and, the volatiles less easily evolved on heating above this critical temperature (mainly hydrogen with reduced quantities of carbon bearing materials). The easily evolved volatiles can be considered as being generated from the weakly bonded amorphous material around the edges of the lamellae. The hydrogen rich fraction is evolved as a result of ring coalescence. The two components are thus identified as: the loosely associated amorphous material; and the lamellae of condensed rings and related O and H atoms.

#### QUANTITATIVE EXPRESSION

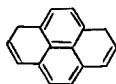
Ayre and Essenhig (3) established first a general equation for the condensed aromatic ring structure. The number of carbon atoms,  $C_L$ , in a condensed aromatic structure containing R rings was shown (3) to be given by

$$C_L = 4 + 3R \quad 1)$$

and the number of hydrogen atoms  $H_L$  for a structure with N double bonds is

$$H_L = 10 + 4R - 2N \quad 2)$$

Equations (1) and (2) are based on naphthalene, and assume ring addition so as to minimize carbon atom addition. As an example



$$\begin{aligned} R &= 4, N = 7 \\ C_L &= 16 \\ H_L &= 12 \end{aligned}$$

Some of the double bonds may be saturated by hydrogen atoms. If n is the fraction that remain unsaturated

$$\begin{aligned} H_L &= 10 + 4R - 2nN \\ &\approx 10 + 4R - 4n(R - 1) \end{aligned} \quad 3)$$

Equation (3) is an approximate expression rarely in error by more than 2. The hydrogen/carbon ratio in the lamellae is therefore

$$H_L/C_L = [10 + 4n + 4(1-n)R]/(4 + 3R) \quad (4)$$

Oxygen and nitrogen have been omitted from the analysis since their proportions of atoms are small.

#### WHOLE COAL ANALYSIS

The next step is to express the hydrogen/carbon ratio in the lamellae in terms of measurable quantities. Identifying the lamella carbon as fixed carbon, Ayre and Essenhigh showed that

$$m_H H_L / m_C C_L = (100/C^*) - 1 - (O^*/C^*) \quad (5)$$

where  $C^*$  and  $O^*$  are weight percent carbon and oxygen; and  $m_H$  and  $m_C$  are molecular weights of hydrogen and carbon. It is not possible to neglect the percentage of oxygen on a weight basis.

To proceed it is necessary to establish relationships between  $C^*$ ,  $H^*$ , and  $O^*$ . Since  $N^*$  and  $S^*$  are usually relatively small we have

$$C^* + H^* + O^* \approx 100 \quad (6)$$

In addition, an empirical linear relationship between  $(O/H) [= (O/C)/(H/C)]$  and  $(O/C)$  was established by Essenhigh and Howard (6) that was recently reconfirmed by Yarzab (7) using the Penn State Coal Analysis Data bank. This is illustrated in Fig. 2, noting that the correlation coefficient for the plot was 0.9889. The further relationship that follows is

$$H^*/C^* = A(O^*/C^*)/[1 + B(O^*/C^*)] \quad (7)$$

where  $A$  and  $B$  are empirical constants with:  $A = 1/(\text{intercept of Fig. 2})$ ; and  $B = (\text{slope of Fig. 2}/\text{intercept of Fig. 2})$ .

In using such data there is often concern expressed that these are whole coal analyses which ignores maceral constituents. As illustrated in Fig. 3, however, Kessler (8) has shown recently, on a somewhat similar plot, that maceral analyses lie on an essentially common band, thus justifying the use of whole coal analyses as in Eq. (7).

It is now possible to solve for  $O^*/C^*$  as a function of  $C^*$ . The relationship between the number of rings per lamella,  $R$  and the total carbon percentage,  $C^*$  is obtained by combining equations (4) and (5)

$$[10 + 4n + 4(1-n)R]/[12(4 + 3R)] = (100/C^*) - 1 - (O^*/C^*) \quad (8)$$

Using equations (6), (7) and (8), the value of  $R$  as a function of  $C^*$  is illustrated in Figure 4 for various values of  $n$ . The best fit line to Hirsch's experimental data is for  $n = 0.6$ , suggesting that between half and three quarters of the double bonds remain unbroken.

The molecular weight of the lamellae,  $M_L$  is then given by

$$M_L = [100 m_C (4 + 3R)]/C^* \quad (9)$$

and is shown in Figure 5 for the case  $n = 0.6$ . Also, the molecular weight of the coal "molecule",  $M$  is given by

$$M = M_L C^*/C_L^* \quad (10)$$

and is shown in Figure 5, using for values of  $C_L^*$  the fixed carbon percentages from Hirsch's original data. The minimum in the whole coal molecular weight is a little unexpected. Walker (9) has suggested it represents the increasing contributions of the greater oxygen percentage in the lignites.

#### DISCUSSION

Figure 4 shows that the predicted behavior parallels the experimental trends. In particular, choosing  $n = 0.6$ , agreement between prediction and experiment is respectable good. Below about 80% carbon the value of  $R$  is constant, and tends to infinity at 100% carbon. This can be explained by considering the process of coalification. The rise in the carbon percentage as coalification proceeds can only occur if a fraction of the primary coal material is eliminated (by coalification as a long term chemical reaction). It is reasonable to assume that the fraction that remains is reorganized so that, as proposed by Ayre and Essenhigh (3)

primary coal material  $\rightarrow$  lamella + material eliminated.

If this is so, raw coal will consist of the lamella with its closely associated fraction of hydrogen, carbon, and nitrogen plus some unchanged parent material. If the unchanged parent material is identified as the amorphous material surrounding the lamellae, then this material contains all the volatile carbon. A plot of fixed carbon versus volatile carbon (Figure 6) is indicative of the growth of lamellae at the expense of the parent material. At about 90% fixed carbon the parent material has run out so that coalification can only continue at the expense of the lamellae, which coalesce. This is consistent with Horton's (10) two stage theory of coalification.

As the number of lamellae increases, the proportion of associated parent material will drop so the molecular weight of the coal molecule will drop slightly as the carbon percentage increases. At about 90% carbon, however, ring coalescence occurs and the molecular weight will rise rapidly. These trends are illustrated in Figure 5.

The model is intended, of course, as a first step in a full model of coal structure. It is clearly lacking in that nitrogen and sulfur are missing. It is also not yet able to predict the degree of detail on pyrolysis described, for example, by Suuberg *et al* (11). The initial agreement between theory and the X-ray results of experiment, however, is encouraging and suggests that the model is probably adequate as a framework or skeleton for further developments.

#### SUMMARY

1. X-ray data suggest that the coal molecule may be viewed in terms of a lamella of condensed aromatic rings of carbon plus a fraction of loosely associated volatile matter.
2. The model described is in agreement with the X-ray data, showing that the number of rings per lamella is constant at 4 or 5 up to about 90% carbon above which it rapidly rises with rank.
3. The model shows that the molecular weight of the coal molecule drops slightly as the carbon percentage rises to 90% above which it rises rapidly with rank.

4. The lamella carbon is identified as the fixed carbon and the amorphous material as the volatile matter as determined by the proximate analysis.
5. The model is consistent with the Two-Component Hypothesis of coal constitution (5) and the Two-Stage Theory of coalification (10).

#### REFERENCES

1. Hirsch, P.B., Proc. Royal Society, 226A, 143 (1955).
2. Van Krevelen, D.W., et al, Fuel, 33, 79 (1954)  
Fuel, 36, 85 (1957).
3. Ayre, J.L. and Essenhigh, R.H., Sheffield Univ. Fuel Soc. Journal, 8, 44, (1957).
4. Essenhigh, R.H., Fuel, 34, 497 (1955).
5. Clark, A.H. and Wheeler, R.V., Trans, Chem. Soc., 103, 1754 (1913).
6. Essenhigh, R.H. and Howard, J.B., The Pennsylvania State University Studies, 31 (1971).
7. Yarzab, R.F., Coal Research Section, The Pennsylvania State University, Private Communication (1976).
8. Kessler, M.F., Fuel, 52, 191 (1973).
9. Walker, P.L. Jr., Department of Material Sciences, The Pennsylvania State University Private Communication (1978).
10. Horton, L., Fuel, 31, 341 (1952).
11. Suuberg, E.M., Peters, W.A. and Howard, J.B., American Chemical Society Fuels Division Preprints, 22 (1), 112 (1977).

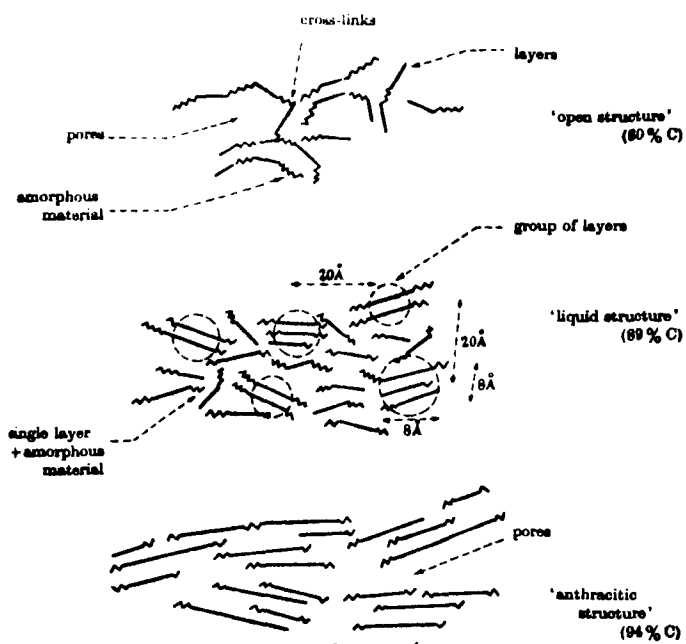


Figure 1 - Coal Structure as a Function of Rank  
(source: Hirsch (1))

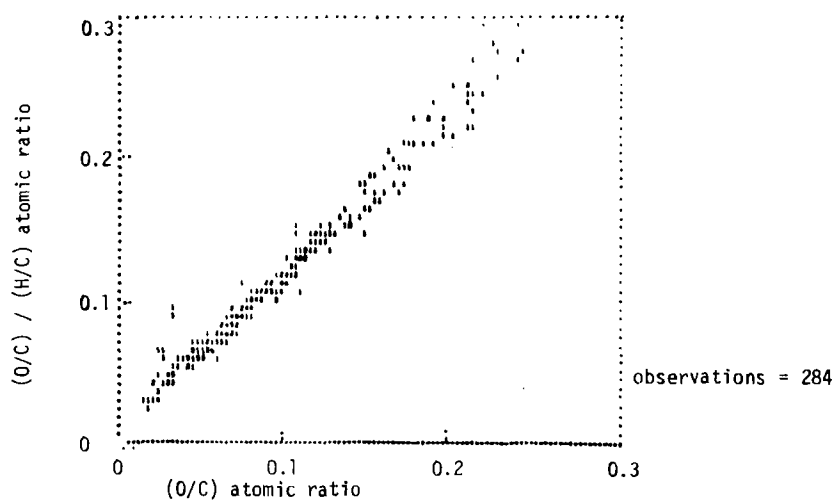


Figure 2 - Variation of  $(O/C) / (H/C)$  with  $(O/C)$  atomic ratios for various coals. (Source: Yarzab, (7)).

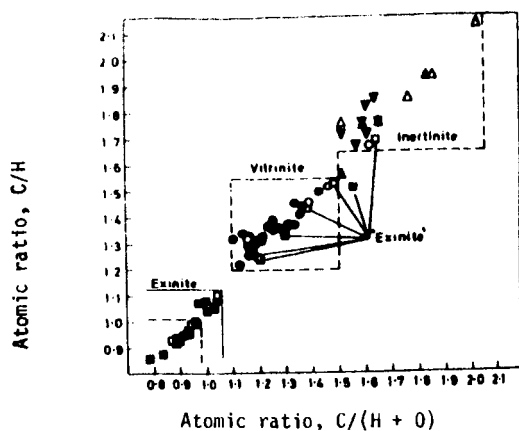


Figure 3 - Variation of C/H ratio with C/(H + O) ratio for various macerals. (Source: Kessler, (8))

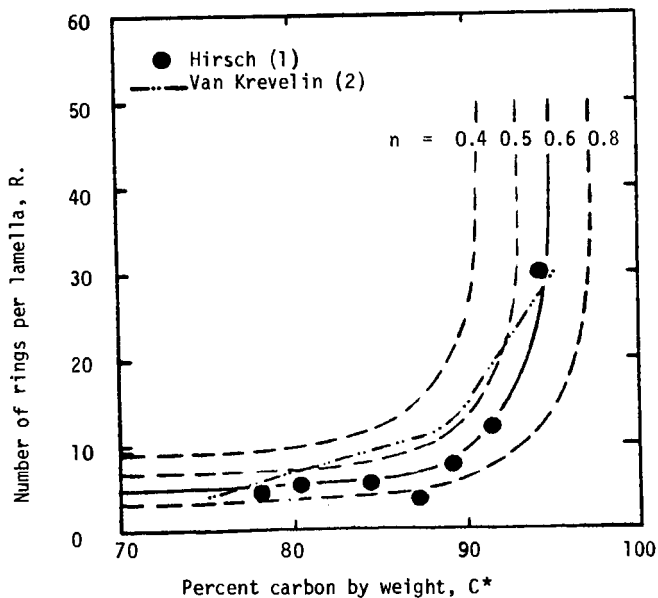


Figure 4 - Variation of number of rings per lamella with carbon percentage by weight.

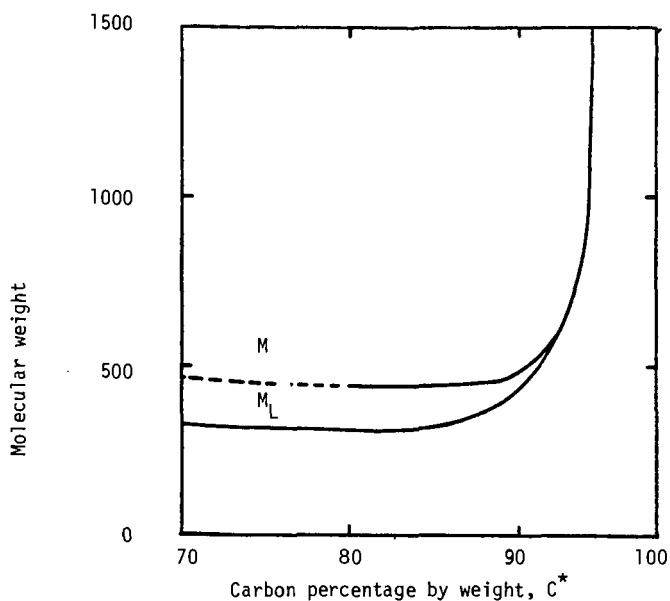


Figure 5 - Variation of molecular weight of lamella and coal molecule with weight percent carbon.

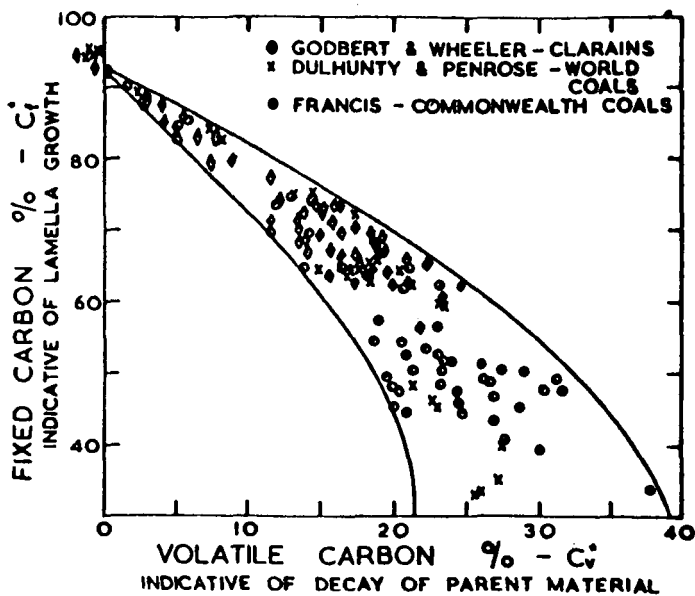


Figure 6 - Relation between lamella growth and decay of parent material. (Source: Ayre and Essenhig, (3))

Organic Structure Studies of Fossil Fuels  
by Nuclear Magnetic Resonance

Victor J. Bartuska and Gary E. Maciel  
Department of Chemistry, Colorado State University  
Fort Collins, Colorado 80523

and

Francis P. Miknis and Daniel A. Netzel  
Laramie Energy Research Center, U.S. Department  
of Energy, Laramie, Wyoming 82070

Nuclear magnetic resonance (nmr) is playing an increasingly important role in the characterization of the organic constituents of fossil fuels.<sup>1-17</sup> The nmr techniques that are currently being applied to fossil fuel characterizations utilize both the <sup>1</sup>H and <sup>13</sup>C nuclides and can conveniently be divided into those that apply to liquid samples and those that apply to solids. For solids one has to contend with line-broadening influences of dipole-dipole interactions and chemical shift anisotropies (especially for carbon) and with long spin-lattice relaxation times; some recent advances have largely circumvented these problems for <sup>13</sup>C.<sup>14-20</sup> For liquids, rapid isotropic molecular tumbling averages dipolar splittings to zero and the chemical shift tensor to its isotropic average, and gives rise to relatively efficient spin-lattice relaxation (permitting one to reduce the wait time between pulse repetitions).

For solid fossil fuels, a considerable amount of structural information can be obtained by modern <sup>13</sup>C techniques.<sup>14-17</sup> Proton experiments on solids determine the amplitude of the free induction decay (FID) following a 90° pulse; this amplitude is a measure of the organic proton content of the sample for oil shales and has been related empirically to the oil yield one can obtain by retorting (Figures 1 and 2).<sup>8,9</sup>

For <sup>13</sup>C studies on solids, rapid spinning of the intact or powdered sample about an axis making an angle of 54° 44', the "magic angle", relative to the field axis eliminates broadening due to chemical shift anisotropy.<sup>17,19,20</sup> High-power <sup>1</sup>H decoupling eliminates broadening due to <sup>13</sup>C-<sup>1</sup>H dipole-dipole interactions.<sup>18</sup> If the high-power <sup>1</sup>H decoupling and <sup>13</sup>C resonance are carried out under conditions obeying the Hartmann-Hahn condition,<sup>18</sup> then the problem of long <sup>13</sup>C spin-lattice relaxation times can also largely be overcome. The net result of applying these techniques to homogeneous, pure organic solids is sharp-line spectra, reminiscent of spectra obtained on analogous liquid samples. For solid fossil fuels, however, the great complexity of mixtures of closely related chemical structures gives rise to resonance "bands", rather broad lines, encompassing the <sup>13</sup>C resonances of a given structural type, e.g., aliphatic carbons. While greater structural detail may sometime be available, (especially from spectra obtained at high field strength), at present the greatest current capability of this approach is a clear distinction between the resonances of aromatic or olefinic carbons and the aliphatic carbon resonances. Typical spectra are shown in Figures 3 and 4.

For liquid samples, standard pulse Fourier transform methods<sup>1-7</sup> are applicable to both <sup>13</sup>C and <sup>1</sup>H. Because of the great chemical complexity typical of samples, very complex spectra are usually obtained. Nevertheless, considerable information can usually be extracted regarding the occurrence of specific structural types.

By combining the various techniques described above, a great deal can be learned about a fossil fuel system and the processes involved in typical characterization procedures and, more importantly, in its conversion into a useable fuel source. We have applied the various nmr techniques described above to solid and liquid samples derived from oil shale of the Green River Formation. The purpose was to explore the potential applicability of nmr methods to answer such questions as: Do procedures for concentrating the kerogen in oil shale alter the distribution of organics in kerogen significantly? How similar are the kerogen, shale oil and bitumen derived from a specific oil shale? What, if any, types of organic structural features are present in the spent shale after retorting?

Using solid-sample techniques one can determine the total organic proton content and the aromatic/olefinic and aliphatic carbon contents of the raw shale, of the solid remaining after bitumens are extracted, of the solid kerogen concentrate obtained from the shale and of the residue from retorted shale. Using standard FT techniques for liquids, analogous information and considerably greater structural detail can be obtained on the bitumens extracted from the shale and on the shale oil retorted from the shale. Examples of relevant spectra are shown in Figures 5-8. In interpreting the intensities of the resonances of such carbon spectra, one has to pay close attention to intensity distortions associated with nuclear Overhauser effects and the dynamics of the cross polarization experiment.<sup>20</sup>

#### References

1. Shoolery, J.N. and Budde, W.L., Anal. Chem., **48**, 1458, (1976).
2. Dorn, H.C. and Wooten, D.L., Anal. Chem., **48**, 2146, (1976).
3. Pugmire, R.J., Grant, D.M., Zilm, K.W., Anderson, L.L., Oblad, A.G. and Ward, R.E., Fuel, **56**, 295, (1977).
4. Wooten, D.L., Coleman, W.M., Taylor, L.T., and Dorn, H.C., Fuel, **57**, 17, (1978).
5. Schweighardt, F.K., Retcofsky, H.L. and Freidel, R.A., Fuel, **55**, 313, (1976).
6. Retcofsky, H.L., Schweighardt, F.K. and Hough, M., Anal. Chem., **49**, 585, (1977).
7. Retcofsky, H.L. and Friedel, R.A., Fuel, **55**, 363(1976).
8. Miknis, F.P., Decora, A.W. and Cook, G.L., U.S. BuMine Rept. Invest. 7984, (1974), 47 pp.
9. Miknis, F.P., Decora, A.W. and Cook, G.L., Science and Technology of Oil Shale (Ed. T. F. Yen), Ann Arbor Science Publishers, 1976, pp. 35-45.
10. Sydansk, R.D., Fuel, **57**, 66 (1978).
11. Halla, A. and Craft, B.D., paper No. 75, 1978, Pittsburgh Cleveland Conference on Analytical Chemistry and Spectroscopy.
12. Gerstein, B.C. and Pembleton, R.G., Anal. Chem., **49**, 75, (1977).
13. Gerstein, B.C., Chow, C., Pembleton, R.G. and Wilson, R.C., J. Phys. Chem., **81**, 565, (1977).
14. VanderHart, D.L. and Retcofsky, H.L., Fuel, **55**, 202 (1976).

15. Bartuska, V.J., Maciel, G.E. and Miknis, F.P., Am. Chem. Soc. Div. of Fuel Chem. preprints, 23, No. 2, 19, (1978).
16. Maciel, G.E., Bartuska, V.J. and Miknis, F.P., Fuel, in press.
17. Bartuska, V.J., Maciel, G.E., Schaefer, J. and Stejskal, E.O., Fuel, 56, 354, (1977).
18. Pines, A., Gibby, M.G. and Waugh, J.S., J. Chem. Phys., 59, 569, (1973).
19. Schaefer, J. and Stejskal, E.O., J. Amer. Chem. Soc., 98, 1031, (1976).
20. Schaefer, J., Stejskal, E.O. and Buchdahl, R., Macromolecules, 10, 384, (1977).

#### Figures

- Figure 1. Proton free induction decay (at 20 MHz) for oil shale before and after heating to remove free water (From Miknis et al, BuMines Rep. Invest. No., 7984 (1974).
- Figure 2. Correlation between proton free induction decay amplitude and average Fischer assay oil yields (From Miknis and Netzel, Magnetic Resonance in Colloid and Interface Science, H.A. Resing and C.G. Wade, Eds., ACS Symposium Series, 34, 182 (1976).
- Figure 3.  $^{13}\text{C}$  nmr spectrum of Hanna (Wyoming) coal, with high-power  $^1\text{H}$  decoupling, cross polarization and magic-angle spinning, obtained at 15.1 MHz. 530 ppm range. Higher shielding on the right.
- Figure 4.  $^{13}\text{C}$  nmr spectrum of Australian oil shale, same conditions as for Figure 3.
- Figure 5.  $^{13}\text{C}$  Fourier transform nmr spectrum of shale oil retorted from Colorado oil shale of Fig. 7. 530 ppm range. Higher shielding on the right.
- Figure 6.  $^{13}\text{C}$  Fourier transform nmr spectrum of bitumen (in  $\text{CDCl}_3$ ) extracted with benzene from Colorado oil shale of Fig. 7. Same conditions as for Fig. 5.
- Figure 7.  $^{13}\text{C}$  nmr spectrum of raw Colorado oil shale. Same conditions as for Fig. 3.
- Figure 8.  $^{13}\text{C}$  nmr spectrum of kerogen concentrate obtained from Colorado oil shale of Fig. 7. Same conditions as for Fig. 3.

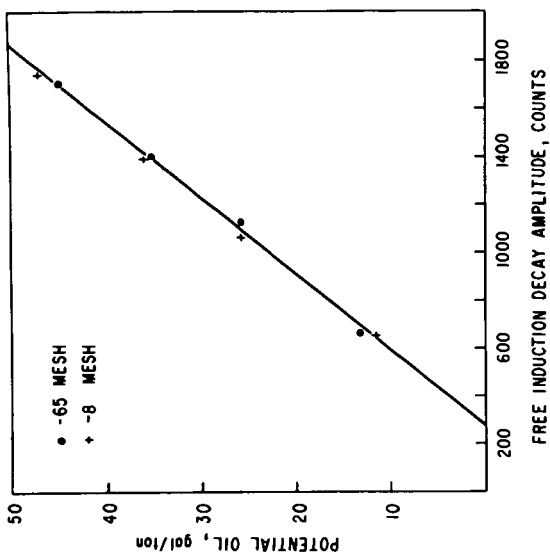


FIG. 2  
CORRELATION BETWEEN FID  
AMPLITUDE AND OIL YIELD

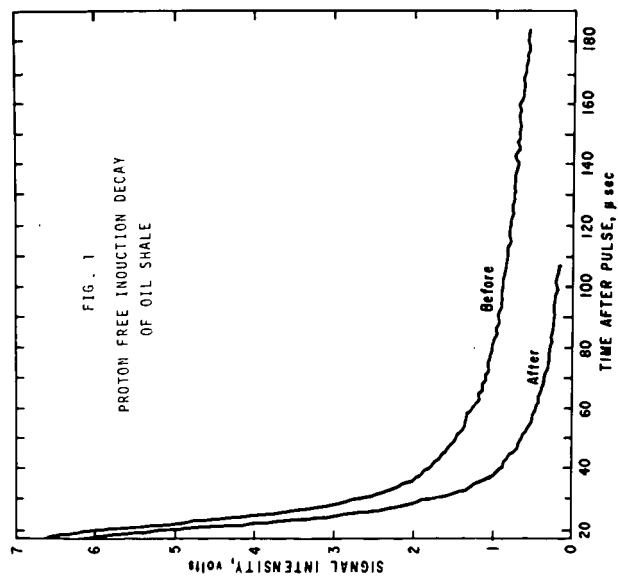


FIG. 3  
 $^{13}\text{C}$  SPECTRUM OF  
HANNA COAL

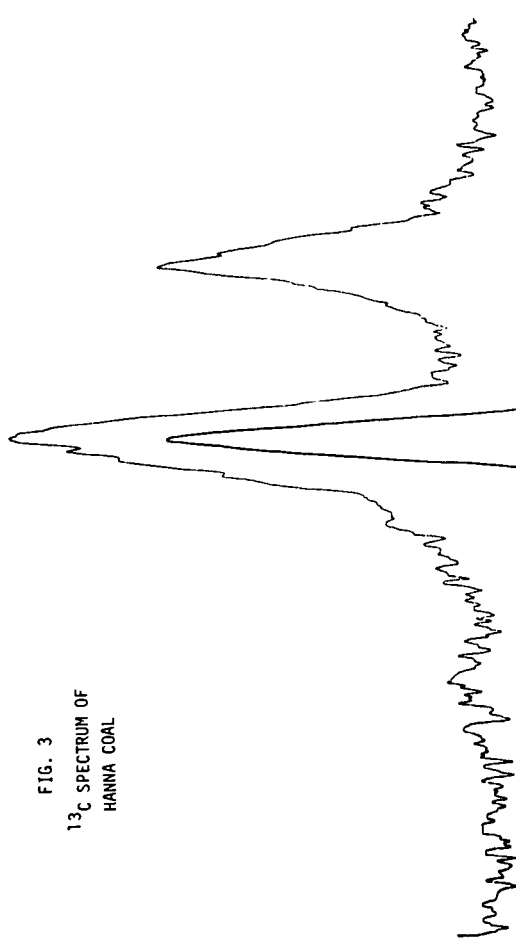


FIG. 4  
 $^{13}\text{C}$  SPECTRUM OF AUSTRALIAN  
OIL SHALE

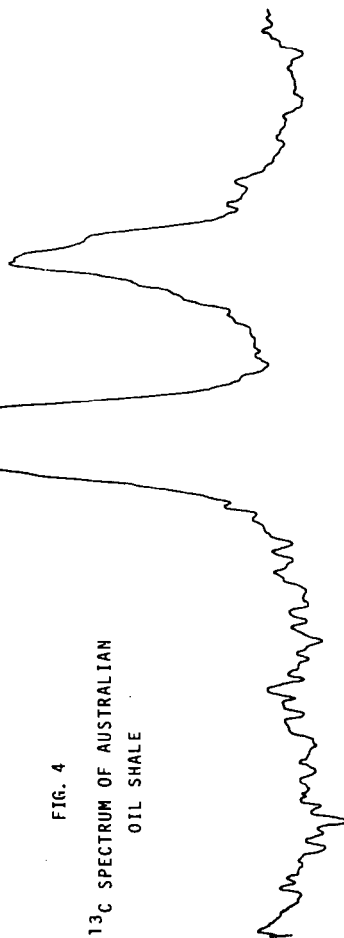


FIG. 5  
 $^{13}\text{C}$  FT SPECTRUM OF SHALE OIL

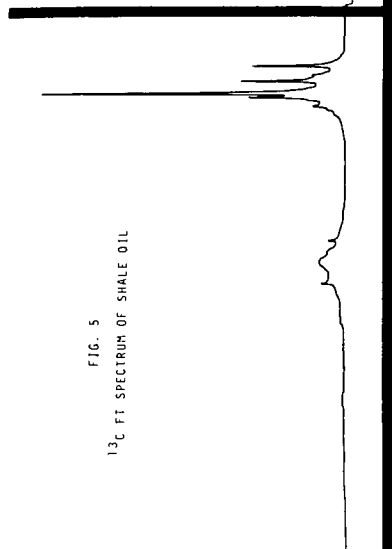


FIG. 7  
 $^{13}\text{C}$  SPECTRUM OF RAW OIL SHALE

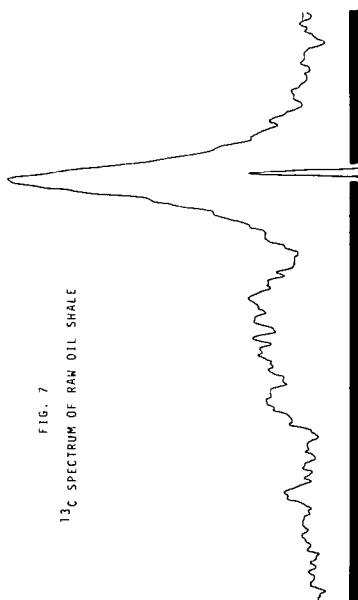


FIG. 6  
 $^{13}\text{C}$  FT SPECTRUM OF  
OIL SHALE BITUMEN

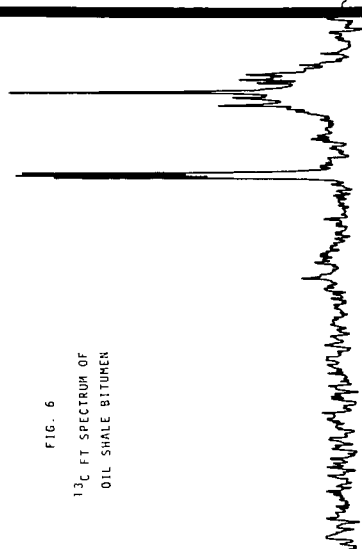
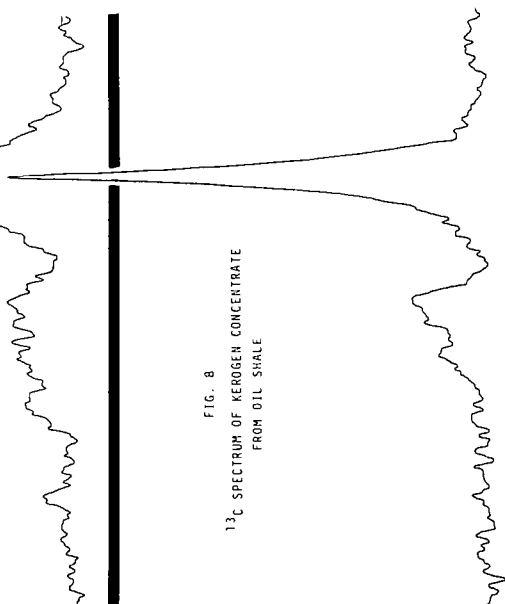


FIG. 8  
 $^{13}\text{C}$  SPECTRUM OF KEROGEN CONCENTRATE  
FROM OIL SHALE



CHEMICAL CHANGES PRODUCED IN COAL THROUGH  
THE ACTION OF LEWIS ACID CATALYSTS

D. P. Mobley, S. Salim, K. I. Tanner, N. D. Taylor and A. T. Bell

Materials and Molecular Research Division  
Lawrence Berkeley Laboratory  
and

Department of Chemical Engineering  
University of California, Berkeley, CA 94720

INTRODUCTION

Molten Lewis acids and in particular  $ZnCl_2$  and  $SnCl_2$  are known to catalyze the conversion of coal to liquid products (1-15). While the degree of liquefaction attainable with different catalysts is known, the manner in which Lewis acids promote liquefaction is not well understood. The present work was undertaken in an effort to establish more clearly the effects of Lewis acids on coal and to identify the specific chemical reactions which these catalysts affect. The results reported here concern experiments conducted with both solvent refined coal (SRC) and a variety of model compounds. The latter were selected to represent the aliphatic, ether, and sulfide linkages which connect the aromatic and hydro-aromatic groups in coal. Several models of fused ring aromatic clusters were also examined.

EXPERIMENTAL

Apparatus

All reactions were conducted in a 300 cm<sup>3</sup> stirred autoclave (Autoclave Engineers, Inc. Model ABP-300). To facilitate the introduction of reactants and the removal of products a snugly fitted glass liner was used to contain the reaction mixture. The temperature and pressure within the autoclave were recorded continuously.

Materials

The SRC used here was produced from a bituminous West Kentucky coal by the Pittsburg and Midway Coal Mining Company in Tacoma, Washington. The SRC was dried overnight in an  $N_2$ -purged oven at 105°C and then ground to pass through an 80 Tyler mesh sieve. The sieved SRC was then stored in a vacuum dessicator until needed for a run.

Model compounds were obtained from a variety of standard commercial sources. These materials were kept dry but were not purified before use.

Lewis acid catalysts were also obtained from several sources. Since several of these materials are hygroscopic (viz.  $\text{AlCl}_3$ ,  $\text{FeCl}_3$ ,  $\text{SbCl}_3$ ) the catalysts were first dried in a vacuum oven overnight at  $105^\circ\text{C}$  and then stored in an  $\text{N}_2$ -purged dry box. Weighing of the catalyst and transfer into the glass liner were also carried in the dry box.

#### Product Analysis

The liquid products obtained from reactions of SRC were disengaged from the reaction solvent and dried. The dried material was then weighed to establish the fraction of the SRC submitted to reaction which had been converted to liquid products. The stoichiometry of the dissolved products was determined by elemental analysis and the ratio of aliphatic to aromatic hydrogens,  $\text{H}_{\text{Al}}/\text{H}_{\text{Ar}}$ , by  $^1\text{H-NMR}$ .

The products obtained from model compound studies were analyzed by gas chromatography. Product identification was established with the aid of a gas chromatograph/mass spectrometer. Where possible product assignments were confirmed by injecting pure compounds into the gas chromatograph/mass spectrometer and comparing their retention times and mass spectra with those of the postulated reaction product.

### RESULTS AND DISCUSSION

#### SRC Studies

Table 1 summarizes the results of screening experiments designed to compare the influence of selected Lewis acid catalysts on the dissolution of SRC in benzene at  $300^\circ\text{C}$ . It is apparent that the stronger acids,  $\text{AlCl}_3$ ,  $\text{FeCl}_3$ ,  $\text{SbCl}_3$ , and  $\text{HgCl}_2$ , cause a decrease in SRC solubility over that obtained without a catalyst. The use of  $\text{ZnCl}_2$  does not alter the benzene solubility of SRC but contributes significantly to raising the  $\text{H/C}$  and  $\text{H}_{\text{Al}}/\text{H}_{\text{Ar}}$  ratios of the soluble product. Similar results were obtained with  $\text{SnCl}_2$  but in this instance a greater fraction of the SRC was dissolved. These results suggest that the acidity of the catalyst should be high enough to promote bond cleavage but not so high as to catalyze rapid retrograde reactions which lead to a diminished solubility of SRC.

The effectiveness of a given catalyst on the solubilization of SRC also depends upon the solvent as shown in Table 2. Here, it is seen that while cyclohexane is a less effective solvent for SRC than benzene, the introduction of either  $\text{ZnCl}_2$  or  $\text{SnCl}_2$  into cyclohexane has a very pronounced effect on the yield of soluble products.

### Model Compound Studies

The cleavage of aliphatic linkages between aromatic nuclei was studied using the model compounds listed in Table 3. To facilitate product identification, cyclohexane was used as the solvent. Reactions were typically carried out for 90 min. at 325°C and 1000 psig of  $H_2$ . The ratio of substrate to catalyst was usually 14.3 mole/mole.

Screening studies performed on the unsubstituted diphenyl alkanes showed that the cleavage of the aliphatic bridge in these compounds required the use of a strong Lewis acid such as  $AlCl_3$ . In the presence of this catalyst diphenyl methane, ethane, propane, and butane reacted readily at temperatures as low as 250°C. The initial products were always benzene and a phenyl alkane, indicating that cleavage had occurred between a benzene ring and the first carbon of the aliphatic bridge. The phenyl alkane product was not stable, however, and was observed to isomerize or crack to shorter chained products. In the cases of diphenyl propane and diphenyl butane, indan and tetralin were observed respectively as major reaction products. While 70 to 80% of the diphenyl alkanes were converted to products under the conditions noted earlier, diphenyl was less reactive and was only 32% converted. The only product obtained from diphenyl was benzene.

A mechanism which summarizes our observations on the cleavage of diphenyl and the diphenyl alkanes is shown below. The lower reactivity of diphenyl is explained by the fact that the phenyl carbonium ion, formed in the first step of the reaction, is less stable than a phenyl alkane carbonium ion.

The addition of a hydroxyl group to one of the phenyl rings of diphenyl methane was found to contribute an inductive effect, facilitating cleavage of the aliphatic linkage. Since phenol was a major reaction product it was concluded that cleavage had occurred preferentially at the ring containing the hydroxyl group. Experiments were also performed to determine whether the inductive effect of the hydroxyl group would now permit  $ZnCl_2$ , a weaker Lewis acid, to cleave the aliphatic bridge. These experiments gave positive results. However, under identical reaction conditions  $ZnCl_2$  provided only half of the substrate conversion obtained with  $AlCl_3$ .

To determine the effects of fused ring nuclei upon the cleavage of aliphatic bridges, experiments were conducted with phenyl naphthalene and benzyl naphthalene. By analogy with diphenyl, phenyl naphthalene was relatively unreactive and could be cleaved only to the extent of 10%. Benzyl naphthalene, on the other hand, was completely converted to naphthalene, benzene, and other aromatic products. The reaction of benzyl naphthalene in the presence of  $ZnCl_2$  was also examined. It was found that while  $ZnCl_2$  is not as effective a catalyst as  $AlCl_3$ , it would bring about a 40% conversion of the substrate to products.

The cleavage of ether and sulfide linkages occurred more readily than the cleavage of aliphatic linkages and could be catalyzed by  $\text{ZnCl}_2$ . Reaction of diphenyl ether at  $325^\circ\text{C}$  yielded phenol and benzene. Under similar conditions diphenyl sulfide yielded thiophenol and benzene. Dibenzyl ether and dibenzyl sulfide followed similar reaction paths. Both of these substrates apparently form benzyl carbonium ions which rapidly alkylate the solvent, benzene, to produce diphenyl methane.

The reactions of benzyl naphthyl ether were also explored. In benzene this substrate yielded 2-hydroxynaphthalene and diphenyl methane. These products again illustrate the preferential cleavage of the linkage to produce a benzyl carbonium ion.

The effects of Lewis acid catalysts on fused ring aromatic clusters was also examined, using naphthalene and phenanthrene as models. In the presence of  $\text{AlCl}_3$ , naphthalene was converted to tetralin which in turn cracked to produce benzene. Phenanthrene reacted to produce 9,10-dihydrophenanthrene and smaller quantities of naphthene and tetralin. Thus both naphthalene and phenanthrene appear to react by first hydrogenating and then cracking to produce products of lower molecular weight. It is interesting to note that for temperatures up to  $325^\circ\text{C}$  no evidence was obtained that  $\text{ZnCl}_2$  could promote reactions similar to those observed with  $\text{AlCl}_3$ .

#### CONCLUSIONS

The following conclusions can be drawn from this work.

- $\text{ZnCl}_2$  and  $\text{SnCl}_2$  are particularly suitable catalysts for the dissolution of  $^2\text{SRC}$  in benzene and cyclohexane.
- The strength of acid required to catalyze the cleavage of aliphatic linkages between aromatic nuclei depends upon the nature of the nuclei, naphthyl and hydroxyphenyl groups being more readily separated from aliphatic linkages than phenyl groups.
- Ether and sulfide linkages are easily cleaved by mild Lewis acids such as  $\text{ZnCl}_2$ .
- The products obtained from the cleavage of aliphatic, ether, and sulfide linkages can be explained by carbonium ion mechanisms.
- Hydrogenation and cracking of fused ring aromatic clusters requires strong Lewis acids such as  $\text{AlCl}_3$ .

#### ACKNOWLEDGMENT

This work was supported by the Division of Chemical Sciences, Office of Basic Energy Sciences, U.S. Department of Energy.

# REFERENCES

- (1) C. O. Hawk and R. W. Hiteshue, U.S. Bureau of Mines Bulletin No. 622(3), 1965.
- (2) C. W. Zielke, R. T. Struck, J. M. Evans, C.P.. Costanza, and E. Gorin, Ind. Eng. Chem. Process Des. Dev., 5(2), 151 (1966).
- (3) C. W. Zielke, R. T. Struck, J. M. Evans, C. P. Costanza, and E. Gorin, Ind. Eng. Chem. Process Des. Dev., 5(2), 158 (1966).
- (4) W. Kawa, S. Friedman, L. V. Frank; and R. W. Hiteshue, Preprints, ACS Fuel Chem., Am. Chem. Soc., 12(3) 4347 (1968).
- (5) Research on Zinc Chloride Catalyst for Converting Coal to Gasoline, Research and Development Report No. 39, Vol. III, Books 1,2, prepared by the Consolidation Coal Company for the Office of Coal Research, 1968.
- (6) R. T. Struck, W. F. Clark, P. J. Dudt, W. A. Rosenhoover, C. W. Zielke, and E. Gorin, Ind. Eng. Chem. Process Des. Dev., 8(4), 546 (1969).
- (7) C. W. Zielke, R. T. Struck, and E. Gorin, Ind. Eng. Chem. Process Des. Dev., 8(4), 552 (1969).
- (8) W. Kawa, H. F. Feldmann, and R. W. Hiteshue, Preprints, ACS Fuel Chem., Am. Chem. Soc., 14(4), Part 1, 19 (1970).
- (9) Project Western Coal: Conversion of Coal Into Liquids - Final Report, Research and Development Report No. 18, prepared by the University of Utah for the Office of Coal Research, May 1970.
- (10) S. A. Qader, K. Duraiswamy, R. E. Wood, and G. R. Hill, AIChE Symposium Series, 69(127), 102 (1973).
- (11) Coal Processing - Gasification, Liquefaction, Desulfurization: A Bibliography 1930-1974, Atomic Energy Commission, October 1974.
- (12) H. Katzman, A Research and Development Program for Catalysis in Coal Conversion Processes, Electric Power Research Institute Report No. 207-0-0, Palo Alto, Calif., 1974.
- (13) C. W. Zielke, W. A. Rosenhoover, and E. Gorin, Preprints, Div. of Fuel Chem., Am. Chem. Soc., 19(2) 306 (1974).
- (14) D. S. Ross and J. Y. Low, "Homogeneous Catalysis - Acid Catalysis", in Homogeneous Catalytic Hydrocracking Processes for Conversion of Coal to Liquid Fuels, Stanford Research Institute, Menlo Park, Calif., Quarterly Report Nos. 2,3, 1976.

- (15) R. E. Wood and W. H. Wiser, Ind. Eng. Chem. Process Des. Dev., 15(1), 144 (1976).

Table 1

Effects of Lewis Acid Catalysts on  
the Liquefaction of SRC in Benzene

Reaction Conditions: T = 300°C      Catalyst mass = 5 gm  
 P = 2000 psig H<sub>2</sub>      SRC mass = 5 gm  
 t = 90 min      Solvent volume = 70 ml  
 ω = 1250 rpm

Catalyst	Sol. (%)	Charac. of Sol. Prod. H/C	H <sub>Al</sub> /H <sub>Ar</sub>
None	46.7	0.85	1.33
AlCl <sub>3</sub> <sup>a</sup>	20.3	0.89	1.32
ZnCl <sub>2</sub>	46.8	1.01	2.54
SnCl <sub>2</sub>	57.9	0.97	2.22
SbCl <sub>3</sub>	38.2	0.95	2.18
HgCl <sub>2</sub>	37.8	0.93	1.79

<sup>a</sup> 1.0 gm AlCl<sub>3</sub> charged

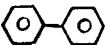
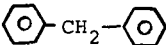
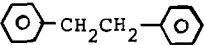
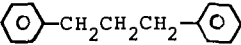
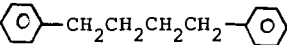
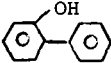
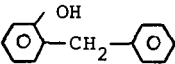
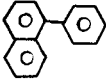
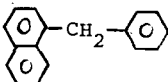
Table 2

## Effects of Solvents on the Liquefaction of SRC

Reaction Conditions: T = 300°C      Catalyst mass = 5 gm  
 P = 2000 psig H<sub>2</sub>      SRC mass = 5 gm  
 t = 90 min      Solvent volume = 70 ml  
 ω = 1250 rpm

Catalyst	Solvent	Sol. (%)	Charac. of Sol. Prod.	
			H/C	H <sub>Al</sub> /H <sub>Ar</sub>
None	Benzene	46.7	0.85	1.33
None	Cyclohexane	15.1	0.91	1.50
ZnCl <sub>2</sub>	Benzene	46.8	1.01	2.54
ZnCl <sub>2</sub>	Cyclohexane	35.4	1.06	3.38
SnCl <sub>2</sub>	Benzene	57.9	0.97	2.22
SnCl <sub>2</sub>	Cyclohexane	29.8	1.00	2.68

Table 3  
Model Compounds Containing Aliphatic Linkages

Compound	Structural Formula
Diphenyl	
Diphenyl methane	
1,2-Diphenyl ethane	
1,3-Diphenyl propane	
1,4-Diphenyl butane	
2-Phenyl phenol	
2-Benzyl phenol	
1-Phenyl naphthalene	
1-Benzyl naphthalene	

# AN ESR INVESTIGATION OF FREE RADICALS IN COALS AND IN COAL CONVERSIONS

L. Petrakis and D. W. Grandy

Gulf Research & Development Company  
P. O. Drawer 2038  
Pittsburgh, PA 15230

## I. Introduction

Free radicals in coal are not well understood or characterized despite their apparent great significance in liquefaction (1). The fate of these thermally generated free radicals is believed to determine the type of product obtained and may be associated with problems in coal conversion such as reactor coking and poor yields. This study of free radicals in coals was initiated to gain some insight as to the number and types of free radicals under a number of conditions that might be significant in coal conversion processes. Since the discovery of free radicals in coals by Uebersfeld (2) and Ingram (3), electron spin resonance (ESR) spectroscopy has been used in the study of coal and coal-derived materials by many workers (2-8).

As a technique, ESR is attractive, since radical concentration and chemical information can be obtained with relative ease in a minimal period of time. The spectral parameters of interest are the g-value of the radicals, radical concentration, peak-to-peak linewidth of the first derivative signal, and in some cases, the spectral lineshape.

## II. Experimental

Six coals, ranging in rank from lignite to low volatile bituminous, were examined by ESR after a variety of treatments. The analytical data for these coals are summarized in Table I. Several sample treatments were used. Four coals were treated by evacuation to  $\sim 10^{-4}$  torr with heating for 2 hours in 2 mm I.D. ESR tubes with subsequent sealing under vacuum. Several coals were treated under liquefaction conditions by mixing them with approximately equal weights of either naphthalene or tetralin in ESR tubes and heating them under 1800 psi of  $H_2$  or  $N_2$ . Some samples were prepared without solvent. The effects of different heating rates, solvents, gases, and residence times on the ESR parameters will be discussed. Duplicate samples were prepared in many cases to check reproducibility. All spectra were recorded at room temperature with Varian V-4500 single- and dual-cavity x-band spectrometers. Details of the measurements and peripheral equipment used are described in Ref. 8. The possible effect of many different factors, such as solid state effects, "skin" effects, sample inhomogeneity, and coal particle fractionation, on these measurements was considered and is discussed elsewhere (8).

## III. "Room Temperature" Experiments

The results obtained in the ESR experiments on coals evacuated at  $\sim 100^\circ C$  and at room temperature are essentially in agreement with the results obtained by earlier workers (4). The g-values show a large difference between the lignite and subbituminous coal and the four higher rank coals. (See Table II.) In the case of the higher rank coals, their g-values are typical of  $\pi$ -type aromatic hydrocarbon radicals (9,10). The subbituminous coal and the lignite have higher g-values indicating that atoms other than carbon and hydrogen are important in the electronic structure of the radical.

The spectral linewidth of all samples was measured as run in vacuum. Several samples yielded spectra which consist of a sharp line ( $\sim 1$  gauss) superimposed on a broader signal. As noted by Retcofsky et. al., a small amount of fusain ( $\sim 1\%$ ) in coal can account for the sharp component seen in spectra of evacuated samples (4).

The radical concentrations for the six coals follow the expected increase with rank with two exceptions. The Kentucky #11 coal has an extremely high free radical concentration for its rank. The Lower Dekoven coal is somewhat lower than expected, probably due in part to its extremely high ash content.

The lineshapes of the spectra were estimated in some cases. The lineshape functions considered were the Lorentzian and Gaussian functions. The samples yielded spectra which range from some nearly equal linear combination of the two functions, as is the case with the Wyodak coal, to the very broadly sloping, multi-component spectra sometimes found for the higher rank coals. The lineshapes of coal spectra are probably affected by unresolved hyperfine, anisotropic effects or the large number of somewhat chemically different radicals found in coals.

#### IV. Heat-Treated Coals

Four of the coals, Wyodak, Pocahontas #3, Illinois #6, and Lower Dekoven, were evacuated and heated to temperatures up to 600°C. Radical concentrations, g-values, and linewidths were measured for each sample. The radical concentration of the coals is seen to change dramatically over the temperature range studied. Up to 400°C, only moderate changes in radical concentration occur. Radical concentration increases sharply between 400°C and 500°C and drops substantially on going to 600°C (8). This behavior is qualitatively in agreement with the work of Smidt and Van-Krevelen, among others (6).

Figure 1 shows the change in g-values of the radicals in the coals as a function of temperature. Two of the coals, the Pocahontas #3 coking coal and the Illinois #6 high-volatile bituminous coal, show a minor decrease in g-values from 2.0029 to 2.0027. Such a change in g-value shows a minor change in radical structure, the radical tending to become more hydrocarbon in nature. The Wyodak sub-bituminous coal shows a very large decrease in g-value, from 2.0037 to 2.0027, which occurs below 500°C. One of the bituminous coals, Lower Dekoven, Illinois, shows some interesting changes in g-value when heated. Between 250° and 500°C the g-value decreases to an abnormally low value of 2.0023. There are several possible explanations for this behavior, among these is the appearance of  $\sigma$ -type radicals. Many  $\sigma$  radicals have g-values around 2.0024 and some are known have g-values as low as 2.0008 (11). From the increase in the g-value of the radicals in the Lower Dekoven coal on heating to 600°C and the decline in radical concentration, it is likely that the  $\sigma$ -radicals are involved in recombination reactions.

#### V. Liquefaction Experiments

Several coals were treated using various temperatures, heating rates, solvents, reagent gases, and residence times to determine their effect on the ESR spectral parameters. The Wyodak subbituminous coal was selected to determine experimental conditions to be used on a series of coals. In our initial experiments, this coal was heated at  $\sim 13^\circ\text{C}/\text{min}$  to 440°C in 1800 psig of  $\text{N}_2$  or  $\text{H}_2$  gas and held at that temperature for 2 hours. Examination of these samples at room temperature by ESR showed essentially no difference in g-values (2.0028), or linewidth (5.1 vs 5.5). Some difference in radical concentration between the samples treated with the two gases does occur, the samples treated in  $\text{H}_2$  having somewhat fewer radicals,  $25 \pm 13 \times 10^{18}/\text{g}$  vs  $45 \pm 3 \times 10^{18}/\text{g}$ . The same coal was reacted with tetralin or naphthalene in 1800 psi of  $\text{H}_2$  or  $\text{N}_2$  at the same temperature, heating rate, and for the same length of time. Linewidths and g-values were the same for all combinations, within experimental error, being about 5 gauss and 2.0027 to 2.0028, respectively. Free radical concentration of tetralin-treated Wyodak coal appears to be the same, around  $25\text{--}30 \times 10^{18}$  whether  $\text{H}_2$  or  $\text{N}_2$  gas is used. Naphthalene-treated coals do show some slight dependence (less than a factor of 2) of the free radical concentration on the gas used, the concentration being lower when  $\text{H}_2$  is used. The difference in radical concentration in this coal in what should be the best donor, tetralin and  $\text{H}_2$ , compared

to the worst donor system, naphthalene and  $N_2$ , is only slightly more than a factor of 2. Using tetralin with  $H_2$  and naphthalene with  $N_2$  as the treatments for the coal samples, the effects of heating rate and residence time were investigated. The radical concentration in samples was reduced in samples heated at a faster rate ( $32^\circ\text{C}/\text{min}$ ) and held at the maximum temperature for a shorter time (10 min). The tetralin- $H_2$ -treated samples showed a reduction in radical concentration that was much larger. The difference in radical concentration between the treatment schemes is about 5 to 1 for the Wyodak coal, again with the naphthalene- $N_2$ -treated samples having more free radicals remaining. Doubling the residence time from 10 minutes to 20 minutes had no apparent effect on tetralin- $H_2$ -treated samples. Some of the radical concentration data collected for different heating rate-residence time treatments for the two solvent-gas treatment schemes are shown in Figures 2 and 3 for the temperature range  $400^\circ$  to  $500^\circ\text{C}$ .

Two other coals, Kentucky #11 and Hagel lignite, were studied by ESR after treatment with the tetralin- $H_2$  and naphthalene- $N_2$  systems. All samples were heated at  $\sim 32^\circ\text{C}/\text{min}$  under 1800 psig and after they were kept at the desired temperature for 10 minutes, the reactor was cooled rapidly ( $\sim 3$  minutes to RT) by high-pressure air. A plot of the g-values of the Kentucky #11 coal radicals as a function of temperature is shown in Fig. 4. Around  $420^\circ\text{C}$  there is a considerable difference in g-values for the samples treated by the donor and non-donor systems. As the temperature is raised to  $\sim 475^\circ\text{C}$ , these differences disappear. The differences in g-values cannot be easily interpreted since all of these fall in the range of hydrocarbon radicals, and differences as large as these seen here are found between the anion and cation of the same radical species (9,10). The Hagel lignite runs show no such temperature dependence of g-values in the  $400^\circ$ - $500^\circ\text{C}$  range, with most of the samples having very similar g-values, between 2.0027 and 2.0028. Spectral linewidths for these two coals show no dependence upon temperature between 400 and  $500^\circ\text{C}$  or the solvent-gas treatment system used. The lignite samples had spectral linewidths generally between 5 and 6 gauss. There was more scatter in the linewidths found for the Kentucky #11 samples, ranging from 4 to 6 gauss. The free radical concentration of the Kentucky #11 samples is shown in Figure 5. Here the differences between the donor and non-donor treatments are apparent, as it was in Fig. 2 for the Wyodak coal. The Hagel lignite shows similar effects due to donor capabilities of the sample treatment; however, there is a generally higher concentration in all cases, the tetralin- $H_2$ -treated samples having radical concentration  $\sim 20 \times 10^{18}$  compared with  $\sim 40 \times 10^{18}$  for the naphthalene- $H_2$ -treated samples. It is believed that the lower radical concentration found for the tetralin- $H_2$ -treated samples is due to hydrogen transfer to the radical sites. A few extraction experiments were attempted on the Wyodak coal samples after the liquefaction treatments to see if a correlation between radical concentration and toluene-insolubles could be made. No significant differences were found, although this may be due to large experimental scatter. Conversions on a toluene soluble, daf basis are from 64 to 77%. Further effort in this area is planned.

#### VI. Solvent-Refined Coal

SRC filter feed, process solvent, and filter wash solvent were obtained from the Pittsburgh & Midway Coal Mining Co. SRC pilot plant near Tacoma, Washington. The samples used in most of this work are the dried filter solids, process solvent, filter wash solvent, the filtrate, which is about 50% process solvent and 50% filter-feed with solids removed, and the filter feed as received. A sample of the solid SRC product from the Catalytic, Inc., SRC pilot plant in Wilsonville, Alabama, was also examined. The results of the ESR measurements are shown in Table III. All values are for the organic paramagnetic species present.

#### VII. Conclusions

In general, concentrations of naturally occurring free radicals are of the order of  $5\text{--}15 \times 10^{18}/\text{g}$ . In coals heated in vacuum, the concentration of radicals is

quite high,  $100-200 \times 10^{18}/g$ , and reaches a maximum between 400 to 500°C, dependent on rank and maceral content. Coals heated to similar temperatures in the presence of a high-pressure (2000 psig) gas have somewhat lower concentrations ( $<100 \times 10^{18}/g$ ). This could result from small molecules or radicals escaping less readily in a high-pressure gas than in vacuum. The gas acts as a solvent. Naphthalene affects free radical concentration in a manner similar to that of the gases by acting as a solvent. Tetralin, as a hydrogen donor solvent, is the most effective treatment among those tried for consuming free radicals. Hydrogen transfer is presumed to occur and in some cases this hydrogen transfer quenches some of the naturally occurring free radicals in coal. The free radical concentration of SRC is similar to that found for other solvent-treated systems.

#### VIII. References

- (1.) R. C. Neavel, Fuel **56**, 237 (1976).
- (2.) J. Uebersfeld, A. Etienne, and J. Combrisson, Nature **174**, 614 (1954).
- (3.) D.J.E. Ingram, J. G. Tapley, R. Jackson, R. L. Bond, and A. R. Murnaghan, Nature **174**, 797 (1954).
- (4.) H. L. Retcofsky, J. M. Stark, and R. A. Friedel, Anal. Chem. **40**, 1699 (1968).
- (5.) D.E.G. Austin, D.J.E. Ingram, P. H. Given, C. R. Binder, and L. W. Hill, p. 344, "Coal Science," Advances in Chemistry, Series #55 ACS, (1965).
- (6.) J. Smidt and D. W. VanKrevelen, Fuel **38**, 355 (1959); COAL, pp. 393-399, Elsevier, Amsterdam (1961).
- (7.) B. C. Gerstein, C. Chow, R. G. Pembleton, and R. C. Wilson, J. Phys. Chem. **81**, 565 (1977).
- (8.) L. Petrakis and D. W. Grandy, Anal. Chem. **50**, 303 (1978).
- (9.) M. S. Blois, Jr., H. W. Brown, and J. E. Maling, FREE RADICALS IN BIOLOGICAL SYSTEM, p. 130, Academic Press, Inc., New York (1961).
- (10.) B. G. Segal, M. Kaplan, and G. K. Fraenkel, J. Chem. Phys. **43**, 4191 (1965).
- (11.) P. Smith, R. A. Kaba, L. M. Dominguez, and S. M. Denning, J. Phys. Chem. **81**, 162 (1977).

Table I  
CHEMICAL ANALYSIS (DAF)

	C	H	O	S	N	ASH(dry)	RANK
Wyodak Gilllete, WY	72.2	5.5	21.0	0.3	1.0	9.2	Subbit C
Hagel-ND*	71.0	4.9	21.8	.72 (total)	1.6	9.7	Lignite
Kentucky #11*	76.4	5.4	10.0	5.1 (total)	2.2	16.0	HVB
Illinois #6	82.0	5.4	9.5	1.0	1.7	6.5	HVB
Lower Dekoven-IL*	80.6	5.8	4.8	7.7	1.8	21.9	HVA
Pocahontas #3-WV	86.4	3.9	6.8	0.9 (total)	1.2	3.3	LV

\*Data supplied by P. Given, Pennsylvania State University.

Table II

ESR PARAMETERS OF COALS  
All samples evacuated 2 hr at 105°C

	<u>g-Value</u>	<u>Linewidth</u>	<u>Raical Concentration</u> <u>per g x 10<sup>-18</sup></u>
Hagel Lignite	2.0040	6.7	4.7
Wyodak Subbit C	2.0037	7.43	5.8
Kentucky #11 HUB	2.0029	1.9	14.1
Illinois #6 HUB	2.0029	1.34 & 6.02	6.8
Lower Dekoven HVA	2.0028	0.86 & 4.14	4.1
Pocahontas #3 LV	2.0029	0.97 & 6.03	15.8

Table III

SRC ESR DATA\*

<u>Sample</u>	<u>g-Value</u>	<u>Linewidth</u> <u>(gauss)</u>	<u>Concentration</u> <u>(spins/g)</u>
SRC Filter Cake Solids	2.0026	2.9	$18 \times 10^{18}$
Filtrate	2.0031	6.4	$0.7 \times 10^{18}$
Filter Feed	2.0027	1.4	$3.5 \times 10^{18}$
Recycle or Process Solvent	2.0029	9.4	$0.2 \times 10^{18}$
Wash Solvent	2.0037	6.8	$6 \times 10^{15}$
Wilsonville SRC Solid Product	2.0028	1.0	$15 \times 10^{18}$

\*All materials are from the P&M SRC pilot plant at Tacoma, Washington, except as noted.

Figure 1. g-Value Vs Temperature

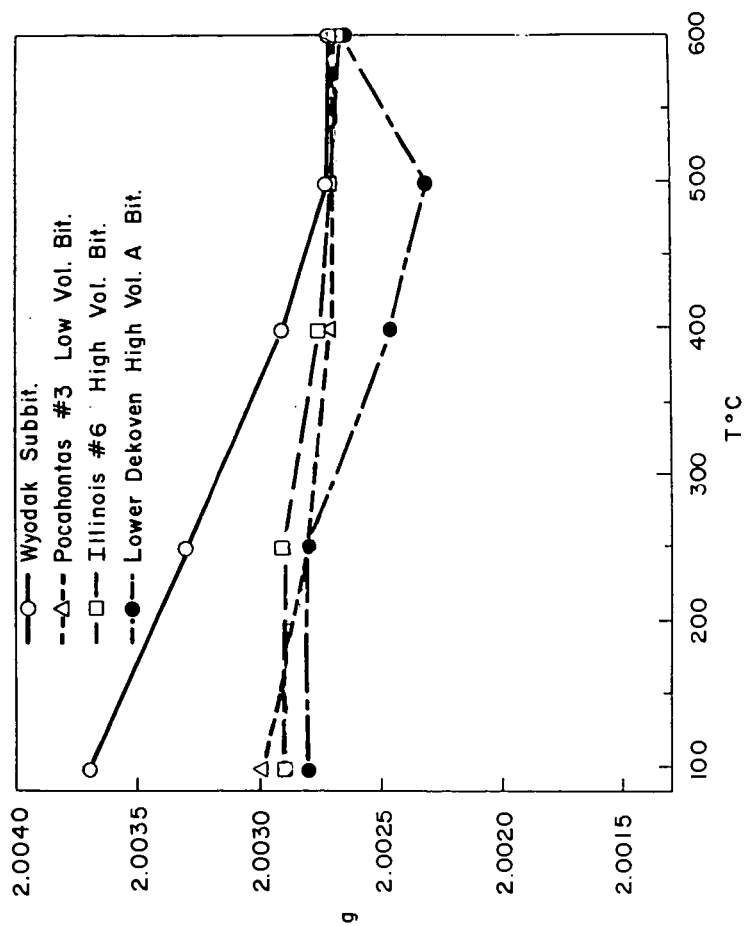


Figure 2. Radical Concentration Vs Temperature

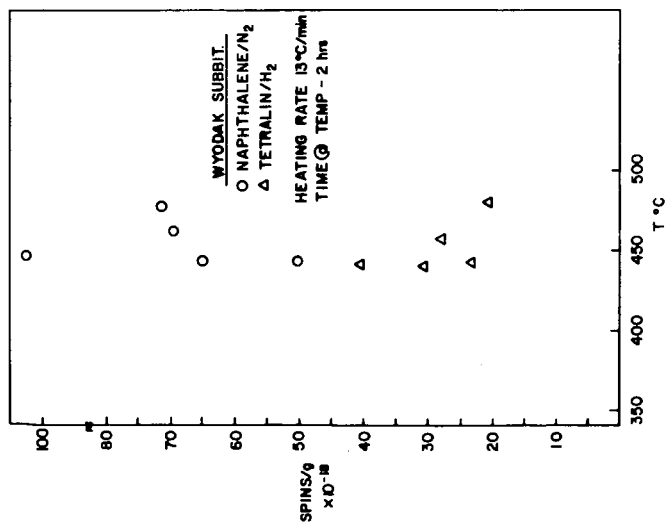


Figure 3. Radical Concentration Vs Temperature

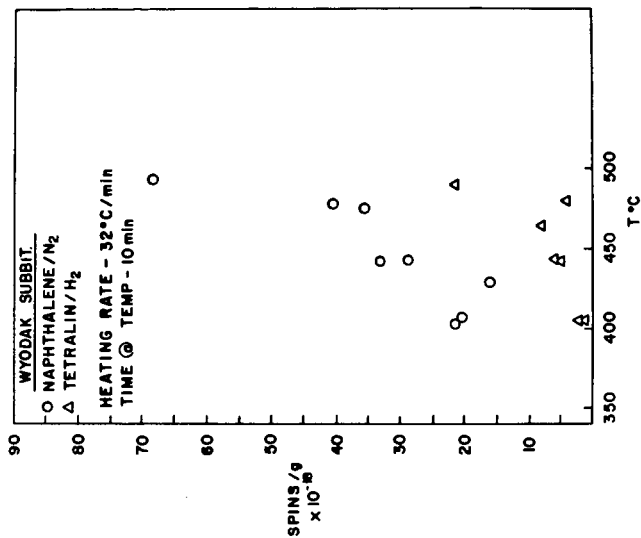


Figure 4. g-Value Vs Temperature

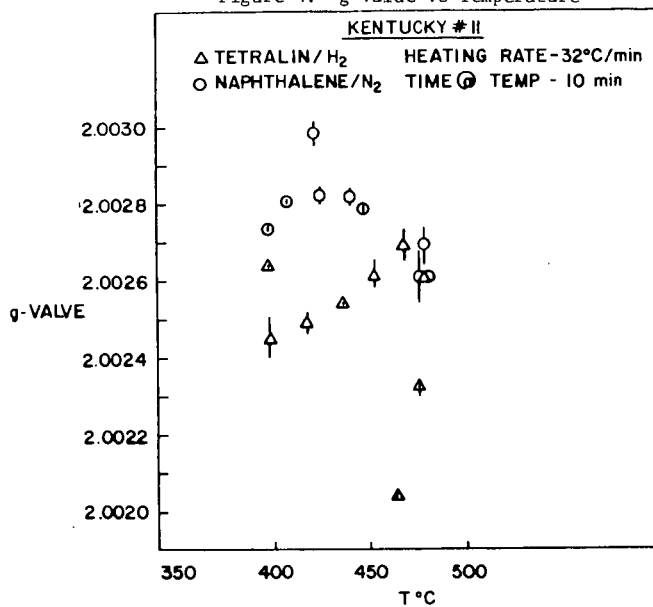
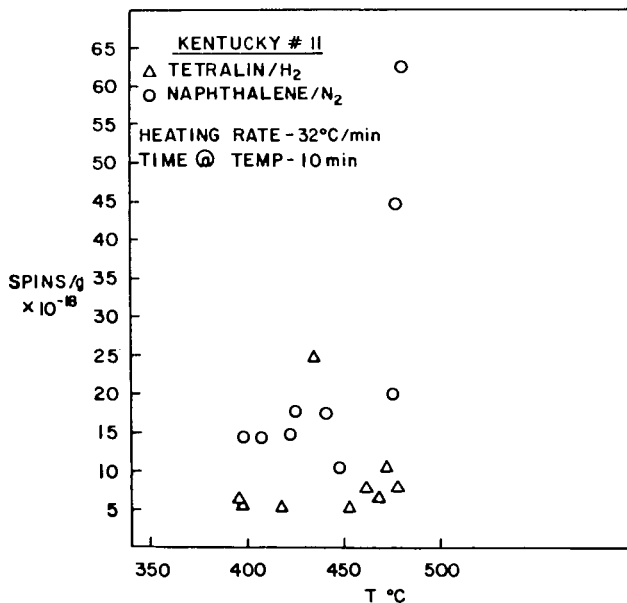


Figure 5. Radical Concentration Vs Temperature



## DEUTERIUM TRACER METHOD FOR INVESTIGATING THE CHEMISTRY OF COAL LIQUEFACTION

Raymund P. Skowronski, Laszlo A. Heredy  
Rockwell International, Atomics International Division  
8900 De Soto Avenue, Canoga Park, California 91304

Joseph J. Ratto  
Rockwell International, Corporate Science Center  
1049 Camino Dos Rios, Thousand Oaks, California 91360

### INTRODUCTION

Conversion of coal to liquids by hydrogenation involves an increase of the hydrogen content of the coal. The effective use of this costly gas is, therefore, of significant importance to commercial hydrogenation processes. An intensive research effort has been under way to obtain a better understanding of the hydrogenation reaction mechanisms and thereby to improve hydrogen utilization and the efficiency of the process. This paper describes the development of a deuterium tracer method for the investigation of the mechanism of coal hydrogenation.

The deuterium tracer method consists of conducting coal hydrogenation experiments with deuterium, or deuterium and a deuterated donor solvent, separating the products by solvent-fractionation and analyzing the fractions for protium and deuterium structural types by proton and deutron NMR spectrometry. In an alternative application of the method, which has been investigated, pairs of hydrogenation experiments are conducted, one with protium and one with deuterium, under identical experimental conditions. The hydrogenated products are separated by solvent-fractionation and the fractions are analyzed for hydrogen structural types by proton NMR spectrometry. The difference between the two spectra gives a quantitative measure of the hydrogen which is incorporated into different structural positions in the coal.

In the past, relatively little use has been made of deuterium as an isotopic tracer for investigating coal chemistry.<sup>(1,2)</sup> Very recently, however, renewed interest in the applications of deuterium to coal science has been evident.<sup>(3-5)</sup>

### EXPERIMENTAL

A high volatile A bituminous coal (81.8% C, dmmf basis) from the Loveridge Mine, Pittsburgh Seam, was used. The coal was ground to -200 mesh and stored under dry nitrogen until used. It then was dried at 115°C for 4 h before use.

High-purity (99.95% according to the supplier's specifications) protium and technical grade (>98.8 atom % deuterium and total hydrocarbons <1 ppm according to the supplier's specifications) deuterium were used. The benzene, hexane isomer mixture, and methanol utilized for the solvent-fractionation analyses were all Baker reagent grade. Chloroform-d was used as the solvent for the NMR spectrometric analyses.

The experiments were performed in a 1-liter stirred autoclave (Autoclave Engineers). The combined solid and liquid products from each of the hydrogenation experiments were solvent-fractionated into oil, asphaltene, benzene-methanol soluble, and residue fractions. Samples of fractions from those experiments in

which deuterium was used were combusted, and the resulting water was collected. The water samples then were analyzed by mass spectrometry (MS) to determine the protium and deuterium contents of each.

The product gases were analyzed by gas-solid chromatography coupled with mass spectrometry (GC-MS) to determine both the amount of each component in the gas phase and its isotopic composition. Both the MS and GC-MS were performed by Shrader Analytical and Consulting Laboratories, Inc.

The NMR spectra of the soluble fractions were obtained using a JEOL FX60Q Fourier Transform NMR Spectrometer. Elemental analyses were conducted with a standard combustion train.

## RESULTS AND DISCUSSION

Exploratory hydrogenation experiments were conducted to establish baseline conditions for the systematic investigation of deuterium incorporation. The criterion that was established for baseline conditions was that the benzene-soluble portion of the products be 25-50 wt % of the total products. Moderate conversion to benzene solubles was desired because it was expected that isotopic scrambling and nonspecific deuterium incorporation could be kept to a minimum under such reaction conditions.

The results of the exploratory experiments indicated that an experiment performed at 400°C, 3200 psig, for 1 h, with a 100 rpm stirring rate, should give the desired quantity of soluble products. Accordingly, the first pair of protium/deuterium experiments (4 and 5) was conducted under these conditions. The second pair of hydrogenation experiments (6 and 7) was performed at a lower temperature and for a shorter reaction time in order to investigate deuterium incorporation at a very low conversion. The parameters for each experiment were 380°C, approximately 3000 psig, and 15 minutes reaction time. The yield of soluble products and the degree of deuterium incorporation were considerably lower than in the first pair of experiments.

The results of both pairs of experiments are summarized in Table 1. In both experiments, the atom percent deuterium content of the fractions increased from the oil (hexane soluble) to the less soluble fractions and it was highest in the insoluble residue.

Table 2 lists the deuterium/protium ratios for the structural positions of the various fractions from Experiment 4. These numbers indicate the relative deuterium content in each position. The higher the number, the greater the deuterium incorporation in this position relative to other structural positions. The term  $2H_x$  refers to the quantity of deuterium that is in a specific structural position and, therefore,  $(2H_x/2H)$  refers to the fraction of the total deuterium that is in a given structural position. Similarly,  $(1H_x/1H)$  refers to the fraction of the total protium that is in a given structural position.

Significant specific deuterium incorporation is noted in the  $\alpha$ -alkyl (benzylic) positions in all the fractions and in the  $\gamma$ -alkyl positions of the asphaltene fraction. Large specific incorporation of deuterium in  $\alpha$ -alkyl positions is illustrated in Figure 1, where the proton and deutron NMR spectra of the oil fraction from Experiment No. 4 are compared. The deuterium incorporation in the  $\gamma$ -alkyl position of the asphaltenes is quite interesting because protium-deuterium exchange is expected to be relatively low in such a structural position. Further research will be conducted to establish whether this finding is related to the mechanism of asphaltene production.

The value for the  $\beta$ -alkyl region of the benzene-methanol fraction is equivalent to the  $\gamma$ -alkyl value for the asphaltene fraction. Data from a number of other experiments, however, indicate that the  $\beta$ -alkyl value is atypical, while the  $\gamma$ -alkyl value is typical.

A coal hydrogenation experiment was conducted with  $^2\text{H}_2$  and tetralin- $\text{d}_{12}$  at  $400^\circ\text{C}$  and 3000 psig. Significant specific deuterium incorporation was observed in the  $\alpha$ -alkyl position in all fractions. Similarly, most of the protium in the recovered tetralin- $\text{d}_{12}$  was concentrated in the  $\alpha$ -alkyl position.

Another set of experiments was designed to test the reactions of coal with deuterium under 3000 psig pressure at different temperatures and under different degrees of contact opportunity. The gaseous products from each of these experiments were analyzed by GC-MS to determine their isotopic composition. Together with data on the composition of the solvent-fractionated liquid and solid products, this information is being used to develop a tentative mechanism for the coal hydrogenation reaction.

The two techniques used to determine into which structural positions in the coal deuterium is incorporated during hydrogenation were discussed in the introduction. The measured values of deuterium incorporation, obtained from deuterium NMR spectrometry, were compared with the calculated values obtained from proton NMR spectrometry. In those cases where the  $^2\text{H}$  content of the sample was over 10-15 atom % there was good agreement between the calculated and measured values for deuterium incorporation.

#### ACKNOWLEDGMENT

This research was supported by the U.S. Department of Energy under Contract EF-77-C-01-2781.

#### REFERENCES

1. Y. C. Fu and B. D. Blaustein, *Chem. Ind.*, 1257 (1967)
2. T. Kessler and A. G. Sharkey, Jr., *Spectrosc. Lett.*, 1, 1977 (1968)
3. F. K. Schweighardt, B. C. Bockrath, R. A. Friedel, and H. L. Retcofsky, *Anal. Chem.*, 48, 1254 (1976)
4. A. F. Gaines and Y. Yürüm, *Fuel*, 55, 129 (1976)
5. J. R. Kershaw and G. Barrass, *Fuel*, 56, 455 (1977)

TABLE 1

## SUMMARY OF RESULTS FOR EXPERIMENTS 4-7

Parameter	Expt. 4	Expt. 5	Expt. 6	Expt. 7
Reactant Gas	$2\text{H}_2$	$1\text{H}_2$	$1\text{H}_2$	$2\text{H}_2$
Reaction Time (h)	1.0	1.0	0.25	0.25
Temperature ( $^{\circ}\text{C}$ )	400	400	380	380
Pressure (psig)	3200	3200	2700	3000
Reactor	1 Liter 250 Milliliters			
Products (%)	Atom % $2\text{H}$ (Expt. 4)		Atom % $2\text{H}$ (Expt. 7)	
Oil	22	22	5	5
Asphaltene	25	25	<1	*
Benzene-Methanol Soluble Fraction	6	6	7	7
Insoluble Residue	47	47	87	87
				19.5

\*Insufficient sample for analysis

TABLE 2  
COMPARISON OF PROTIUM AND DEUTERIUM  
DISTRIBUTIONS IN COAL HYDROGENATION PRODUCTS  
(EXPERIMENT 4)

Functional Region	$(^2\text{H}_x/^2\text{H})/(^1\text{H}_x/^1\text{H})$ Ratio		
	Oil	Asphaltene	BMS
Experiment 4			
$\gamma$ - Alkyl	0.6	1.2	0.9
$\beta$ - Alkyl	0.5	0.6	1.2
$\alpha$ - Alkyl*	2.2	1.9	1.5
Aromatic**	0.9	0.8	0.8

\*Includes  $\alpha^2$ - Alkyl Region

\*\*Includes Phenolic Region

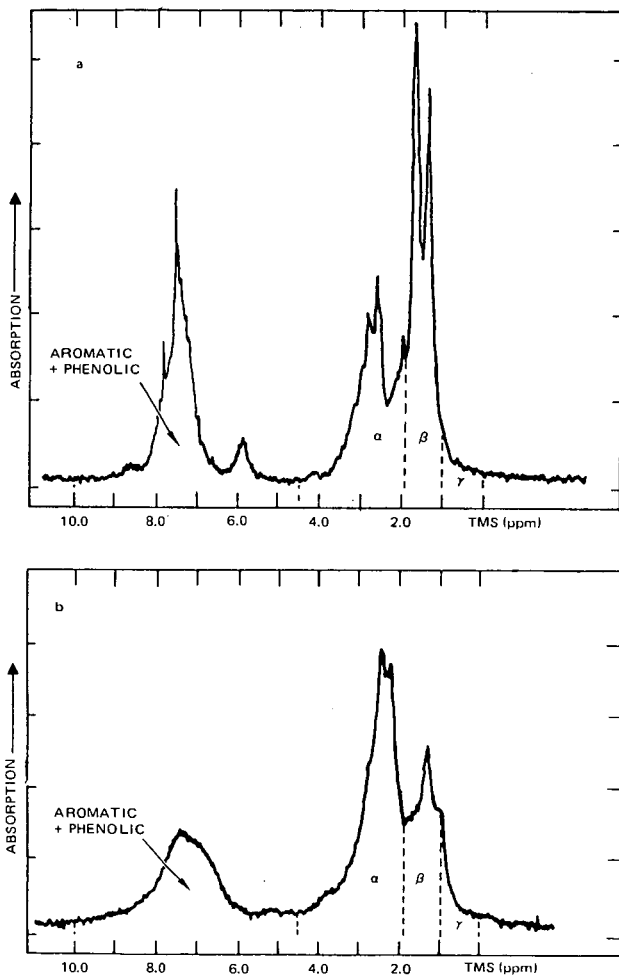


FIGURE 1. PROTON(a) AND DEUTERON(b) NMR SPECTRA OF THE OIL FRACTION FROM EXPERIMENT No. 4

## THE ROLE OF OXYGEN FUNCTIONAL GROUPS IN THE MECHANISMS OF COAL LIQUEFACTION

A. J. Szladow and P. H. Given

Department of Materials Science and Engineering,  
The Pennsylvania State University, University Park, Pa. 16802

The hypothesis that the generation of soluble products in coal liquefaction is related to the cleavage of ether bridges or cross-links was proposed by Fisher et al. (1) and reiterated 20 years later by Takegami et al. (2). Recently, several workers have reported investigations on related topics, which include reductive alkylation (3,4), behavior of model compounds (5), and the distribution of oxygen-containing functional groups in liquefaction products (6). Nevertheless, the role of oxygen functionalities in coal liquefaction seems to us still to be obscure, and we therefore report here some attempts to clarify the matter. We have restricted our study to coal-tetralin interactions and relatively short contact times, in order to study phenomena in the early stages of the process.

### EXPERIMENTAL

A high volatile bituminous coal having a low mineral matter content was chosen for the study (Table 1). Liquefaction runs were simulated in microreactors (~45 cc stainless steel tubes, with Swagelok fittings) charged with 5g of dried coal and 10 cc tetralin. Reactions were carried out at temperatures of 340 to 400°C and at contact times up to 30 minutes. Rapid heating of the contents was achieved by immersion of the vessels in a preheated fluidized sand bath; cooling was achieved by plunging the vessels into cold water. To ensure good mixing microreactors were vertically oscillated 450 times per minute with an amplitude of 1.25 cm. A more detailed description of the reactor assembly was given in (7). After reaction was completed, the contents were transferred to a 500 cc flask, diluted with hexane to a total volume of 500 cc, stirred and left for 24 hours to allow the precipitate (asphaltenes, preasphaltenes and residue) to be formed. To ensure that no change of sample properties occur during handling, such as oxidation or condensation of oxygen functional groups, a procedure was designed to avoid exposure to air, elevated temperatures or vacuum. The precipitate was filtered, washed with hexane and dried at room temperature in a stream of nitrogen for 24 hours. To correct analysis and extraction yields for adsorbed solvent, a portion of precipitate was dried in a vacuum ( $<10^{-1}$  torr) at 100°C and the weight loss noted.

The following determinations were carried out on the hexane-insoluble precipitate. Figure 1 presents the procedure in block diagram.

1. Hydroxyl groups were determined by acetylation (8). The procedure was modified by using a larger excess of acetic anhydride.

2. Carbonyl groups were determined from the nitrogen uptake during reaction with hydroxylamine hydrochloride (9). We are aware that the amounts reported may not strictly correspond to carbonyl groups, but may include other functionalities. However, since carbonyl groups probably constitute the major part of the functionalities determined we will refer to all of them as carbonyls. This problem does not affect the conclusions expressed in a later part of this paper.

3. Benzene and pyridine solubilities were determined by exhaustive extraction under a nitrogen atmosphere in a Soxhlet apparatus.

4. High temperature ash was determined according to ASTM procedure D 271.

This value was used to calculate coal conversion to gases and hexane-solubles using the following equation derived from material balance considerations:

$$\% \left[ \begin{array}{c} \text{hexane-solubles} \\ + \text{gases} \end{array} \right] = \frac{A_i - A_o}{A_o} \frac{10^4}{M_o} \quad 1)$$

where

$A_i$  = ash content of precipitate

$A_o$  = ash content of coal

$M_o$  = mineral matter in coal.

5. Elementary analyses including direct oxygen were determined using a Perkin-Elmer Model 240 microanalyzer.

The loss of total oxygen was calculated from the difference between direct oxygen determinations and is reported per total initial oxygen in coal. The values will include a portion of the inorganic oxygen, estimated to be no more than 5-10% of the total oxygen; this error will presumably be the same for coal and insoluble reaction products.

A special sample of liquefied coal was prepared to investigate the effect of hydrogen bonding on benzene solubilities. Samples were prepared by reacting coal with tetralin at 400°C for 10 minutes, and then following the above described procedure to obtain the hexane-insoluble precipitate.

We were able to introduce different quantities of trimethylsilyl groups on to the hydroxyl groups by varying the reflux time of 2g of sample in 40 cc tetrahydrofuran and 10 cc hexamethyldisilazane. After reaction, the contents were diluted with hexane, filtered and the residue was washed with hexane. Because some hexane-soluble materials were generated by the above procedure, the filtrate was collected and solvent plus unreacted hexamethyldisilazane removed by distillation, after which the undistilled material was weighed. The number of hydroxyl groups blocked was estimated from the change in H/C atomic ratios between a blank run (sample + THF), and the products of silylation (residue + dry solid from filtrate).

Differences in solubilities between blank and blocked samples are reported as the increase of benzene solubilities.

## RESULTS AND DISCUSSION

Yields of pyridine-solubles, benzene-solubles and hexane-solubles plus gases are plotted *versus* the loss of oxygen for various contact times and temperatures in Figures 2a-d. There appear to be correlations between the various sets of data, from which it is tempting to draw mechanistic conclusions. Thus, as already noted, Fisher et al. (1) used a similar correlation to that in Figure 2a, between conversion to benzene-soluble products and loss of total oxygen content, to infer that splitting of ethers was a rate-determining step. But other correlations found here (Figures 2b and 2c) could support alternative hypotheses, such as that the elimination of hydrogen-bonding between hydroxyl groups is crucial to liquefaction. In any case, there is a correlation between loss of total oxygen and oxygen as OH (Figure 3). Thus we believe that in coal liquefaction, where a number of processes are undoubtedly occurring concurrently, unambiguous conclusions about mechanisms cannot be drawn directly from correlations such as those illustrated in Figures 2a-d. Nevertheless, we believe that useful conclusions can be drawn from the data, though in a less direct way.

In examining the magnitude of changes of the oxygen functionalities during generation of pyridine-soluble materials, we have observed that the major loss of

oxygen occurred with the so-called unaccounted oxygen (unaccounted = total - hydroxyl - carbonyl) and very little change was detected in the contents of hydroxyl and carbonyl groups at these stages of liquefaction (Figure 4). If we presume that the unaccounted oxygen is comprised primarily of the ether oxygen, then Figure 4 strongly suggests an important contribution of these functionalities to generation of pyridine-soluble materials. Although we cannot estimate an exact amount of the ether oxygen being cleaved, we can, however, estimate the maximum amount of the ether oxygen linkages being cleaved per 100 initial carbon atoms in coal. From a material balance we can show that:

$$\left[ \begin{array}{c} \text{amount of ether} \\ \text{oxygen cleaved} \end{array} \right] \leq \left[ \begin{array}{c} \text{total oxygen} \\ \text{loss} \end{array} \right] - \left[ \begin{array}{c} \text{hydroxyl + carbonyl} \\ \text{oxygen loss} \end{array} \right] \quad 2)$$

making the reasonable assumption that the amount of oxygen in the hexane-solubles is insignificant. Figure 5 shows the right side of the above inequality *versus* generation of pyridine-soluble materials plus gases (conversion of coal). The regression equation for the line is:

$$y = -0.230 + 0.0336x \quad 3)$$

The second coefficient (slope) has a standard deviation  $\sigma = 0.0030$ . The amount of ether oxygen linkages,  $\phi$ , being cleaved per 100 initial carbon atoms was calculated from the slope using the equation:

$$\phi = \left( \frac{12}{16} \right) \times \left( \frac{10^4}{\% C} \right) \times (\text{slope}) \quad 4)$$

where  $\% C$  = percent carbon in coal, dmmf.

Substituting  $\% C = 83.47$ , slope = 0.0336

gives  $\phi = 3.0 \pm 0.3$

This number is slightly larger than the amount estimated by Ignasiak et al. (4) in their study of products from reductive alkylation of a high-rank vitrinite, i.e., two ether linkages cleaved per 100 original C atoms. The difference in rank of vitrinites could explain the discrepancy. The question arises, is ether cleavage, in the amount indicated, sufficient to generate the observed yields of pyridine-soluble materials, or does the ether cleavage have only a contributing role, like that discussed below for the effect of hydrogenolysis of hydroxyl groups on generation of benzene-soluble materials.

It should be noted that the plot in Figure 5 is purely empirical. The points represent data obtained in runs at different temperatures and reaction times, so it is somewhat surprising that they lead to a linear regression of high significance. One possible inference from the finding is that the coal behaves in a manner characteristic of a uniformly cross-linked polymer.

We have conjectured from Figure 2c that since hydrogenolysis of hydroxyl groups cannot result in substantial lowering of the molecular weight, the effects observed are due to elimination of hydrogen bonding by removal of the hydroxyl groups. If this is true, then by replacing the hydroxyl hydrogen with a substituent like trimethylsilyl, we should decrease the number of hydrogen bonds and increase the benzene solubility. The results of the treatment with hexamethyldisilazane are shown in Figure 6. A marked increase of benzene solubility suggests that, during liquefaction, hydrogenolysis of hydroxyl groups can play an important role in the generation of benzene-soluble materials. (By extrapolation, the results indicate that over 80% of the total pyridine-soluble material could become benzene-soluble). However, if

we compare the rate (slope) of generation of benzene solubles when hydroxyl groups are blocked to the rate (slope) when hydroxyl groups are removed during liquefaction (dashed line, predicted from Figure 2c by correcting for yield of gases), we must concede that hydrogenolysis of hydroxyl groups during liquefaction cannot account for more than 40% of the benzene-soluble materials generated. The remainder, presumably, is generated via different mechanistic routes.

Suppose it should prove possible to make hydrogenolysis of hydroxyl groups more competitive by introducing selective catalysts. Would we gain anything from such a modification of the liquefaction process? In terms of hydrogen consumption the answer seems to be, yes. To produce more benzene solubles merely by hydrogenolysis of OH groups, we would have to add about 0.8% of hydrogen (w/w of pyridine-soluble materials). On the other hand, Whitehurst et al. (5) give 2.2% for the actual hydrogen consumption in the hydrogenolysis of asphaltols from a similar coal to benzene solubles under SRC liquefaction conditions.

In view of the large amount of experimental work involved, we have only studied one coal. One principal finding is that "unaccounted" oxygen, mostly ether, is removed much more rapidly in the early stages of liquefaction than other oxygen-containing groups, and a maximum amount of ether groups split has been estimated. It has been shown that hydrogenolysis of OH groups has an important effect on the solubility of liquefaction products. The quantitative, or semi-quantitative, aspects of these conclusions probably will not apply to other coals, but it seems likely that the qualitative identification of important phenomena will be relevant generally.

#### SUMMARY

A number of processes taking place during liquefaction are concurrent and, therefore, no mechanistic inferences can be made from simple relationships between generation of different classes of soluble materials and loss of coal functionalities, such as oxygen functional groups.

The amounts of ether oxygen being cleaved during the process are not larger than  $3.0 \pm 0.3$  ether oxygen linkages per 100 initial carbon atoms in the coal studied, and loss of "unaccounted" oxygen, assumed to be principally ether, increases linearly with conversion, as measured by pyridine solubility.

Blocking of hydroxyl oxygen with trimethylsilyl groups results in an increase in the benzene solubilities of pyridine-soluble materials. However, comparison of the rates of increase when hydroxyl groups are blocked with the rates when hydroxyl groups are removed during liquefaction leads to the inference that during liquefaction no more than 40% of benzene-soluble materials are generated from benzene-insoluble, pyridine-soluble materials by the mechanism of hydrogenolysis of oxygen functional groups.

#### ACKNOWLEDGEMENT

This work was supported by U.S. D.O.E. under Contract No. EX-76-C-01-2494, for which the authors wish to express their appreciation.

#### REFERENCES

1. C. H. Fisher and A. Eisner, Ind. Engng. Chem., 29, 1371 (1937). H. H. Storch, C. H. Fisher, C. O. Hawk and A. Eisner, Bureau of Mines TP 654 (1943).
2. Y. Takegami, S. Kajiyama and C. Tokokawa, FUEL (Lond.), 42, 291 (1963).

3. H. W. Sternberg, 172nd ACS Meeting, San Francisco, Aug. 1976, Fuel Chem. Div. Preprints Vol. 21, No. 7, 11.
4. B. S. Ignasiak and M. Gawlak, FUEL (Lond.), 56, 216 (1977).
5. D. D. Whitehurst, M. Farcasiu, T. O. Mitchell and J. S. Dickert, Jr., EPRI Report AF-480, July, 1977, "The Nature and Origin of Asphaltenes in Processed Coals".
6. D. C. Cronauer and R. G. Ruberto, EPRI Report AF-422, January, 1977, "Investigation of Mechanism of Reactions Involving Oxygen-Containing Compounds in Coal".
7. P. H. Given et al., Quarterly Progress Report to ERDA, FE-2494-2, "The Relation of Coal Characteristics to Coal Liquefaction Behavior", 1977.
8. J. Knotnerus, J. Inst. of Petrol., 42, 355 (1956).
9. L. Blom, L. Edelhausen and D. W. van Krevelen, FUEL (Lond.), 36, 135 (1957).

TABLE 1  
Elemental Analysis, PSOC-330, Middle Kittanning Seam, Pa.  
all data on dry mineral-containing basis

Mineral Matter	7.96%	Oxygen (direct)	9.03%*
Carbon	76.83%	Hydroxyl oxygen	3.8%
Hydrogen	4.97%	Carbonyl oxygen	1.2%
Nitrogen	1.71%	Vitrinite content	71.4%
Sulphur (organic)	0.67%	Pyridine solubility	13.2%
Oxygen (by difference)	7.86%	Pyritic sulphur	2.08%

\*not corrected for interferences by mineral matter.

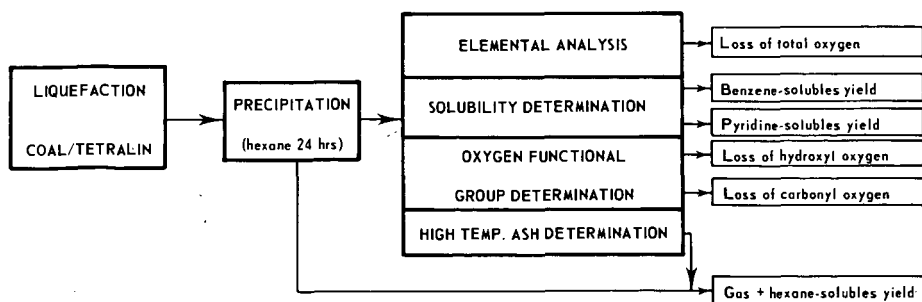


Fig. 1 PROCEDURE BLOCK DIAGRAM

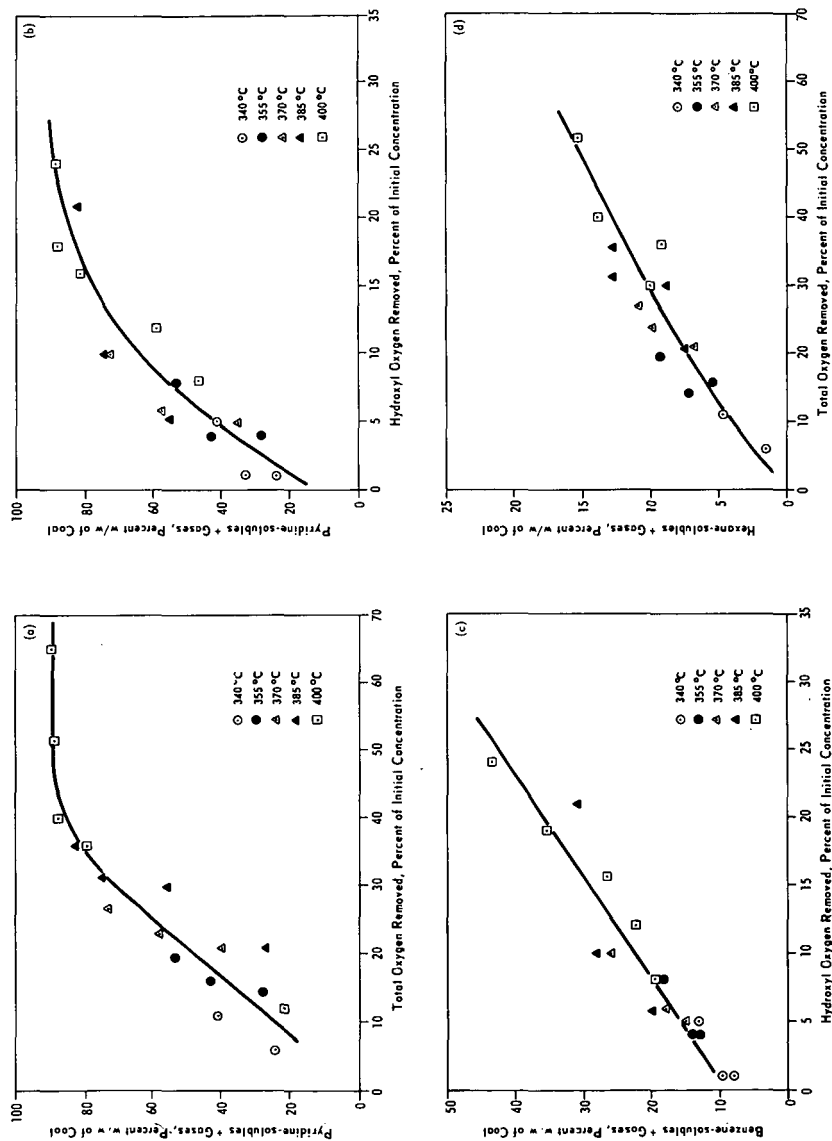


Fig. 2 RELATIONSHIPS BETWEEN GENERATION OF (a) PYRIDINE-SOLUBLE MATTER AND LOSS OF TOTAL OXYGEN, (b) PYRIDINE-SOLUBLE MATTER AND LOSS OF HYDROXYL OXYGEN, (c) BENZENE-SOLUBLE MATTER AND LOSS OF TOTAL OXYGEN, (d) HEXANE-SOLUBLE MATTER + GASES AND LOSS OF TOTAL OXYGEN, ALL ON DRY COAL BASIS

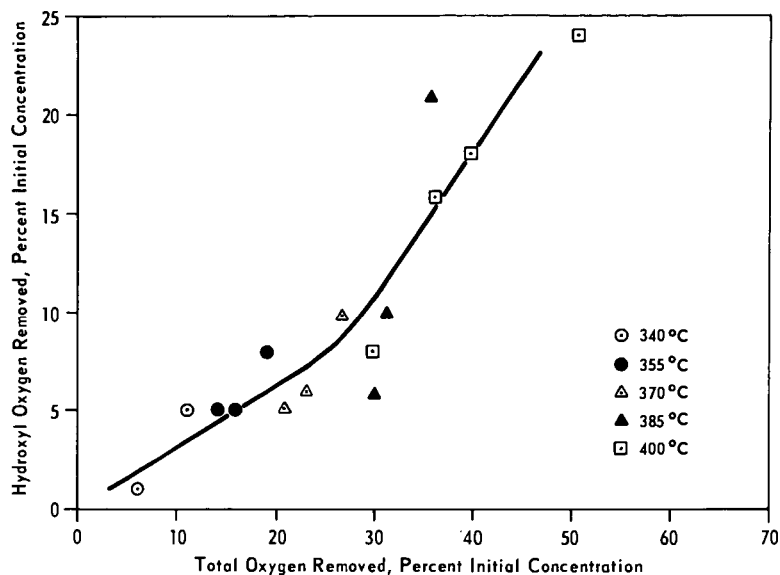


Fig. 3 RELATIONSHIP BETWEEN LOSS OF HYDROXYL OXYGEN AND TOTAL OXYGEN

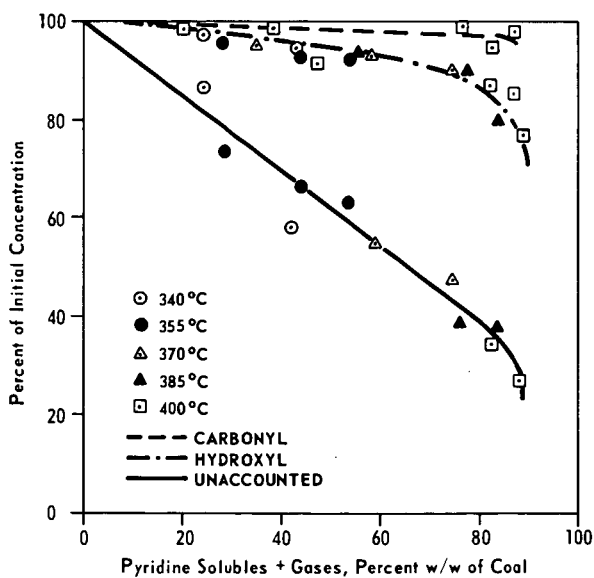


Fig. 4 LOSS OF OXYGEN FUNCTIONAL GROUPS VS GENERATION OF PYRIDINE SOLUBLE MATTER, DRY COAL BASIS

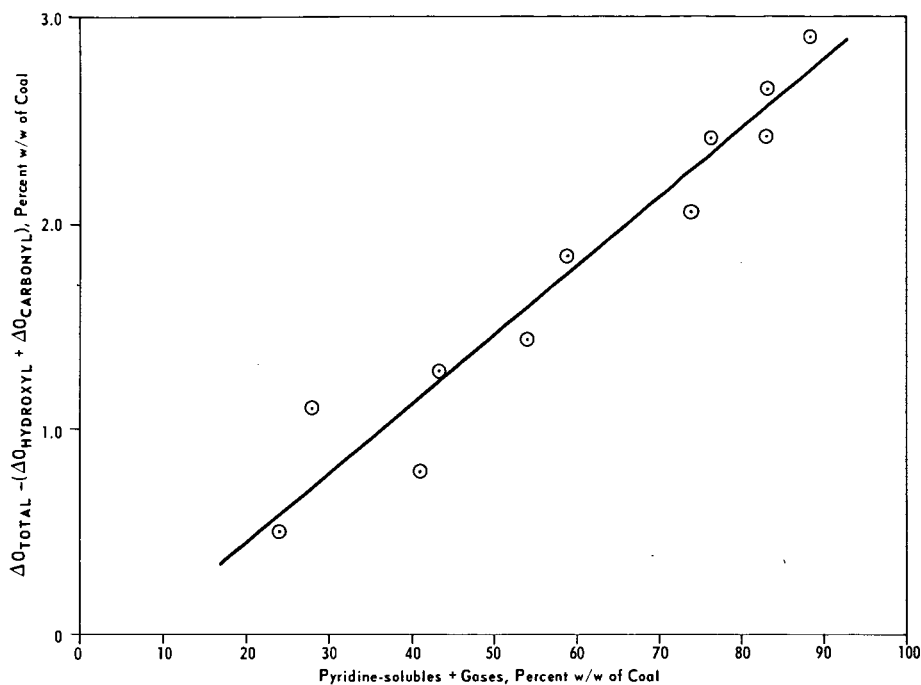


Fig. 5 RELATIONSHIP BETWEEN MAXIMUM ETHER OXYGEN CLEAVED AND GENERATION OF PYRIDINE SOLUBLES + GASES, PERCENT W/W OF COAL

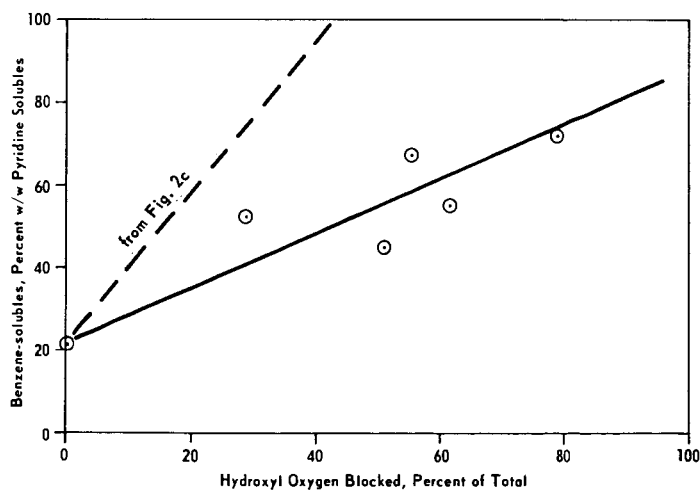


Fig. 6 EFFECT OF HYDROXYL HYDROGEN SUBSTITUTION ON BENZENE SOLUBILITIES

# THE KINETICS OF COAL LIQUEFACTION IN A HYDROGEN DONOR SOLVENT

BY: A. ATTAR

Department of Chemical Engineering  
University of Houston, Houston, Texas 77004

## 1. Introduction

One of the most important liquefaction processes involves the treatment of coal with hydrogen donors (HD). HD solvents are materials that can donate hydrogen at the reaction conditions. The industrially important HD's are those which can be regenerated with molecular hydrogen.

Quantitative data on liquefaction was published by Orchin (1944), Orchin and Storch (1948), Oele *et al.*, (1951), Curran *et al.*, (1966), Hill (1966) and Neavel (1976).

In hydrogen donor, liquefaction is believed to proceed by a free-radicals mechanism (Hill (1966), Curran *et al.*, (1966).) However, because of the complexity of the system coal-HD-ASH and catalyst, (when added), little quantitative work if any has been published on modeling coal liquefaction as a free radical depolymerization process. Several empirical models were published however, e.g., Curran *et al.* (1966), Hill (1966), Oele *et al.* (1951), Wen and Han (1975) and Yoshida *et al.* (1976).

The main objective of the present work is to present a fundamental approach to the modeling of coal liquefaction in hydrogen donors, which will permit predictions relevant to the processing of coals at different conditions. The discussion concentrates on liquefaction to heavy boiler fuel although it could be extended to modeling of liquefaction to gasoline.

## 2.1 Arguments of Material Balance

Conversion of coal to oils requires production of material with a smaller molecular weight and with a larger ratio of hydrogen to carbon. One hydrogen have to be added per each 3-6 carbon atoms in order to obtain the desired H/C ratio for boiler fuels.

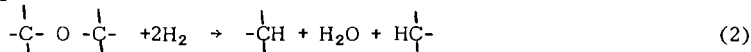
If it is assumed that on the average, each time a bond is broken, two fragments will be formed with approximately equal molecular weights, then each coal molecule will have to be broken 2-4 times to form heavy oil, or 3-6 times to form gasoline.

As an example, consider a "molecule" of bituminous coal with molecular weight of 3000 and ultimate composition of  $\text{CH}_{0.88} \text{O}_{0.132} \text{N}_{0.016} \text{S}_{0.0174}$  (MWU= 15.77). Each such coal molecule will have an average of 190 carbon atoms. Typical hydrogenation products may have ultimate composition of  $\text{CH}_{1.0} \text{O}_{0.09} \text{N}_{0.016} \text{S}_{0.016}$  (MWU= 14.34) and molecular weight of about 400, and will contain an average of 28 carbon atoms. Such product can be obtained if the original molecule is broken on the average 2.75 times and if 0.32-0.51 hydrogen atoms are added per each carbon atom in the original molecule.

Reduction in the molecular weight can be achieved by elimination of certain "side chained" functioned groups, e.g. OH, C=O, SH etc., or by breaking the HC structure of the main molecule, e.g., by reactions like:



or by



Elimination of side chains can result in a reduction in the molecular weight of the order of 16-32 units/group. Breaking of the main chain could result in a much more significant reduction in the molecular weight. The products of the latter reaction could have half the molecular weight of the original molecules. Opening of rings with or without the elimination of a heteroatom does not change significantly the molecular weight.

Most of the oxygen is present in coal in the form of hydroxylic (-OH) ketonic (C = O), and to a lesser extent heterocyclic or etheric (C-O-C) groups (Dryden (1963), (p. 267)). However, products with significantly reduced molecular weight result only when etheric oxygens or sulfidic sulfur are eliminated. Elimination of an OH group requires two hydrogen atoms but elimination of other groups requires four hydrogen atoms.

Data on the concentrations of etheric and sulfidic sulfur indicate that elimination of the etheric oxygen and the sulfidic sulfur could in some coals be sufficient to produce products with sufficiently low molecular weight. However, some saturation of  $\pi$  and c-c bonds is also required in order to bring the H/C ratio to the desired range. If each coal molecule has to be broken 2-6 times to produce heavy oil, then breaking of 1-3 etheric oxygen (if present) bonds and 2-3 sulfur-carbon or carbon-carbon bonds will result in product with M.W. in the range required for boiler fuel. When low volatile bituminous coal is processed breaking of c-c bonds may occur more than 2-3/ coal molecule.

## 2.2 Fundamental Assumptions

The most important assumptions of the present model are:

1. each coal consists of an assembly of functional groups or bonds with a given initial distribution which is specific to the particular coal.
2. the kinetic parameters, the activation energy and the frequency factor, for the reaction of each functional group with a given reagent, are function only of the reagent and the group, and are independent of the specific coal involved. Once such parameters are evaluated they can be used to model the kinetics of the reactions of similar groups in every coal.
3. the coal "molecules" are large and therefore have a small translational motion. The donor molecules and radicals are much smaller and much more mobile in the solution.
4. the bonds of each coal molecule break according to the hierarchy of the bond energies in each molecule, the weakest bonds first.
5. the depolymerization proceeds by a free radicals mechanism for which the steady state approximation can be applied.
6. the rate of the chemical reaction controls and not the rate of mass transport.
7. the solvent is present in a large excess.

Several additional assumptions are introduced latter which apply to specific cases.

### 3. Development of the Kinetic Model

A model is developed which describes the depolymerization in solution of a single high molecular weight compound. Classical chemistry of free radicals reactions is built into the model, and that permits to attribute physical significance to some of the reaction parameters. The rate of change of the average molecular weight of the solution is then discussed, and the model is extended to include the kinetics of the redistribution of the molecular weight of a system which initially contains compounds with different molecular weights.

#### 3.1 Chemistry of Free Radicals Depolymerization in a Hydrogen Donor

A free radicals reaction mechanism consists of three types of processes:

1. initiation reactions - which form more radicals than they consume.
2. propagation reactions - which do not affect the number of free radicals in the system.
3. termination reactions - which consume free radicals.

In the system coal-hydrogen-donor, initiation can proceed by various mechanisms, the most plausible ones are:

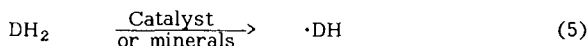
1. decomposition of very weak bonds in the coal macromolecule.



The radicals  $1n_1 \cdot$  react with the hydrogen donor,  $DH_2$ , and form the donor radical  $DH \cdot$

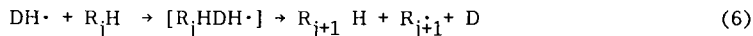


2. interaction between the hydrogen donor molecules,  $DH_2$ , and the mineral matter or catalysts.



The number of weak bonds that can initiate a chain of radicals per unit mass of coal is finite and probably small. Therefore, the rate of initiation, by the decomposition of bonds decreases during the course of an isothermal decomposition. However, since the solvent is usually in a large excess, the rate of initiation by the interaction of the solvent and heterogeneous inorganic minerals is approximately constant.

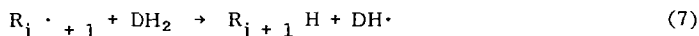
The radical  $\cdot DH$  can break carbon-carbon and carbon-oxygen bonds. In the process, the donor molecules are converted into dehydrogenated donor molecules, D. The coal molecules break into smaller molecular fragments; i.e:



This is a propagation reaction.

The index  $j$  is used to denote the number of times that the macromolecule has been broken prior to that reaction. All the molecules  $R_j H$  and the radicals  $R_j \cdot$  are large (M.W. 300-3000) and contain several aromatic rings. It is therefore plausible to assume that they are not very mobile in the solution. Moreover, it is reasonable to assume that the activated complex that is formed in reaction (6),  $[R_j HDH \cdot]$  dissociate at the weakest carbon-carbon or carbon-oxygen bond of the macromolecule. Therefore, the weakest bond in the  $R_{j+1} H$  product is stronger than that in the parent molecule,  $R_j H$ . In other words,

the decomposition of the original coal macromolecule,  $RoH$ , proceeds by the hierarchy of the strength of the bonds. The propagation step is completed by the fast reaction:



which replenishes the concentration of the radicals  $DH \cdot$ .

Since the radicals  $R_j \cdot$  are much more bulky than  $DH \cdot$ , they are less mobile. Therefore, it is reasonable to assume that the dominant termination reaction is:



We were not able to detect the dimer di-tetralin in studies on model compounds. Therefore, reaction (8) describes the dominant mode of termination.

### 3.2 Modeling of The Depolymerization of a Single Component Macromolecule

Let the initiation reactions proceed at a rate  $I = I(t)$ , and assume that the steady-state approximation can be applied. Then, the rate of initiation has to be equal to the rate of termination, since the propagation reactions do not change the total concentration of free radicals and because termination is assumed to occur predominantly by binary collisions of  $DH \cdot$ , then:

$$2k_t [DH \cdot]^2 = I \quad (9)$$

$$[DH \cdot] = \sqrt{\frac{I}{2k_t}} \quad (10)$$

The rate of change of the component  $R_j H$  is described by the equation:

$$\begin{aligned} \frac{d[R_j H]}{dt} &= k_{pj-1} [DH \cdot] [R_{j-1} H] - k_{pj} [DH \cdot] [R_j H] = \\ &= \sqrt{\frac{I}{2k_t}} (k_{pj-1} [R_{j-1} H] - k_{pj} [R_j H]) \end{aligned} \quad (11)$$

Denote:

$$\Pi_j = \frac{[R_j H]}{[R_0 H]_0} \quad (12)$$

$$d\theta = k_{po} \sqrt{\frac{I}{2k_t}} dt \quad (13)$$

Thus:

$$\frac{d\Pi_j}{d\theta} = \frac{k_{pj-1}}{k_{po}} \Pi_{j-1} - \frac{k_{pj}}{k_{po}} \Pi_j \quad \Pi_j = \beta_{j-1} \Pi_{j-1} - \beta_j \Pi_j \quad (14)$$

where:

$$\beta_j = \frac{k_{pj}}{k_{po}} \quad (15)$$

$$\text{Also: } \frac{d[R_0H]}{dt} = -k_{po} \frac{I}{2k_t} [R_0H] \quad (16)$$

$$\text{or: } \frac{d\bar{\Pi}_0}{d\theta} = -\bar{\Pi}_0 \quad (17)$$

$$\beta_0 = 1 \quad (18)$$

$$\text{Initially, } \bar{\Pi}_j = 0 \quad j > 0 \quad (19)$$

$$\bar{\Pi}_0 = 1 \quad j = 0 \quad (20)$$

Let us assume that an integration constant is chosen so that  $\theta(t=0) = 0$ . If the process is isothermal, then all the  $k$ 's are constant. Thus, it is possible to solve equation (15) by Laplace transform with respect to  $\theta$ :

$$m \bar{\Pi}_j = \beta_{j-1} \bar{\Pi}_{j-1} - \beta_j \bar{\Pi}_j \frac{\beta_{j-1}}{m+\beta_j} \quad (21)$$

$$\bar{\Pi}_j = \frac{\beta_{j-1}}{m+\beta_j} \bar{\Pi}_{j-1} = \bar{\Pi}_0 \prod_{j=1}^j \frac{\beta_{j-1}}{(m+\beta_j)} \quad (22)$$

$$\text{But: } \bar{\Pi}_0 = \frac{1}{1+m} \quad (23)$$

$$\text{Therefore: } \bar{\Pi}_j = \frac{1}{1+m} \prod_{j=1}^j \frac{\beta_{j-1}}{m+\beta_j} \quad (24)$$

The last equation has poles at every  $m = -\beta_j$ , and will therefore have slightly different solutions when all the  $\beta_j$  are distinct and different or when some of them are identical. The solutions for the case where all the  $\beta_j$ 's are different and for the case where all the  $\beta_j$ 's  $j \geq 1$  are the same as listed in tables 1 and 2.

Table 1: The Kinetics of Isothermal Coal Liquefaction by Successive Depolymerization in Hydrogen Donor Distinct and Different Rates for each Step\*

$$\begin{aligned} j & \quad \bar{\Pi}_j \\ 0 & \quad \bar{\Pi}_0 = e^{-\theta} \\ 1 & \quad \bar{\Pi}_1 = \frac{1}{1-\beta_1} (e^{-\beta_1\theta} - e^{-\theta}) \\ 2 & \quad \bar{\Pi}_2 = \beta_1 \left[ \frac{e^{-\theta}}{(\beta_1-1)(\beta_2-1)} + \frac{e^{-\beta_1\theta}}{(1-\beta_1)(\beta_2-\beta_1)} + \frac{e^{-\beta_2\theta}}{(1-\beta_2)(\beta_1-\beta_2)} \right] \\ 3 & \quad \bar{\Pi}_3 = \beta_1\beta_2 \left[ \frac{e^{-\theta}}{(\beta_1-1)(\beta_2-1)(\beta_3-1)} + \frac{e^{-\beta_1\theta}}{(1-\beta_1)(\beta_2-\beta_1)(\beta_3-\beta_1)} + \frac{e^{-\beta_2\theta}}{(1-\beta_2)(\beta_1-\beta_2)(\beta_3-\beta_2)} + \right. \end{aligned}$$

$$\begin{aligned}
& + \frac{e^{-\beta_3 \theta}}{(1-\beta_3)(\beta_1-\beta_3)(\beta_2-\beta_3)} \Bigg) \\
4 \quad \Pi_4 = & \beta_1 \beta_2 \beta_3 \left[ \frac{e^{-\theta}}{(\beta_1-1)(\beta_2-1)(\beta_3-1)(\beta_4-1)} + \frac{e^{-\beta_1 \theta}}{(1-\beta_1)(\beta_2-\beta_1)(\beta_3-\beta_1)(\beta_4-\beta_1)} + \right. \\
& \frac{e^{-\beta_2 \theta}}{(1-\beta_2)(\beta_1-\beta_2)(\beta_3-\beta_2)(\beta_4-\beta_2)} + \frac{e^{-\beta_3 \theta}}{(1-\beta_3)(\beta_1-\beta_3)(\beta_2-\beta_3)(\beta_4-\beta_3)} + \\
& \left. \frac{e^{-\beta_4 \theta}}{(1-\beta_4)(\beta_1-\beta_4)(\beta_2-\beta_4)(\beta_3-\beta_4)} \right] \\
& \text{etc.}
\end{aligned}$$

$$* \quad \beta_0=1, \quad \beta_j \neq \beta_i \quad i \neq j.$$

Table 2: The Kinetics of Isothermal Coal Liquefaction by  
Successive Depolymerization in Hydrogen Donor -

Initial Unique rate followed by steps with an identical rates\*

$$\begin{aligned}
j \quad & \Pi_j \\
0 \quad & \Pi_0 = e^{-\theta} \\
1 \quad & \Pi_1 = \frac{1}{1-\beta} (e^{-\beta \theta} - e^{-\theta}) \\
2 \quad & \Pi_2 = \frac{\beta}{(1-\beta)^2} e^{-\theta} + \beta e^{-\beta \theta} \left[ \frac{\theta}{(1-\beta)} - \frac{1}{(1-\beta)^2} \right] \\
3 \quad & \Pi_3 = \frac{\beta^2}{(1-\beta)^3} e^{-\theta} + \beta^2 e^{-\beta \theta} \left[ \frac{\theta^2}{2(1-\beta)} - \frac{\theta}{(1-\beta)^2} + \frac{1}{(1-\beta)^3} \right] \\
4 \quad & \Pi_4 = \frac{\beta^3}{(1-\beta)^4} e^{-\theta} + \beta^3 e^{-\beta \theta} \left[ \frac{\theta^3}{6(1-\beta)} - \frac{\theta^2}{2(1-\beta)^2} + \frac{\theta}{(1-\beta)^3} - \frac{1}{(1-\beta)^4} \right] \\
& \text{etc.}
\end{aligned}$$

$$* \quad \beta_0 \neq \beta_j \quad j > 0$$

$$\beta_j = \beta_1 = \beta \quad i, j > 0$$

### 3.3 Analysis of Models of the Initiation Reaction

Four models are proposed which describe various modes of initiations:

### 3.3.1 Decompositions of Unstable Bonds in the Coal:

It is assumed that initially a finite number of labile bonds exist per unit mass, and that these bonds decompose in a first order reaction.

$$I = - \frac{d[ln]}{dt} = 2k_i [ln] \quad (25)$$

Then, if the systems is isothermal:

$$[ln] = [ln]_0 e^{-2k_i t} \quad (26)$$

and:

$$d\theta = k_{po} \sqrt{\frac{I}{2k_t}} dt = k_{po} \sqrt{\frac{2[ln]_0 k_i}{2k_t}} e^{-k_i t} dt \quad (27)$$

$$\theta = \frac{k_{po}}{\sqrt{2k_t k_i}} \sqrt{2[ln]_0} (1 - e^{-k_i t}) \quad (28)$$

(Denoted as Model B)

### 3.3.2 Catalytic Interaction Between the Donor and Inorganic Materials:

When the minerals can catalyze the decomposition of the donor, the initiation rate constant will depend on the type of mineral matter, its surface area, quantity, and its porosity. The rate of initiation,  $I$ , will be more or less constant, since the concentration of donor and the mineral matter remains more or less constant. In such a case:

$$d\theta = k_{po} \frac{I_0}{2k_t} d\theta \quad (29)$$

and

$$\theta = k_{po} \frac{I_0}{2k_t} t \quad (30)$$

since  $\theta(t=0) = 0$  (Denoted as Model A)

### 3.3.3 Combination Models of Initiation:

In reality, initiation can occur both by decomposition of unstable bonds and by catalytic reactions. In such a case, the rate of initiation will have the former:

$$I = I_0 + k_i [ln]_0 e^{-k_i t} \quad (31)$$

and:

$$d\theta = k_{po} \sqrt{\frac{I}{2k_t}} dt = k_{po} \sqrt{\frac{I_0 + 2k_i [ln]_0 e^{-k_i t}}{2k_t}} dt \quad (32)$$

(Denoted as Model C)

$\theta(t=0) = 0$

When the coal contains more than one type of bond that can dissociate and initiate a chain, one obtains:

$$I = 2k_{i1} [1n]_{10} e^{-2k_{i1} t} + 2[1n]_{20} k_{i2} e^{-2k_{i2} t} \quad (33)$$

and:

$$d\theta = \sqrt{\frac{p_0}{2k_t}} (2k_{i1} [1n]_{10} e^{-k_{i2} t} + 2k_{i2} [1n]_{20} e^{-k_{i2} t})^{\frac{1}{2}} dt \quad (34)$$

and

$$\Theta(t=0) = 0 \quad (35)$$

(Denoted as Model D)

### 3.4 Modification of the Liquefaction Model to Real Coals

Extraction of coals with different solvents yield a given amount of the various fraction, e.g. asphaltenes, hexane solubles etc. If, it is assumed that the molecular weight and the functionality of these fractions are similar to that of the same fractions which are produced by the liquefaction of coal, then they will contribute to the rate of accumulation of the various fractions. To include these effects in the model, the dimensionless initial concentration of each group,  $\Pi_i^0$ , have to be taken into account. The equations that result are listed in Table 3. Note should be made that it has been assumed that each fraction depolymerize with a specific set of parameters which is a function only of the particular fraction. It could be shown (Attar, 1978) that fractions which are isolated by the "solvent soluble/insoluble" method should have molecular volume or weight and functionality in a given range. "Functionality" is defined in this context as the sum  $\sum F_i N_i$ , where  $N_i$  are the number of atoms of the i-th kind and  $F_i$  the energy parameter as described by Small (1953): Whithurst et. al., (1976) examined SRC fractions and noted that the molecular weight and composition of the various fractions is independent of the conversion, in accord with the semi-theoretical prediction of Attar (1978). Therefore, in the following text it will be assumed that each j group could be identified with a given "solvent soluble/insoluble" fraction.

Table 3: Kinetics of the Depolymerization of Coal

$$\Pi_j^0 \neq 0 \quad \beta_j \neq \beta_i, \quad i \neq j$$

$$j \quad \Pi_j$$

$$o \quad \Pi_0 = \Pi_0 e^{-\theta}$$

$$1 \quad \Pi_1 = \frac{\Pi_0^0}{1-\beta_1} (e^{-\beta_1 \theta} - e^{-\theta}) + \Pi_1^0 e^{-\beta_1 \theta}$$

$$2 \quad \Pi_2 = \beta_1 \Pi_0^0 \left\{ \frac{e^{-\theta}}{(\beta_1 - 1)(\beta_2 - 1)} + \frac{e^{-\beta_1 \theta}}{(1 - \beta_1)(\beta_2 - \beta_1)} + \frac{e^{-\beta_2 \theta}}{(1 - \beta_2)(\beta_1 - \beta_2)} \right\} + \frac{\Pi_1^0 \beta_1}{\beta_1 - \beta_2} (e^{-\beta_2 \theta} - e^{-\beta_1 \theta}) + \Pi_2^0 e^{-\beta_2 \theta}$$

$$\begin{aligned}
3 \quad \Pi_3 = & \beta_1 \beta_2 \Pi_0^0 \left\{ \frac{e^{-\theta}}{(\beta_1-1)(\beta_2-1)(\beta_3-1)} + \frac{e^{-\beta_1 \theta}}{(1-\beta_1)(\beta_2-\beta_1)(\beta_3-\beta_1)} + \right. \\
& \left. \frac{e^{-\beta_2 \theta}}{(1-\beta_2)(\beta_1-\beta_2)(\beta_3-\beta_2)} + \frac{e^{-\beta_3 \theta}}{(1-\beta_3)(\beta_1-\beta_3)(\beta_2-\beta_3)} \right\} + \\
& \Pi_1^0 \beta_2 \beta_3 \left\{ \frac{e^{-\beta_1 \theta}}{(\beta_2-\beta_1)(\beta_3-\beta_1)} + \frac{e^{-\beta_2 \theta}}{(\beta_1-\beta_2)(\beta_3-\beta_2)} + \frac{e^{-\beta_3 \theta}}{(\beta_1-\beta_3)(\beta_2-\beta_3)} \right\} + \\
& \frac{\Pi_2^0 \beta_3}{\beta_2-\beta_3} (e^{-\beta_3 \theta} - e^{-\beta_2 \theta}) + \Pi_3^0 e^{-\beta_3 \theta}
\end{aligned}$$

and so on.

#### 4. Estimation of Parameters

The parameters which are needed are divided into two groups:

1. parameters associated with the propagation -  $\beta_j$ ,  $j \geq 1$ .
2. parameters associated with the initiation and the termination

The kinetics parameters associated with the propagation reaction depend mainly on the structure of the molecules. The kinetic parameters associated with the initiation and the termination depend on the structure of the molecules and will have a different form which depends on which initiation mechanism is assumed.

##### 4.1 Estimation of the Propagation Parameters

The rate limiting step in the propagation is reaction (6)

The corresponding rate parameter is  $\beta_j$ :

$$\beta_j = \frac{k_{pj}}{k_{po}} = \frac{A_{pj} e^{-\frac{E_{pj}}{RT}}}{A_{po} e^{-\frac{E_{po}}{RT}}} = \frac{A_{pj}}{A_{po}} e^{-\frac{(E_{pj} - E_{po})}{RT}} \quad (36)$$

It is convenient to evaluate separately the values of  $A_{pj}/A_{po}$  and  $E_{pj}-E_{po}$ .

##### 4.1.1 Depolymerization of Analogue Bonds.

Application of the polanyi relation yield:

$$E_{pj} - E_{po} = \alpha(\Delta H_j - \Delta H_o) \quad (37)$$

If the absolute rate theory is applied to equation (36) and it is assumed that the activated complex is similar to the molecule  $R_jH$ , one obtains for the frequency factor

$$A_{po} = A_{pj} \approx \frac{kT}{hQ_{DH}} \quad (38)$$

The last equation shows that to a first order approximation the frequency factor is independent of  $j$ , therefore,:

$$\beta_j = e^{-\frac{\alpha(\Delta H_j - \Delta H_o)}{RT}} \quad (39)$$

#### 4.1.2 Depolymerization by the Hierarchy of the Functional Groups

Following the initial solubilization of the coal, the various functional groups will compete for the hydrogen donors radicals. However, if the heat of reaction of the depolymerization of a particular group is much smaller than that of the other groups it will be eliminated at a much larger rate than the others.

The functional groups which are believed to be present in coal in substantial concentrations can be arranged in the order of increasing stability toward an attack by a hydrogen donor radical. The author calculates that at the initial stages of the liquefaction etheric bonds are broken first and subsequently methelenic bridges are broken at the benzylic position along with sulfidic sulfur. Other groups like  $-OH$ ,  $C=O$  also react, but their elimination will not result in a major decrease in the molecular weight of large coal molecules. If the first bond that is broken is an etheric bond, the second will be either etheric or benzylic and the third, and subsequent bonds that are broken are benzylic bonds. Based on these arguments, the activation energies for breaking the various bonds will probably be  $j=0$ , 7.8 kcal/mole,  $j=1$ , 9.0 kcal/mole,  $j=2$ , 9.9 kcal/mole,  $j=3$ , 10.5 kcal/mole,  $j=4$ , 11.1 kcal/mole.

#### 4.2 Estimation of the Initiation and Termination Parameters

The rate of termination was assumed to be diffusion controlled and equal to  $2 \cdot 10^9$  lit/mole sec.

The parameters associated with different initiation models are different and can not be estimated by simple assumptions. Two types of parameters are needed: rate constants and initial concentrations. The values of the rate constants for the decomposition of specific bonds is independent of the coal used. However, different values of the initial concentrations are expected to be present in different coals.

The rates of initiation by the decomposition of weak bonds are determined by the thermodynamic bond-dissociation energy and entropy. If initiation occurs by the decomposition of bonds which become unstable around  $350^\circ C$ , for example:



The activation energy of such reactions will be about the same as the bond energy. For reaction (40),  $E_a \sim \Delta H \sim 76.4$  kcal/mole. at  $400^\circ C$ . Also,  $\Delta S \sim 41.57$  cal/mole $^\circ K$  and by  $\log k_o \sim 22.26$ . The rate constant for the decomposition at  $400^\circ C$  is  $2.87 \cdot 10^{-3} \text{ sec}^{-1}$ . Since the number of moles of such relatively weak bonds is finite, and depend on the aromaticity of the coal, the number of chains that could be initiated by such a mechanism is finite and depend on the aromaticity of the coal. For coals with an aromaticity of 0.84 and  $H/C \sim 0.757$  the concentration of such groups can not exceed  $8 \cdot 10^{-2}$  mole/mole carbon and will probably be no larger than  $3 \cdot 10^{-2}$  mole/mole

carbon. The concentration of such groups is in effect smaller since the solvent further dilutes the solution.

The value of the kinetic parameters which determine  $k_{po}$  is assumed to be  $E_{po} = 7.8$  kcal/mole  $A_{po} = 2.2 \cdot 10^7$  (lit./mole sec).

## 5. Results and Discussion of the Results

In order to apply the model one needs to have data on the initial condition of the coal and on the conditions of the reaction. The data needed on the initial condition of the coal are: 1. the ultimate analysis and the aromaticity. 2. the mineral content and composition; and 3. the distribution of oxygen and sulfur functional groups. Detailed accurate knowledge of the groups distribution is not necessary since the mathematical model lumps many molecules and reduces the sensitivity to the value of  $\beta_i$ . The data needed on the condition of the reaction are 1. the temperature, 2. the solvent, 3. the pressure and type of gas, and 4. the catalyst.

The concentration of etheric oxygen determine the kinetic parameters chosen for the first and possibly the second propagation step.

The temperature and the solvent determine the values of the rate constants and of the relative rate parameters  $\beta_i$ . The type of gas and its pressure determine whether solvent regeneration should be included in the model or not. The effect of hydrogen is more important when catalyst is present and/or when deep liquefaction is considered. The catalyst effects mainly the rate of initiation and in a sense, (its effect) is analogous to that of certain components of the mineral matter, e.g.  $FeS_2$  and  $FeS$ . Catalysts will permit the liquefaction process to continue after the labile bonds decomposed.

### 5.1 Case Study: Analysis of the Liquefaction of a Bituminous Coal

The coal is treated in this case study as a single macromolecule so that the relationships among the various fractions will be more clear. The data used are described in table 4. The results of applying the model are described in figures 1 and 2. Figure 1 shows the dimensionless amount of the various fractions in a batch operation, as a function of the dimensionless time parameter  $\theta$ . To obtain the dependence of  $\Pi_j$  on the real time  $t$ , use Figure 2 which shows the dependence of  $t$  on  $\theta$  for various initiation models. Figure 2 shows also the change in the dimensionless average molecular weight of the SRC as a function of time.

Acknowledgement: The author wishes to thank the U.S. DOE for its support of this work. (Grant No. EF-77-G-01-2735). The author is in debt to Mr. David Agar, to Mr. Steven Shen and to Mr. Glenn Swin for their help in the calculations.

Note: Because of space limitations, several sections of the manuscript, case studies and calculations have been removed. The complete paper will be published soon. The main sections that were omitted include the rate of desulfurization and deoxygenation, the change in the molecular weight, several case studies, and the references.

Table 4: Case Study: Liquefaction of a Medium  
Volatile Bituminous Coal in Tetralin at 427°C

Approximate initial ultimate analysis:

$C_{10}H_{0.88}O_{0.132}N_{0.016}S_{0.174}$

Ash: 14.7 wt.%

Pyritic Sulfur: 1.3 wt.%

j	Bond Broken	Initial Conc. of Fractions	Epj Kcal/mole	Apo lit/mole sec)
0	-O- very weak	100	7.8	$2.2 \cdot 10^7$
1	-O- weak	-	9.0	
2	$\phi$ -CH <sub>2</sub> CH <sub>2</sub> $\phi$	-	9.9	
3	$\phi$ -CH <sub>2</sub> - $\phi$	-	10.5	
4	$\phi$ -CH <sub>2</sub> - $\phi$	-	11.1	

Initiation and Termination Models:

$$I_0 = 8 \cdot 10^{-6}$$

$$I = I_0 + k_{i1} [lni]_0 e^{-k_{i1} t}$$

$$k_{i1} = k_{i10} e^{-\frac{E_{i1}}{RT}} =$$

$$[lni]_0 = 0.01$$

$$2k_t = 2 \cdot 10^9$$

$$k_{i10} = 2 \cdot 0 \cdot 10^{22} \text{ sec}^{-1}$$

$$E_{i10} = 76.4 \text{ kcal/mole.}$$

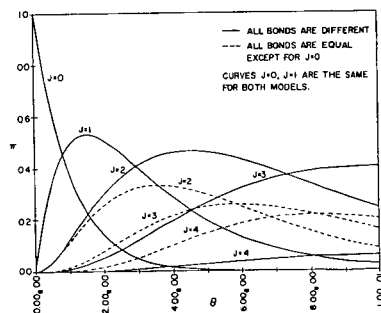
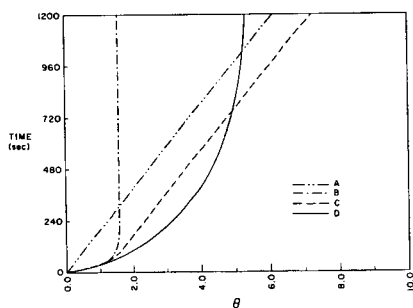


Figure 1: The Kinetics of Coal Liquefaction in  
Hydrogen Donor

Molecular Weight Distributions of Reductively  
Alkylated and Depolymerized Coals

J.W. Larsen, P. Choudhury<sup>1</sup> and L. Urban<sup>1</sup>

Department of Chemistry, University of Tennessee  
Knoxville, Tennessee 37916

and  
Oak Ridge National Laboratory\*, P.O. Box X  
Oak Ridge, Tennessee 37830

The intellectual starting point for this work is our belief that bituminous coals consist of largely aromatic "clusters" linked together by various bridges to form a three dimensionally cross-linked macromolecular network in which some extractable molecules are dissolved. The simplest way of making the coal soluble is to cleave enough bridges to destroy the network. Soluble fragments should result. By looking at the molecular weight distribution of these fragments produced by selectively cleaving bridges, the relative importance of the various types of bridges can be determined. Two well developed ways for accomplishing such cleavage are the well known Heredy-Neuworth depolymerization<sup>2</sup> and the Sternberg reductive alkylation,<sup>3</sup> which cleave methylene bridges and primarily ethers respectively. Their chemistry has been reviewed.<sup>4</sup> We will concentrate here on the Heredy-Neuworth depolymerization.

Figure 1 shows the results of depolymerizing Bruceton coal. The fraction soluble in benzene ethanol (70/30 v/v) is stable and passes through a 0.5  $\mu$  filter. The pyridine "solution" is stable, in that nothing precipitates on standing. However 6.8% of the "dissolved" material is removed by a 2.7  $\mu$  filter. The remaining solution will not pass a 0.5  $\mu$  filter. Ultracentrifugation of the pyridine "solution" (60,000 rpm; 3 hrs) results in precipitation of 40% of the pyridine solubles. Before centrifugation, the number average molecular weight ( $M_N$ ) of the pyridine "solubles" was 400, quite comparable with results reported by others.<sup>5</sup> After centrifugation,  $M_N$  was 1,000. The increase is due to the removal of colloidal material and the latter number is the true  $M_N$  for the dissolved material. Similar results have been obtained with a vitrinite sample (PSOC 126). As a result of these observations, all  $M_N$  values reported for products of Heredy-Neuworth depolymerization must be regarded as questionable and probably erroneous. We are currently determining whether the colloidal material emerges from the coal unchanged or whether it is a reaction product.

The molecular weight distribution measured for the benzene-ethanol soluble fraction of depolymerized Bruceton coal by gel permeation chromatography ( $\mu$ -Styragel columns 10<sup>5</sup>, 500, 100 A°, THF solvent) followed by vapor pressure osmometry of individual fractions is shown in Fig. 2. Several important points emerge. First, there must be association in THF as indicated by the higher  $M_N$  for the fraction in that solvent. Separation on the gpc columns is only partly on the basis of size. Finally, silylation of the depolymerized coal does not decrease its  $M_N$  in pyridine, apparently there is little association via hydrogen bonds involving CH groups in that solvent.

Acknowledgment. We thank the U.S. Department of Energy for support of this work.

\*Operated by Union Carbide Corporation under contract W-7405-eng-26 with the U.S. Department of Energy.

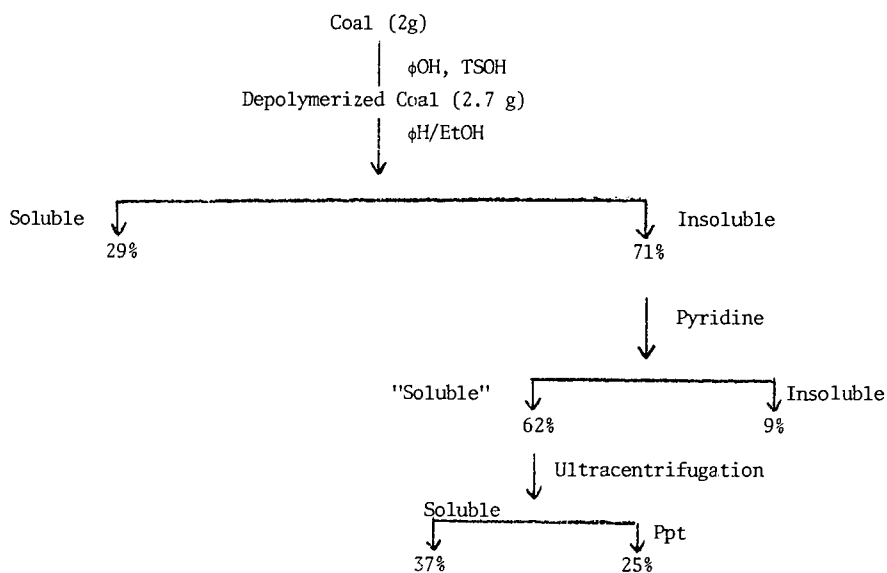
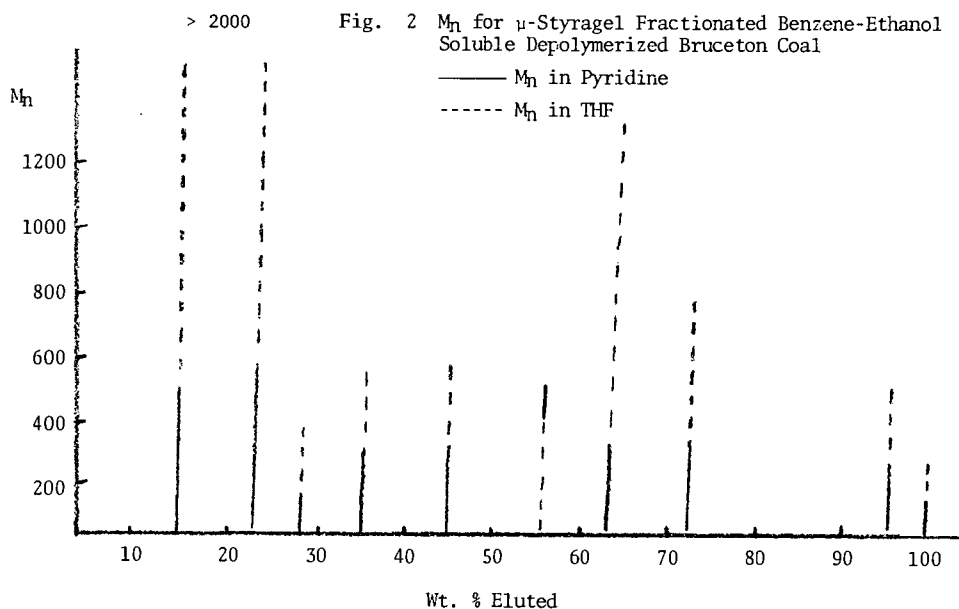


Fig. 1 Solvent Fractionation of Depolymerized Bruceton Coal



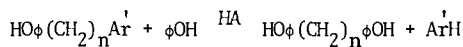
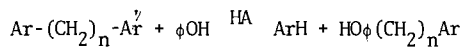


Figure 3. The Depolymerization Reaction

Coal	C (wt %, daf)	Alkylation technique	Solvent	Mol. wt.	Extract- ability (wt %)
W. Va. 1vb	90.6	HNO <sub>3</sub> -φOH/BF <sub>3</sub> -Ac <sub>2</sub> O	CHCl <sub>3</sub>	530	14
Clarian hvb	60.0	HNO <sub>3</sub> -φOH/BF <sub>3</sub> -Ac <sub>2</sub> O	CHCl <sub>3</sub>	1725	84
Ohio 8 Hvab	80.9	HNO <sub>3</sub> -φOH/BF <sub>3</sub> -Ac <sub>2</sub> O	CHCl <sub>3</sub>	645	95
McFarlane Hvcb	67.3	HNO <sub>3</sub> -φOH/BF <sub>3</sub> -Ac <sub>2</sub> O	CHCl <sub>3</sub>	375	96
Japanese	75.8	φOH/PTS	Pyridine	320	98
	78.0	φOH/PTS		340	100
	81.7	φOH/PTS		440	90
	81.9	φOH/PTS		450	96
	83.1	φOH/PTS		460	98
	84.6	φOH/PTS		500	92
	86.2	φOH/PTS		480	98
	89.6	φOH/PTS		1100	32
Lignite	71	φOH/BF <sub>3</sub>	φOH	300	21
			φH-MeOH	300	48
Sub-bituminous	77	φOH/BF <sub>3</sub>	φOH	350	2
			φH-MeOH	290	15
High-volatile vitrain	82	φOH/BF <sub>3</sub>	φOH	920	13.5
			φH-MeOH	525	25
High-volatile bituminous	85	φOH/BF <sub>3</sub>	φOH	930	7
			φH-MeOH	730	15
High-volatile bituminous	86	φOH/BF <sub>3</sub>	φOH	750	19
Low-volatile bituminous	91	φOH/BF <sub>3</sub>	φOH	360	5.4

Figure 4. Phenol Free Molecular Weights (Number Average) of Depolymerized Coals (From J.W. Larsen and E.W. Kuemmerle, Fuel, 55, 162 (1976)).

Figure 5. Molecular Weight Distribution of the True Pyridine Solubles After Centrifugation

Fraction No.	Wt. %	Cumulative Wt. %	$\bar{M}_N$
1	< 0.5		
2	14.7	14.7	> 3000
3	20.3	35.0	> 3000
4	15.2	50.2	> 3000
5	15.5	65.7	2960
6	12.8	78.5	2440
7	7.0	85.5	880
8	5.9	91.4	560
9	4.3	95.7	560
10	2.7	98.4	370
11	1.6	100.0	370

#### References

1. University of Tennessee.
2. L.A. Heredy and M.B. Neuworth, Fuel, 41, 221 (1962).
3. H.W. Sternberg, C.L. Delle Donne, P. Pantages, E.C. Moroni, and R.E. Markby, Fuel, 50, 432 (1971).
4. J.W. Larsen and H.W. Kuemmerle, Fuel, 55, 162 (1976).

# Characterization of Solvent Refined Coal by High Pressure Liquid Chromatography and other Analytical Techniques

C.D. Hathaway, C.W. Curtis, S. Meng, A.R. Tarrer, and J.A. Guin

Chemical Engineering Department  
Auburn University  
Auburn, Alabama 36830

Solvent Refined Coal (SRC) has previously been investigated by gel permeation chromatography (GPC)(1-3) and open column liquid chromatography (4,5). These studies have concentrated on comparison among various untreated coals and SRC's along with the determination of classes of chemical compounds present in SRC. In this paper the basic chemical nature of SRC is investigated, both on a molecular size basis and on a component basis.

By determining the basic chemical characteristics of SRC, important ground work can be laid for understanding the structure of SRC and for a fundamental understanding of the parent coal. Through knowledge of the molecular size distribution of SRC it may be possible to determine the process parameters which control the product composition. Knowledge of the chemical entities composing SRC, should make it possible to better structure the process so as to enhance product quality.

To provide a better understanding of the chemical makeup of SRC, this work presents an in-depth study of its chemical characteristics. SRC is analyzed at three different separation levels: 1) initially, the THF soluble portion of SRC is analyzed by GPC and the molecular size distribution is obtained; 2) GPC is used as a preanalysis step in which individual fractions are collected according to their elution time for subsequent detailed analysis; and 3) the SRC fractions are separated into component peaks or chromatographic bands by high pressure liquid chromatography (HPLC) and gas chromatography (GC).

## Experimental

### Materials Studied

Four SRC's, Amax, Western Kentucky 9/14, Monterey and Illinois #6, and their respective feed coals were obtained from the Wilsonville SRC Pilot Plant. The light recycle oil was obtained from Southern Services, Inc.

### Chromatographic Analyses

GPC and HPLC were performed on a Waters ALC/GPC 202 high pressure liquid chromatograph equipped with a differential refractometer and a Schoeffel Spectroflow SF 770 variable wavelength ultraviolet-visible detector. For dual wavelength analyses, an Altex Model 153 Analytical UV Detector was used with a 254 nm filter. All chromatographic solvents were prefiltered through a 0.2  $\mu$ m Fluoropore filter before use.

GPC was performed using three  $\mu$ -styragel columns, sizes 500 $\text{\AA}$ , 100 $\text{\AA}$ , 100 $\text{\AA}$ , in series with tetrahydrofuran (UV grade, Burdick and Jackson) as mobile phase. Injection volumes and effective concentrations for analytical separations and for preparative analysis were 10  $\mu$ l at 10 mg/ml and 100  $\mu$ l at 50 mg/ml, respectively. Polyethylene glycol standards of molecular weights 285-315, 380-415, 570-670, 950-1050 and 3000-3700 from Union Carbide, and various polynuclear aromatics were used as calibration standards.

HPLC was performed for each of the six fractions obtained from GPC analysis. Reverse phase chromatography was employed for fractions 5 and 6 using two  $\mu$ -Bondapak C<sub>18</sub> columns (30 cm long, 4 mm in diameter) with a mobile phase of equal volume portions of acetonitrile (nanograde, Mallinckrodt), 2-propanol (spectroquality, J.T. Baker) and water (glass-distilled). Ultraviolet detection, set at 254 nm and

0.1 AUFS, monitored the sample.

Fractions 1-4 were separated by normal phase chromatography employing a  $\mu$ -porasil column (30 cm in length and 4 mm diameter) and a two-component mobile phase of hexane and 2-propanol. Isocratic solvent systems ranging from 100% hexane to 75% hexane/25% 2-propanol were used to effect a separation.

Gas chromatographic analysis of fractions 5 and 6 was performed on a Varian Model 1800 GC equipped with a flame ionization detector (FID) with nitrogen as the carrier gas. A Varian Model 3700 GC equipped with a flame photometric detector (FPD) with helium as the carrier gas was used for sulfur compound analysis. In both analyses, temperature programming and a methyl phenyl silicon column (10 feet by 1/8 inch) were used.

#### Analytical Methods Used in Fractional Analysis

Elemental analysis was performed on a Perkin Elmer Model 240 Elemental Analyzer equipped with a Microbalance and a Model 31 Tektronix Calculator. Samples were prepared by open-air evaporation of the THF from each fractional residue.

Fluorescence spectroscopy was performed on a Farrand Mark I Fluorescence Spectrometer with a standard quartz sample cell. Sample preparation consisted of dissolving each fraction in THF at concentration levels ranging from 1 to 10 mg/ml.

Infrared spectroscopy for fractions 1-4 was performed on a Digilab FTS 10 System I Fourier Transform infrared spectrometer (FTIR) and fraction 5 on a Perkin-Elmer 621 infrared spectrometer. Fractions 1-4 were run as KBr pellets and fraction 5 as a thin film.

Mass spectral analysis was performed on approximately 100 mg of each fraction with a Dupont Model 21-491 Mass Spectrometer equipped for solid sampling.

Ultraviolet spectroscopy was performed on a Cary 17 UV/Vis Recording Spectrometer using a standard 1 cm path length quartz cell and UV grade THF as solvent.

#### Results and Discussion

In this study, GPC is used as a method for the characterization of four SRC's and their respective feed coals, as well as a means of preliminary separation for the SRC's. The molecular size distributions of the tetrahydrofuran soluble portion of Amax, Illinois #6, Western Kentucky 9/14 and Monterey SRC's as determined by GPC is shown in Figure 1. The molecular size distributions of Western Kentucky SRC and Monterey SRC have higher molecular weight distributions than those of Illinois #6 and Amax SRC.

A comparison of the molecular size distributions of the THF soluble portion of SRC to the THF soluble portion of the feed coals is also shown in Figure 1. A large difference in the relative solubility of SRC and the feed coal is observed (See Table 1). The differences in the molecular weight distributions of the coals and SRC's are portrayed by their initial and final elution times as shown in Table 2. Two SRC's, Amax and Illinois #6, and one coal, Amax, show substantial differences in elution time. Both SRC's are delayed in initial elution time and continue past the experimental elution time for the smallest aromatic compound, benzene. The final elution time of Amax coal is also delayed - 33.0 minutes - compared to approximately 30.0 minutes for the other coals. These increased elution times can be attributed to partial adsorption of the components on the  $\mu$ -styragel columns.

#### GPC Fractional Analysis

To analyze the chemical nature of solvent refined coal, the SRC must first be subdivided into smaller analyzable fractions. To accomplish this, the GPC eluent of Amax SRC was arbitrarily divided into six fractions. These fractions were collected at three minute intervals beginning at approximately 15.5 minutes, where the SRC eluent was first detected by the differential refractometer. The elution times of the Amax SRC fractions are compared in Figure 2 to the elution times of calibration standards and to known SRC asphaltene and oil fractions from Soxhlet extractions. The elution times from an autoclave reaction mixture, which most

closely approximates SRC process conditions, show that asphaltenes elute between 15.5 and 26.6 minutes and that the oil elutes between 23.6 and 32.2 minutes. Therefore, according to their elution times, Amax SRC GPC fractions 1-3 primarily consist of asphaltenes\*, fraction 4 is a combination of oil compounds and asphaltenes, and fractions 5 and 6 are primarily composed of the oil fraction consisting of small condensed ring systems. (6)

#### Mass Spectrometry

Each GPC fraction was analyzed by electron impact mass spectrometry. The largest m/e value obtained for each fraction as shown in Table 3 is essentially limited by the volatility of each fraction at the maximum probe temperature 3000°C. This fact is exemplified by the nearly equivalent m/e values obtained for Amax SRC and GPC fraction 5 - 579 and 580 respectively. Residues remained on the mass spectrometer probe from each fraction and SRC sample indicating that only a portion of each sample was analyzed. Since all of the fractions, including the two oil fractions 5 and 6, have high molecular weight compounds, the GPC fractions of Amax SRC cannot be easily correlated to a molecular weight separation.

The mass spectral fragmentation pattern of fractions 1 and 5 are shown in Figure 3. These fragmentation patterns clearly illustrate the substantial differences in the chemical compositions of the GPC fractions. The fragmentation pattern of fraction 1 has mass peaks covering the entire mass range while fraction 5 has an intense cluster of mass peaks resembling a Gaussian distribution between mass number 150 to 400. The fragmentation pattern of fraction 2 closely resembles that of fraction 1; whereas, the fragmentation pattern 4 is similar to fraction 5. The fragmentation patterns of fractions 3 and 6 are both weak and sparse. These fragmentation patterns give an indication of the compounds composing the fractions. Fractions 1 and 2 contain easily fragmented compounds - such as heteroatom-containing aromatics or substituted aromatics. The concentrated Gaussian distribution of mass peaks in fractions 4 and 5 appears to be a true distribution of the molecular ions of the compounds present in the fractions, suggesting that these fractions contain compounds which give strong parent peaks and which do not easily fragment such as polynuclear condensed ring aromatics.

#### Fluorescence and Ultraviolet Spectroscopy

The fluorescence emission spectra of fractions 3, 4, and 5 are shown in Figure 4. The apparent fluorescence maxima for the three fractions range from 434 nm to 450 nm and the fluorescence bandwidths at half-height range from 144 to 168 nm. These values correspond to the apparent wavelength maxima and bandwidths of various polynuclear aromatics and coals as described by Retcofsky (7). Retcofsky and co-workers have shown that the apparent fluorescence wavelength maxima for polynuclear aromatic compounds of three or more condensed rings range from 383 to 482 nm. Retcofsky reports that the pyridine extracts from 5 coals have an apparent wavelength maxima ranging from 390 to 455 nm (with four of the coals ranging from 440-455 nm) and have an apparent bandwidth at half-intensity between 120-140 nm. Comparison of the apparent emission maxima and bandwidth of the SRC fractions (see Figure 4) to the fluorescence of the coals and standard polynuclear compounds gives strong evidence that the types of compounds present in fractions 3, 4 and 5 are polynuclear aromatic compounds of three or more condensed rings.

Ultraviolet spectroscopy of the Amax SRC GPC fractions compared to Amax SRC (THF soluble portion) and recycle oil show (Figure 5) considerable variation in the band structure. The UV spectra of fraction 1 shows definite band structure at 217, 243, and 262 nm; fraction 2 has absorption bands at 218, 242 and 264 nm. Fractions 3, 4, 5 and 6 show no band structure. The absorption bands of Amax SRC - 217, 241 and 261 nm - are very similar to fractions 1 and 2. In contrast,

\* Preasphaltenes are not considered due to their insolubility in THF.

the numerous absorption bands of light recycle oil are shifted to longer wavelengths - 272, 278, 283, 285, 319 and 336 nm. This shift agrees with the fact that the oil is composed essentially of condensed polynuclear aromatic compounds of 2, 3, and 4 rings (6). The band structure in fractions 1 and 2 and Amax SRC is obviously due to a prominent functional group present in these samples but absent or in much lower concentration in the other GPC fractions and light recycle oil.

#### Elemental Analysis and Infrared Spectroscopy

Elemental analysis performed on each GPC fraction indicates considerable variation in the carbon and nitrogen percentages (see Table 4). Fractions 1-3 have a significantly lower carbon percentage than do fractions 4 and 5. In contrast, the percentage of nitrogen is definitely higher in fractions 1 and 2 as compared to fractions 4 and 5. The hydrogen values vary among the different fractions but not in any predictable fashion.

Infrared analysis of Amax GPC fractions 1-5 shows distinctive differences in the aliphatic band stretches,  $\text{CH}_2$  at  $2920\text{ cm}^{-1}$  and  $\text{CH}_3$  at  $2960\text{ cm}^{-1}$ , and the aromatic CH stretch at  $3000\text{--}3100\text{ cm}^{-1}$ . Table 5 shows the ratio of the aromatic C-H to the aliphatic  $\text{CH}_2$  stretch and the ratio of  $\text{CH}_3$  to  $\text{CH}_2$  stretch for the Amax GPC fractions. Information concerning the types of compounds present in these fractions can be obtained from the ratios of the band stretches. With increasing elution time, GPC fractions 1-5 show increased aromaticity. A substantial increase in the  $\text{CH}/\text{CH}_2$  ratio is seen in fraction 5. The  $\text{CH}_3/\text{CH}_2$  ratio increases in fractions 1-3 and levels off at fraction 4; however, fraction 5 shows a dramatic increase in the  $\text{CH}_3/\text{CH}_2$  ratio. These ratios along with the elemental analysis (see Table 4) give strong evidence that fractions 1 and 2 have either more heteroatoms or less aromatic compounds than do fractions 3, 4, and 5. Fractions 1 and 2 also have a greater percentage of methylene groups indicating that they have either longer hydrocarbon chains or more saturated cyclic groups in comparison to the other fractions. Fractions 3 and 4 have increased aromatic structure and shorter side-chains or fewer saturated cyclic compounds than 1 and 2. The large change in both the aromatic/ $\text{CH}_2$  and the  $\text{CH}_3/\text{CH}_2$  ratios show that fraction 5 is totally different from the other fractions. Fraction 5 is largely aromatic with more methyl than methylene groups.

#### HPLC and GC Chromatographic Analysis of GPC Fractions

The Amax SRC GPC fractions are further separated by HPLC and GC into their component species (fractions 5 and 6) or into chromatographic bands (fractions 1-4). Since the elution times of fractions 5 and 6 correspond to that of oil and since both 5 and 6 are soluble in the reverse phase solvents, reverse phase affinity mode separations are successfully used.

As shown in Figure 6a, fraction 6 is separated into 30 peaks - some only partially resolved - by reverse phase HPLC. Several peaks in fraction 6 have been tentatively identified by spiking; they are: naphthalene, phenanthrene, fluoranthene, and pyrene. GC analysis of fraction 6 shows one major peak, identified by spiking as pyrene. Several other peaks - phenanthrene, fluoranthene and dibenzothiophene - have been identified by spiking as shown in Figure 6b.

Reverse phase HPLC separates fraction 5 into 35 peaks (see Figure 6c). There are more peaks present in fraction 5 than in fraction 6. At the same total concentration level the UV absorption of the chromatographic peaks is much greater in 5 than in 6. The gas chromatogram of fraction 5 shown in Figure 6d shows three major peaks which have been identified by spiking as phenanthrene, fluoranthene and pyrene. Fourteen intermediate and minor peaks are also present. Two of these components - dibenzothiophene and chrysene - have been identified.

The components identified in fractions 5 and 6 are essentially all 2, 3, and 4 condensed ring polynuclear aromatic compounds with one heteroaromatic sulfur species. Many of the compounds present in fractions 5 and 6 are also present in recycle oil (8). The origin of some of these polynuclear aromatic compounds in the final SRC product

can be attributed to one of two sources: 1) these compounds may be residual recycle oil which is not completely distilled or 2) these compounds may be an integral portion of the SRC organic matrix.

Normal phase HPLC separations of fractions 1-4 have been attempted since reverse phase HPLC is totally unsuccessful due to the lack of solubility of fractions 1-4 in reverse phase solvents. Analytical separations of fractions 1-4 are difficult due to their insolubility in many solvents; however, some progress has been made as shown in Table 6. Under normal phase conditions with a mobile phase of hexane (95%) and 2-propanol (5%), no bands in fraction 1 and 2 elute before 20 column volumes. With the same solvent system fractions 3 and 4 show some resolution into peaks and chromatographic bands at  $k' < 20$ . When a more polar mobile phase is used - hexane (75%)/2-propanol (25%), all the components in fractions 3 and 4 elute as a single band while fractions 1 and 2 elute as two broad bands in less than four column volumes. Under both mobile phases, condensed ring standards - such as phenanthrene, anthracene, dibenzothiophene and rubrene - all elute at the void volume of the column. Considering the mobile phase necessary to effect a separation, fractions 1 and 2 appear to have a composition quite different from fractions 3 and 4. Fractions 1 and 2 appear to be composed of polar compounds or condensed ring systems with high molecular weights; while fractions 3 and 4 appear to be composed of more non-polar but high molecular weight compounds.

### Conclusions

GPC clearly shows that the molecular weight distribution of SRC is consistent with SRC being partially composed of oil and asphaltenes. The fractions, collected from the GPC elution of Amax SRC, are fairly well-defined: fractions 1-3 are composed of asphaltenes, fraction 4 is a combination of oil and asphaltenes, and fractions 5 and 6 are oil. The major constituents of fractions 5 and 6 have been identified as mainly three or four condensed ring polynuclear aromatics; fraction 6 contains primarily pyrene and fraction 5 contains three major components - phenanthrene, fluoranthene and pyrene. From the experimental evidence, fractions 1-4 can be characterized by their bonding type and chromatographic behavior. Fractions 1 and 2 appear to be somewhat polar, high molecular weight compounds dominated by chain structure possibly within an aromatic framework, while fractions 3 and 4 seem to be fairly high molecular weight but essentially non-polar compounds with a more prominent aromatic structure. Future HPLC work is planned to effect more complete separations of the components in fractions 1-4 for subsequent compound identification.

### References

1. H. M. Coleman, D. L. Wooton, H. C. Dorn, and J. T. Taylor, Anal. Chem., 49 (4), 533 (1977).
2. H. M. Coleman, D. F. Wooton, H. C. Dorn, and J. T. Taylor, J. Chrom., 123, 419 (1976).
3. D. T. Wooton, H. M. Coleman, J. T. Taylor, and H. C. Dorn, Fuel, 57 (1), 17 (1978).
4. M. Farcasiu, Fuel, 56 (1), 9 (1977).
5. M. Farcasiu, T. O. Mitchell, D. D. Whitehurst, Chemtech, 7 (11), 680 (1977).
6. J. W. Prather, A. R. Tarrer, J. A. Guin, D. R. Johnson, and W. C. Neely, Prepr., Div. Fuel Chem., Am. Chem. Soc., 21 (5), 144 (1976).
7. H. L. Retcofsky, T. J. Bendel and R. A. Friedel, Nature Physical Science, 240, 18 (1976).
8. J. A. Guin and A. R. Tarrer, U. S. Department of Energy Report No. FE-2454-1, November, 1977.

TABLE 1. Solubility of Amax SRC and Four Demineralized Feed Coals in Tetrahydrofuran

<u>Material</u>	<u>Percent Soluble in THF*</u>
Amax SRC	86.65
Amax Coal	8.75
Monterey Coal	5.02
Western Kentucky Coal	3.88
Illinois #6 Coal	1.60

\*Concentration level: 100 mg/ml

TABLE 2. Comparison of Elution Time for Solvent Refined Coals and their Feed Coals

	<u>Elution Time (minutes)</u>	
<u>SRC</u>	<u>Initial</u>	<u>Final</u>
Amax	24.40	46.75
Monterey	16.25	31.75
Illinois #6	21.90	43.25
Western Kentucky	15.50	29.75
<u>Feed Coals</u>		
Amax	15.75	33.00
Monterey	16.00	30.35
Illinois #6	15.90	30.48
Western Kentucky	15.00	28.75

TABLE 3. Highest Mass Spectral for Amax SRC Fractions and Amax SRC

<u>Fractions</u>	<u>m/e*</u>
1	650
2	640
3	370
4	680
5	580
6	658
Amax SRC	579
Asphaltenes (Amax Coal)	693

Probe temperature: 300°C  
Ionizing voltage: 1400 V

TABLE 4. Elemental Analysis of Amax GPC Fractions and Amax SRC

GPC Fractions	% C	% H	% N
1	81.25	5.24	1.69
2	79.12	5.80	1.38
3	80.30	6.26	1.68
4	82.98	4.40	1.27
5	84.55	6.58	0.75
Amax SRC (THF insoluble portion)	84.18	4.64	1.60
Amax SRC	86.07	5.17	1.52
Recycle Oil	89.22	8.44	0.85

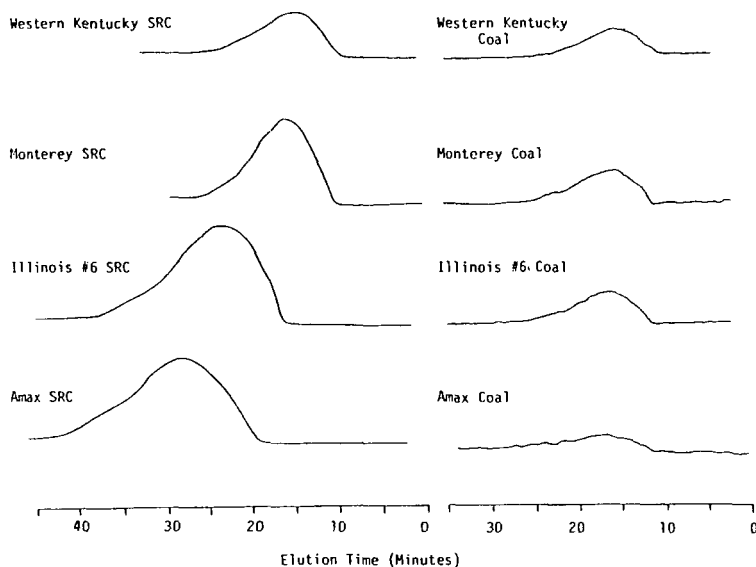
TABLE 5. Infrared Ratios of Amax SRC GPC Fractions

Fractions	Ratios	
	Aromatic/Aliphatic (CH/CH <sub>2</sub> )	Methyl/Methylene (CH <sub>3</sub> /CH <sub>2</sub> )
1	0.077	0.79
2	0.151	0.81
3	0.201	0.92
4	0.298	0.88
5	0.837	1.28

TABLE 6. Normal Phase HPLC Analysis of Fraction 1-4

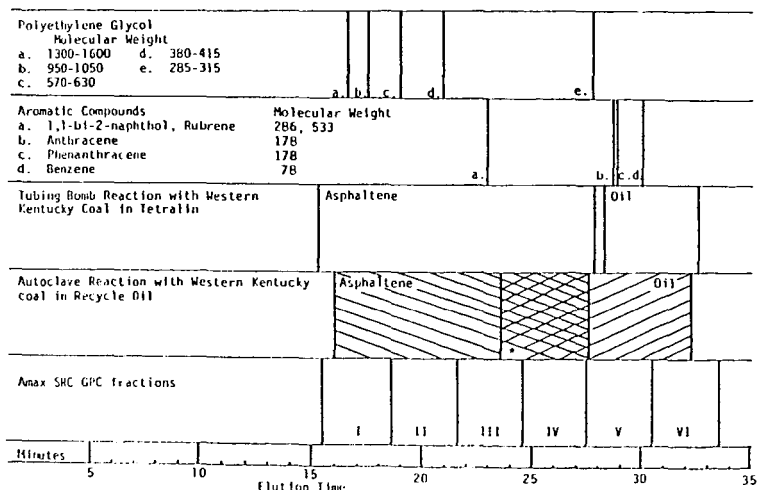
Fraction	Mobile Phase	
	Hexane (95%)/2-Propanol (5%)	Hexane (75%)/2-Propanol (25%)
1	No bands to $k' = 20$	Two broad bands, $1 < k' < 4$
2	No bands to $k' = 20$	Two broad bands, $0 = k' < 1.8$
3	13 peaks (poorly resolved) $k' < 20$	Single broad band, $k' = 0$
4	3 bands, $0 < k' < 1$	Single band, $k' = 0$

Figure 1. GPC<sup>a</sup> of the SRC's and the Feed Coals<sup>b</sup>



- a. UV detection at 300 nm  
b. Coals demineralized (ASTM)

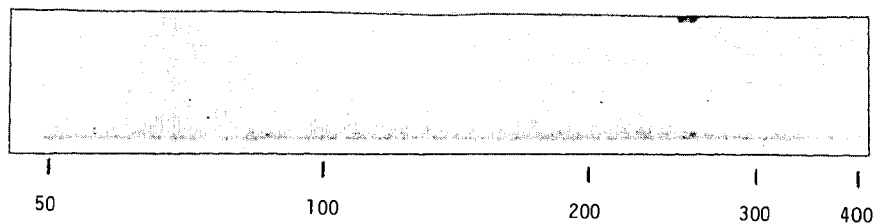
Figure 2. Comparison of the Elution Times of Amax SRC GPC Fractions to Known Standards



\*Overlapped peak includes both asphaltene and oil fractions.

Figure 3. Mass Spectra of Two Amax SRC  
GPC Fractions

Fraction 1



Fraction 5

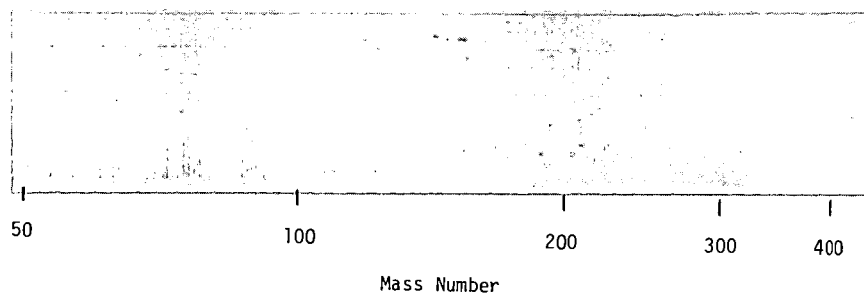
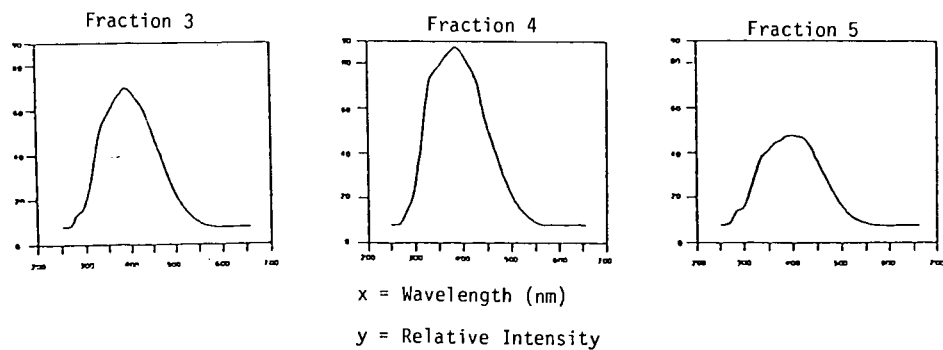


Figure 4. Fluorescence Spectra<sup>a</sup> of Three Amax SRC GPC Fractions



a) Uncorrected emission spectra

Figure 5. Ultraviolet Spectra of Amax SRC,  
Light Recycle Oil and Amax SRC  
GPC Fractions

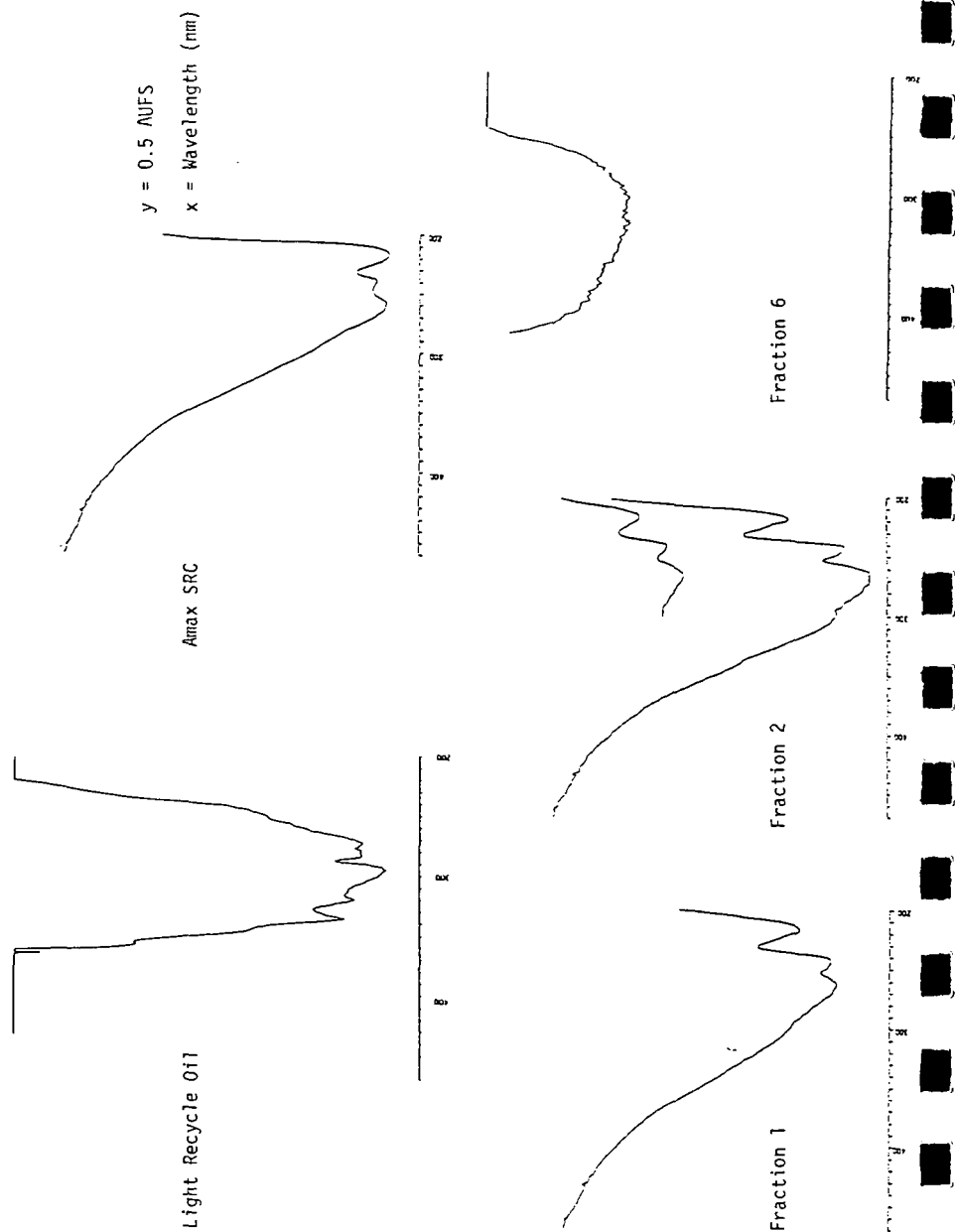
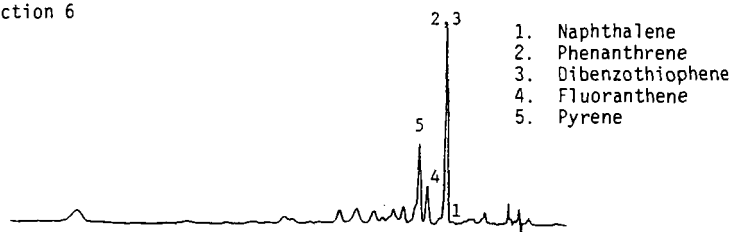
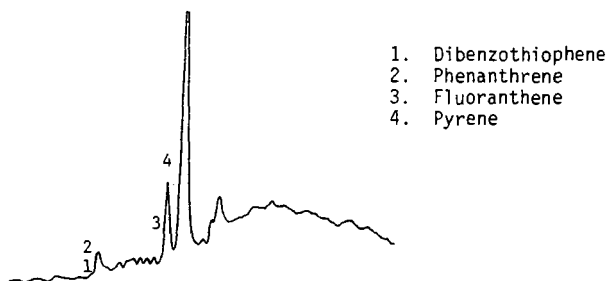


Figure 6. Liquid and Gas Chromatograms of Fractions 5 and 6

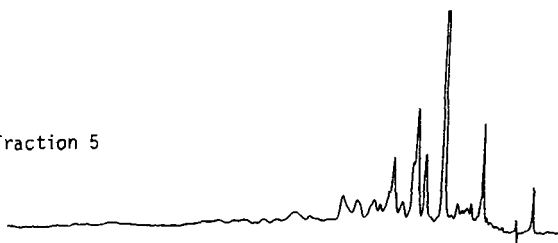
a) HPLC of Fraction 6



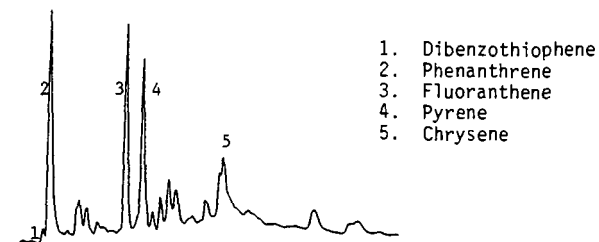
b) GC of Fraction 6



c) HPLC of Fraction 5



d) GC of Fraction 5



Chemistry of Texas Lignite  
Liquefaction in a Hydrogen-Donor  
Solvent System

C. V. Philip and Rayford G. Anthony

Department of Chemical Engineering  
Texas A&M University  
College Station, Texas 77843

INTRODUCTION

Lignite can be converted to clean fuels and chemicals by reacting it with hydrogen in the presence or absence of a hydrogen donor solvent. The polymeric organic constituents of the lignite are cleaved pyrolytically to produce gases and liquids. The ratio of gas to liquid which is produced depends on the temperature, pressure, presence and type of solvent, the use of hydrogen and whether dry or wet lignite is used. The complexity of the liquid product is a function of the severity of the degree of processing.

Alkalies and oxidizing agents have been used (1) to study the structure of different types of coals at mild processing conditions. The use of milder reaction conditions minimizes reactions between coal-derived products, which produce a complex mixture whose components have little resemblance to the original lattice structure of the coal (2). While this approach can be used to reveal the structure of certain predominant moieties in coal, these reagents fail to completely depolymerize the coal. The products may also react with each other even though the process conditions are mild.

The reaction of lignite at temperatures less than 750°F in the presence of hydrogen and tetralin produces a liquid mixture containing a substantial fraction of aliphatic compounds. The chemical nature of the products released from the lignite into the tetralin phase, their structural relationship to lignite, and a procedure for characterizing the reaction products are discussed in this paper.

EXPERIMENTAL

Freshly mined lignite is ground, sieved through a 10 mesh net and used immediately to avoid moisture loss and air oxidation. Technical grade tetralin is used as the hydrogen donor solvent. The reaction vessel is a 300 cc autoclave without the stirrer assembly. Eighty grams of lignite slurried in 60 grams of tetralin is the normal charge to the autoclave. The reactor is flushed of any traces of oxygen and finally hydrogen or helium is added at room temperature to a pressure of approximately 1200 psi. It takes about 30 minutes to heat the reactor with the charge to 700°F. Both gas and liquid samples are collected through the sampling valves during the course of the reaction. At the end of the reaction the reactor is cooled and the pressure is released. Reaction conditions are reported in Table 1.

The products consist of a tetralin-rich liquid phase, a residue saturated with the tetralin-rich liquid, and a water-rich phase. The tetralin-rich phase contains liquid components derived from the lignite which are soluble in tetralin and components which result from dehydrogenation of tetralin due to hydrogen transfer. The saturated residue contains components in the tetralin and water phases, components insoluble in tetralin and water, mineral matter and unreacted lignite. The tetralin-rich liquid is analyzed by use of gel permeation chromatography (GPC) and gas chromatography (GC). The saturated residue is extracted with tetrahydrofuran (THF) by use of a soxhlet extractor. The extract is concentrated in a rotary evaporator to give a solution containing approximately 50% THF and 50% extract. The extract, therefore, contains the same components present in the tetralin-rich phase as well as components

which are insoluble in tetralin. The extract plus THF were then analyzed by use of GPC and GC. The water-rich phase was not analyzed.

The GPC separations were done on a Waters Associate Model ALC/GPC 202 Liquid Chromatograph equipped with a refractometer (Model R 401) and a UV detector. A valve injector is used to load the column with the sample. Generally a 200 $\mu$ l of undiluted sample was used. Two 100 Å  $\mu$ Styragel columns (7.8 mm id X 300mm) were used through out the work. Reagent grade THF which had been distilled after refluxing over sodium wire to ensure that it is completely dry and devoid of any peroxide inhibitor, is used as the GPC solvent. THF was stored under dry nitrogen and all the separations were conducted in an anaerobic atmosphere to prevent the formation of peroxides. The tetralin-rich phase and extract were separated into three fractions as shown in Figure 1. Fraction 1 contains mostly colloidal carbon and some high molecular weight species. Fraction 2 was carefully evaporated to remove THF from the lignite-derived product. The product was then analyzed by GC and by GC-MS (3,4). Fraction 3 contains tetralin, tetralin-derived species and low molecular weight species derived from the lignite. Fraction 3 is collected and analyzed by use of GC which separates the low molecular weight species, tetralin and tetralin-derived products.

The gas samples were analyzed by use of a five column, three valve, automated gas chromatograph which is dedicated for gas analysis. The system is composed of a Carle GC and a Hewlett Packard 3385A automation system.

#### RESULTS AND DISCUSSION

When tetralin is used as the solvent in the liquefaction of lignite, most of the lignite-derived products are soluble in the tetralin-rich (liquid) phase. GPC can be used to separate the major constituents into three fractions. Figure 1 shows the separation obtained when 200 $\mu$ l of the liquid product are injected into the GPC. The first fraction is composed of species with boiling points greater than 500°C as well as colloidal carbon. This fraction can be collected and analyzed by use of NMR. Since most of the high molecular weight species have a limited solubility in the solvent system composed of tetralin and tetralin-derived products, fraction 1 represents only a small portion of the lignite-derived products. For all practical purposes fraction 2 represents the bulk of the lignite-derived products. Figure 3 shows the separation of the second fraction obtained by GC. Most of the components are identified by GC-MS and listed in Table 2 in the order that they appear in the chromatogram shown in Figure 3. The third fraction in Figure 1 is composed of low molecular weight lignite-derived products, tetralin, naphthalene, decalin and dihydronaphthlene. A gas chromatogram of this fraction is shown in Figure 2.

Comparison of the gas chromatograms shown in Figures 2 and 3 of fractions 2 and 3 reveals the success of the GPC separation of the lignite-derived products from the solvent and its reaction products. The amount of tetralin and tetralin-derived products in fraction 2 is insignificant. The lignite-derived products with boiling points close to the boiling point of tetralin, as well as, compounds of molecular size and weight comparable to that of tetralin are concentrated in fraction 2. The lignite-derived products are concentrated in fraction 2 because, (1) aliphatic compounds of comparable molecular weight are larger in molecular size relative to tetralin, and (2) the polar compounds hydrogen bond with the GPC solvent, tetrahydrofuran, which increases their effective molecular size relative to tetralin. Those products which appear in fraction 3 are readily separated by gas chromatography as shown in Figure 2.

Since the lignite-derived products are concentrated in fraction 2, GPC can be used to monitor the rate of liquefaction of lignite. Figure 4a-d illustrate gel permeation chromatograms of reaction samples which were collected at different time intervals during a liquefaction experiment. The GPC area representing fraction 2 increases with the reaction time. As more lignite-derived products are produced the peak resolutions between fractions 1 and 2 are lost due to overloading the column with a 200 $\mu$ l undiluted liquid sample. However, the areas due to fractions 1 and 3 do

not change. The formation of peaks in fraction 3 is due to a nonlinearity in the refractivity due to the concentration of tetralin in THF. The linearity of the area due to fraction 2 with an increase in lignite derived concentration is checked by obtaining GPCs of samples diluted with tetralin and with THF. The samples diluted with tetralin yielded chromatograms which show separations similar to Figure 4a. The sample diluted with THF yielded the same pattern for fraction 2 but, also, yielded a single narrow peak for fraction 3. The area due to fraction 1 decreases in direct proportion to the extent of dilution. The product collected in fraction 1, therefore, does not necessarily increase with the reaction time or the extent of liquefaction.

Monitoring the rate and extent of liquefaction by analyzing the tetralin-rich phase by GPC is based on the following assumptions: (1) The tetralin phase has a homogeneous composition throughout the system (i.e. the tetralin-rich phase inside the porous structure of unreacted lignite is the same as that in the bulk phase.) (2) The tetralin does not bind with the lignite lattice to create a solvent system with different solubility functions. (3) The majority of the lignite-derived products are dissolved in the tetralin-rich phase. Some polar compounds will dissolve in the water-rich phase and others may be only partially soluble in the tetralin and water phases. To determine the difference in the composition of the tetralin-rich phase and the components contained in the porous structure of the unreacted lignite, the products collected by extracting the saturated residue with THF were separated by GPC and fraction 2 was analyzed by GC. The products obtained are shown in Figure 5. The components contained in fraction 2 from the tetralin-rich liquid phase are shown in Figure 6. The relative peaks of the two gas chromatograms indicate the difference in concentration of the lignite-derived products in the tetralin-rich phase and the residue phase. The relative peak heights of the nonpolar compounds in the chromatograms are the same, therefore, the analysis of the tetralin phase may be used to estimate the extent of liquefaction with respect to the nonpolar components.

The liquid products produced due to primary reactions between lignite and tetralin may undergo further chemical rearrangement. To determine the extent of secondary reactions, the lignite-derived products were analyzed by GPC and GC after a reaction time of 7 hours. The gas chromatogram of fraction 2 from the GPC is shown in Figure 7.

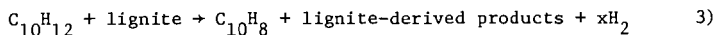
The relative intensity of the alkane peaks in Figures 5, 6, and 7 are similar. Since the product distribution of the lignite-derived liquid does not change for reaction times ranging from a few minutes to several hours, it appears that the alkanes and most of the major components do not rearrange or undergo secondary reactions after they are released from the lignite lattice. Careful examination of the smaller nonalkane peaks reveals that a few of the minor components have had a change in relative peak heights and hence concentrations. These components are undoubtedly participating in secondary reactions.

Some gas production always occurs in the liquefaction of lignite. The composition of the gas phase as a function of reaction time is presented in Table 3. The concentration of carbon dioxide reaches a maximum value after a reaction time of approximately one hour and then slowly decreases. The concentration of hydrogen sulfide follows a similar pattern. The concentration of carbon monoxide is essentially constant during the entire reaction. Production rate of methane decreases after an initial surge and the production rate of hydrogen appears to be constant. Since the hydrogen production rate and CO concentrations are constant it appears that the following reactions are not major pathways for the production of CO<sub>2</sub>, CO and H<sub>2</sub>.



Tetralin acts as a hydrogen donor and as a solvent for the products released

from lignite i.e.



Pyrolysis and direct hydrogenation can also, cleave the lignite lattice to produce the products listed in Table 2 (3,4,5). The conversion of tetralin to naphthalene as a function of time is illustrated in Figure 8 by plotting the ratio of naphthalene to tetralin as a function of reaction time. The extent of this conversion is directly related to the amount of lignite-derived product obtained in fraction 2 from the GPC.

The dehydrogenation of tetralin to naphthalene appears to be independent of the gaseous atmosphere in the system. Even when hydrogen is initially in the system, the hydrogen required for liquefaction is provided by the tetralin.

#### CONCLUSIONS

The conditions used in these experiments were mild enough to prevent both excessive gas production due to high temperature pyrolysis and chemical rearrangement of products released during the liquefaction process. Since the possibility of the water gas reaction is excluded, the production of carbon dioxide is due to the carboxylic acid groups present in the lignite lattice and alkanes constitute the bulk of the lignite liquefaction products. The alkanes can be produced from lignite by pyrolysis, by pyrolytic hydrogenation using hydrogen or hydrogen donor solvents at the same temperatures and pressures.

Although pyrolysis gives the smallest yield and the hydrogen donor solvent system gives the largest yield, the relative composition of alkanes is essentially constant. The lignite lattice contains alkane chains in varying lengths and they are released during liquefaction without fragmentation. The other major products listed in Table 2 are alkylated aromatics, alkylated indanes and alkylated phenols. Some of these products undergo secondary chemical rearrangements during prolonged reaction times. Lignite is one of the youngest members of the coal family and still contains intact some of the original plant structural skeleton. Formation of these lignite structural constituents from wood lignin can be easily envisioned.

#### ACKNOWLEDGMENTS

The financial support of the Texas Engineering Experiment Station, the Texas A&M University Center for Energy and Mineral Resources, and Dow Chemical Co., Freeport, Texas is very much appreciated. The lignite was furnished by Alcoa at Rockdale, Texas and by Dow Chemical Co.

#### REFERENCES

1. F. R. Mayo, "The Chemistry of Coal Liquefaction" Preprints ACS Fuel Div., 22 No. 5, 103, Chicago (Aug. 1977).
2. R. Hayatsu, R. E. Winans, R. G. Scott, L. P. Moore, and M. Studier, "Oxidative Degradation Studies of Coal and Solvent Refined Coal" Preprints ACS Fuel Div., 22 No. 5, 156, Chicago (Aug. 1977).
3. C. V. Philip and R. G. Anthony, "Characterization of Liquids and Gases Obtained by Hydrogenating Lumps of Texas Lignite" Preprints ACS Fuel Div., 22 No. 5, 31, Chicago, (Aug. 1977).
4. C. V. Philip and R. G. Anthony, "Hydrogenation of Texas Lignite" TEES Publications, Tech Bn., 78-2, 10(1978).
5. C. V. Philip and R. G. Anthony, "Organic Chemistry of Coal," ACS Symposium Series, In Press.

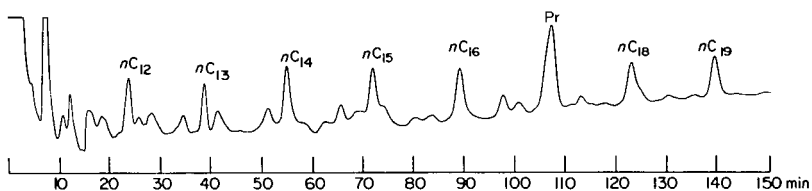
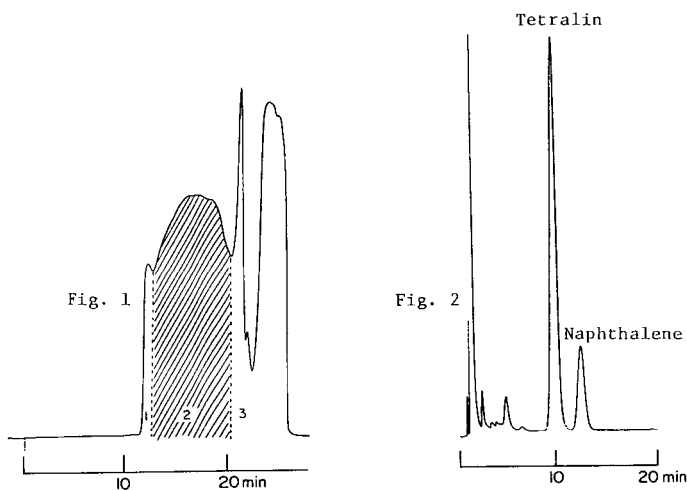


Fig. 3

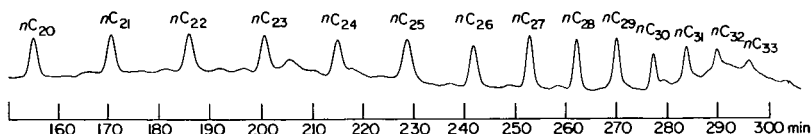


Figure 1. GPC separation of products in the tetralin-rich phase. 1. Colloidal carbon and high molecular weight species; 2. lignite-derived products; 3. tetralin and naphthalene and low molecular weight species.

Figure 2. Gas chromatogram of fraction 3 on a 10% SP2250 on 100/120 supelcoport, 1/4" id x 3'SS: column at 160°C isothermal.

Figure 3. Gas chromatogram of fraction 2 on a 10% SP2100 on 100/120 supelcoport 1/4" x 8'SS; temperature program: 80 - 270°C at 0.5°/min. The peaks were identified by GC-MS and are listed in Table 2.

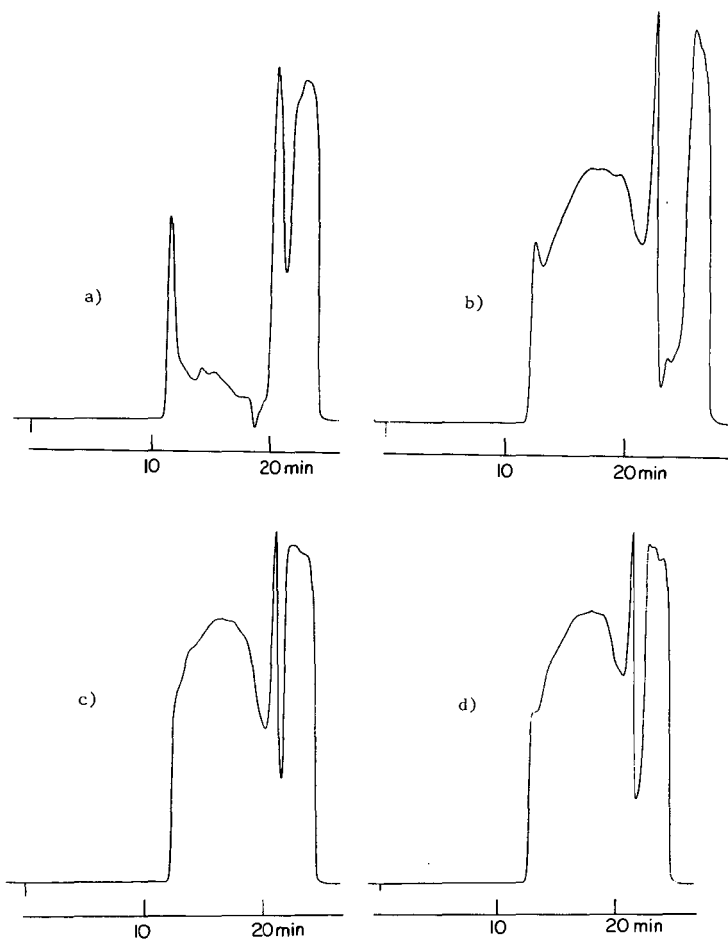


Figure 4. Gel permeation chromatograms of 200 $\mu$ l samples of tetralin-rich phase from run #56 (reaction conditions are listed in Table 1) at reaction times of a) 1 hr. b) 1 1/2 hrs. c) 2 hrs. and d) 7 hrs.

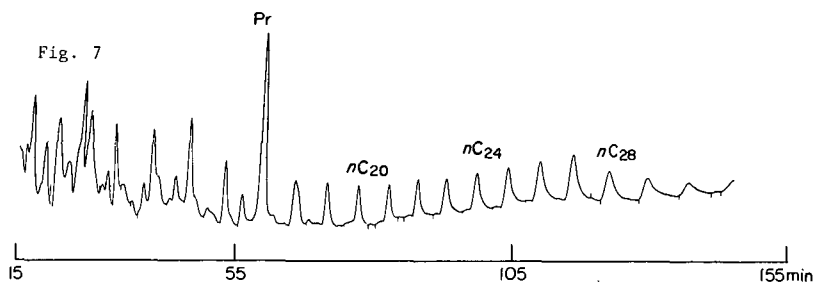
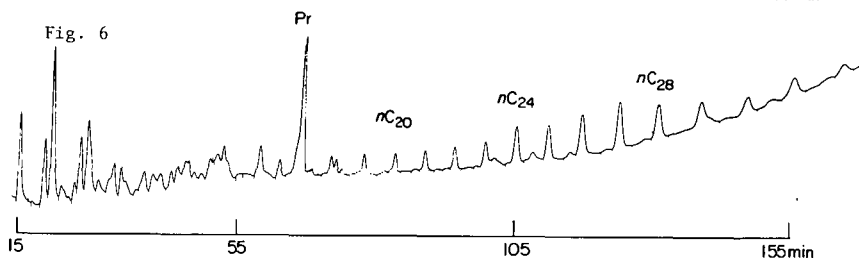
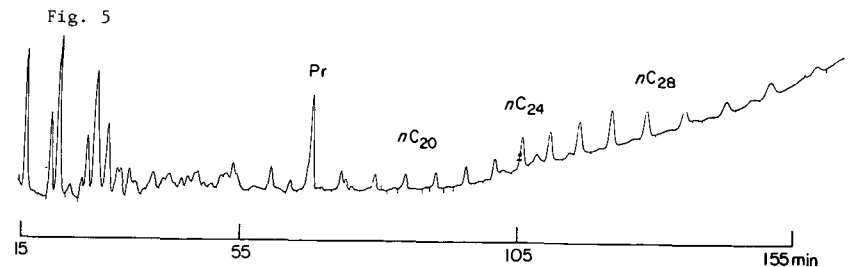


Figure 5. Gas chromatogram of the GPC fraction 2 of the extract of lignite derived products after 2 hrs. of reaction. GC conditions are the same as in Figure 2 except the temperature program of 80 - 250°C was 1.5°C/min. For peak identification, see Table 2.

Figure 6. Gas chromatogram of the GPC fraction 2 of the tetralin-rich phase after 2 hrs. of reaction. Figure 5 GC conditions. For peak identification see Table 2.

Figure 7. Gas chromatogram of the GPC fraction 2 of the tetralin-rich phase after 7 hrs. of reaction. GC conditions are the same as in Figure 5.

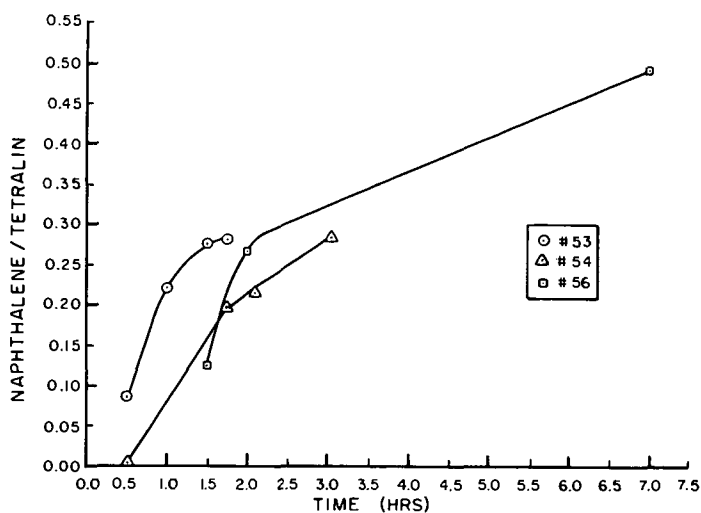


Fig. 8. Naphthalene to tetralin ratio in the tetralin-rich phase during lignite liquefaction process as a function of time.

Table 1. Reaction Conditions of Liquefaction Experiments

No.	Lignite (grams)	Gas	Tetralin (grams)	Initial Pressure (psig)	Max. Pressure (psig)	Reaction Time (Min)	Average Temperature °F
53	80.1	H <sub>2</sub>	60	1250	4400	235	715±15
54	80.0	He	60	1250	5100	130	705±15
56	100.0	H <sub>2</sub>	60	1100	5200	420	718±15

Table 2. Identification of Major Compounds in GPC Fraction 2

Peak No.	Compound	Peak No.	Compound
1	Phenol	26	Trimethylnaphthalene (iso.)
2	1-Ethyl-3-methylbenzene and Decane	27	C <sub>16</sub> H <sub>34</sub> and Trimethylnaphthalene (iso.)
3	<i>o</i> -Cresol	28	<i>n</i> -Hexadecane
4	<i>p</i> -Cresol	29	Diethyl methyl-naphthalene
5	<i>n</i> -Undecane and methylcresol	30	C <sub>17</sub> H <sub>36</sub> and Tetramethylnaphthalene
6	<i>o</i> -Ethylphenol	31	<i>n</i> -Heptadecane
7	2,6-Dimethylphenol	32	Alkylated naphthalene
8	<i>p</i> -Ethylphenol	33	C <sub>18</sub> H <sub>38</sub>
9	<i>p</i> -Cymene	34	<i>n</i> -Octadecane
10	C <sub>12</sub> H <sub>26</sub> and 1,3-Dimethylindan	35	C <sub>19</sub> H <sub>40</sub>
11	<i>n</i> -Dodecane and 2-Methyl-6-ethylphenol	36	C <sub>19</sub> H <sub>40</sub>
12	3-Methyl-6-ethylphenol	37	C <sub>19</sub> H <sub>40</sub>
13	C <sub>12</sub> H <sub>16</sub>	38	<i>n</i> -Nonadecane
14	3-Methyl-6-ethylphenol	39	<i>n</i> -Eicosane
15	C <sub>13</sub> H <sub>28</sub> and 1,6-Dimethylindan	40	<i>n</i> -Heneicosane
16	1,2-Dimethylindan	41	<i>n</i> -Docosane
17	<i>n</i> -Tridecane	42	<i>n</i> -Tricosane
18	C <sub>11</sub> H <sub>16</sub> (Methylated benzene) and C <sub>14</sub> H <sub>30</sub>	43	<i>n</i> -Tetracosane
19	<i>n</i> -Tetradecane	44	<i>n</i> -Pentacosane
20	Dimethylnaphthalene	45	<i>n</i> -Hexacosane
21	2,3-Dimethylnaphthalene	46	<i>n</i> -Hepacosane
22	C <sub>15</sub> H <sub>32</sub>	47	<i>n</i> -Octacosane
23	<i>n</i> -Pentadecane	48	<i>n</i> -Nonacosane
24	Pentamethylindan	49	<i>n</i> -Triacontane
25	C <sub>6</sub> -Alkylindan	50	<i>n</i> -Hentriacontane
		51	<i>n</i> -Dotriacontane
		52	<i>n</i> -Tritriacontane
		53	<i>n</i> -Tetratriacontane

EFFECTS OF NITROGEN COMPOUNDS ON  
DEPOSIT FORMATION DURING SYN FUEL STORAGE\*

John W. Frankenfeld and William F. Taylor

Exxon Research and Engineering Company  
Linden, New Jersey 07036

INTRODUCTION

Both the U.S. and world petroleum reserves are being depleted at a rate that can no longer be ignored. As a result, the development of alternate fuel sources is a virtual necessity within a few decades. Two of the most promising new sources are shale rock and coal. Although processes are available for the production of synthetic liquids from shale and coal, the investment costs associated are very large and the fuels produced will unquestionably be significantly different in chemical composition from present day petroleum-derived materials. Despite considerable variation from various sources and methods of liquification, some generalizations can be drawn: shale liquids will be higher in oxygen and nitrogen, more aromatic and olefinic than petroleum-based fuels; coal liquids will be higher in oxygen content but lower in nitrogen than shale, extremely rich in aromatics and have a somewhat lower olefin content (1). Some of the differences between synthetic and petroleum fuels can be corrected by known processing techniques. However, these are expensive and may never be completely effective. It is important, therefore, to determine which types of variations from known fuels will be deleterious and which can be tolerated.

One of the substances most difficult to remove is nitrogen. In addition, it is known that nitrogen content can adversely effect fuel stability. This is illustrated by Figure 1, where three jet fuels, prepared by catalytic hydrotreating shale liquids, were subjected to the standard JFTOT thermal stability test (2). Clearly, the higher the nitrogen content of a fuel, the poorer its thermal stability. Some of the samples were severely hydrotreated yet still retained significant amounts of nitrogen and exhibited poor thermal stability (2).

Recent work at Exxon has shown that nitrogen compounds, especially of the pyrrole type, promote sediment or sludge formation in JP-5 jet fuel stored under ambient conditions. The reaction is first noted by an almost immediate darkening of the fuel. This is followed by the appearance of sludge which continues to increase on standing. The reactions to form sediments were strongly influenced by light, acids and oxygen present in the fuel.

As a result of these preliminary observations, the present study was undertaken to investigate this phenomenon further. The major objectives of this program are: (1) to determine whether other nitrogen containing species, likely to occur in synfuels, will have effects similar to pyrroles, (2) to test for interactions between nitrogen compounds and other impurities, (3) to determine the effects of storage parameters such as light, temperature and oxygen content of the fuel on sediment formation and (4) to elucidate the chemical structure and mechanism of formation of the sediments produced.

EXPERIMENTAL

The test compounds were the highest quality commercially available. They were purified by distillation when necessary. High quality n-decane was employed

\*Sponsored by NAVAIR 310C, Contract No. N00019-76-C-0675, Dr. Hyman Rosenwasser, technical monitor.

Table 3. Components in Gas Samples Collected at  
Various Time Intervals and Reaction Conditions Listed in Table 1

Number	Time (min)	H <sub>2</sub>	CO <sub>2</sub>	C <sub>2</sub> H <sub>6</sub>	CH <sub>4</sub>	CO	C <sub>3</sub> H <sub>8</sub>	C <sub>3</sub> H <sub>6</sub>	i-C <sub>4</sub> H <sub>10</sub>	H <sub>2</sub> S	n-C <sub>4</sub> H <sub>10</sub>
53-1	40	76.8	10.8	0.3	0.8	0.3	0.2	0.05	0.04	0.1	0.07
53-2	70	75.3	16.5	0.7	1.8	0.5	0.4	0.06	0.06	0.2	0.10
53-3	98	66.2	22.9	1.5	3.5	0.7	0.9	0.06	0.10	0.2	0.18
53-4	120	68.3	21.5	1.6	3.7	0.6	0.9	0.04	0.10	0.2	0.19
53-5	235	67.9	18.6	1.7	4.1	0.5	1.0	0.04	0.12	0.2	0.28
54-1	40	0.2	15.0	0.4	1.1	0.3	0.3	0.06	0.03	0.7	0.07
54-2	80	0.3	12.4	0.4	1.5	0.4	0.3	0.04	0.04	0.5	
54-3	110	0.5	14.8	0.8	2.2	0.4			0.06	0.6	
54-4	130	0.7	14.1	0.9	2.4	0.5	0.5	0.04	0.03	0.3	0.13
56-1	120	63.6	24.3	1.9	5.2	0.8	1.0	0.07	0.09	1.2	0.22
56-2	240	53.6	31.2	4.6	10.7	0.7	2.5	0.07	0.22	1.6	0.59
56-3	420	57.6	27.7	4.2	12.6	0.6	1.4	0.02	0.08	0.6	0.17

TABLE 1  
Effects of Nitrogen Compounds on Sediment Formation in Purified n-Decane

Compound Added (1)	Storage (2) Conditions	Cumulative Sediment (g/500g Decane)					Comments
		1 Day	5 Days	20 Days	30 Days	60 Days	
None	Light	-	-	-	-	-	Clear, Colorless
None	Dark	-	-	-	-	-	Throughout
2,5-Dimethylpyrrole	Light	.362	.718	1.13	1.30	1.69	Dark Brown Solution
2,5-Dimethylpyrrole	Dark	.036	0.100	.353	.524	1.05	Dark Brown Solution
Indole	Light	.012	.021	.022	.036	.043	Pink Solution
Indole	Dark	-	-	-	-	-	Colorless
Carbazole	Light	Trace	Trace	.019	.020	.051	Yellow Solution
Carbazole	Dark	-	-	-	-	-	Yellow Solution
2,4,6-Trimeethylpyridine	Light	-	-	-	-	-	Clear, Colorless
2,4,6-Trimeethylpyridine	Dark	-	-	-	-	-	Clear, Colorless
Quinoline	Light	-	-	Trace	Trace	Trace	Light, Yellow Solution
Quinoline	Dark	-	-	-	-	-	Clear, Colorless
2,6-Dimethylamine	Light	-	.004	.004	.005	.005	Purple Solution
2,6-Dimethylamine	Dark	-	.001	.001	.002	.002	Purple Solution
n-Hexylamine	Light	-	-	-	-	-	Clear, Colorless
n-Hexylamine	Dark	-	-	-	-	-	Clear, Colorless
Methylcyclohexylamine	Light	-	-	-	-	-	Yellow Solution
Methylcyclohexylamine	Dark	-	-	-	-	-	Light Yellow Solution
2-Methylpiperidine	Light	Trace	Trace	.001	.001	.001	Light Yellow Solution
2-Methylpiperidine	Dark	-	-	Trace	.001	.001	Light Yellow Solution
n-Caproamide	-	-	-	-	Trace (3)	Trace (3)	Light Yellow Solution
n-Caproamide	-	-	-	-	Trace (3)	Trace (3)	Light Yellow Solution

(1) Each compound added to purified n-decane at 2000 ppm N level.

(2) Light = (UV) irradiation (366 nm, 1100  $\mu\text{W}/\text{cm}^2$ ); Dark = stored in darkness.

(3) Trace of liquid appeared after 30 days.

as the diluent. This was further purified by percolation through columns of activated alumina to remove traces of reactive, polar materials. The nitrogen compounds were tested at the 2,000 ppm level (nitrogen basis) which is within the limits expected from fuels derived from shale or coal (1). The compound 2,5-dimethylpyrrole was employed as a standard. The oxygenated compounds were added in amounts equivalent to 500 ppm O.

Duplicate sets of samples were set up using glass bottles. One set was stored in darkness at ambient temperature (24°C). The second set was irradiated with long wave (366 nm) UV light with an intensity of 1100  $\mu\text{W}/\text{cm}^2$  (3). A separate sample of *n*-decane with 4,000 ppm N as 2,5-dimethylpyrrole was exposed to normal sunlight to serve as a control. The bottles were removed from storage at intervals, the precipitate filtered and dried under vacuum at 110°C for 1-1/2 hours before weighing and subsequent analysis.

## RESULTS AND DISCUSSION

### Effects of Various Nitrogen Compounds

Compound type analyses of various light distillates of shale liquids have been reported (4). They show that pyrroles, quinolines, and pyridines are the dominant species present along with lesser amounts of amides, anilides and alkyl amines. Compounds of these types were, therefore, chosen for this study. The effects of various representative nitrogen-containing compounds on sediment formation in purified *n*-decane are given in Table 1. It is clear from this data that sediment formation is not unique to 2,5-dimethylpyrrole (DMP) although of those compounds tested, DMP easily produced the greatest amount. It is interesting that the three compounds giving the most sediment were all of the pyrrole type, DMP, indole and carbazole. Of the other compounds studied, only 2,6-dimethylaniline and 2-methylpiperidine afforded any measurable sediment. However, several of the primary amines produced colored solutions which intensified with time. Their effects on long term storage stability is unknown.

### Importance of Light as a Promoter

The importance of light as a catalyst for sediment formation is illustrated by the plots in Figure 2. The difference between the irradiated and dark-stored samples is quite large early in the period and tends to get much smaller later. Thus, with DMP, sediment in the irradiated sample exceeded that for the dark sample by a factor of ten after one day but was only about 38% greater after 60 days. This suggests that exclusion of light will retard but not prevent sediment formation.

The sample stored in sunlight formed sediment slightly more rapidly than the UV irradiated material (Figure 2). This effect is not of practical significance but may have a bearing on the mechanism of sediment formation.

It should be noted that the build up of sediment in the dark follows a straight time relationship while the light catalyzed reaction does not. The dark reaction appears to be at least "pseudo" zero order while the catalyzed reaction is of a higher order. It should also be emphasized that the shape and general magnitude of the curves obtained in *n*-decane is in excellent agreement with those from actual JP-5 fuel.

### Influence of Organic Acids and Phenols

Pyrroles are oxidized more rapidly in acidic than neutral media (5). As a result, it was of interest to determine whether organic acids, likely to be present in synfuels, would catalyze the formation of sediments in hydrocarbon media.

FIGURE 1

VARIATION OF JFTOT BREAKPOINT TEMPERATURE  
WITH NITROGEN LEVEL AFTER HYDROTREATMENT

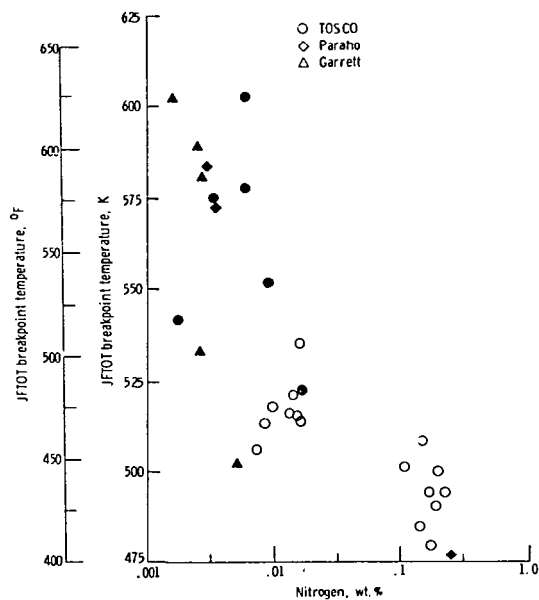
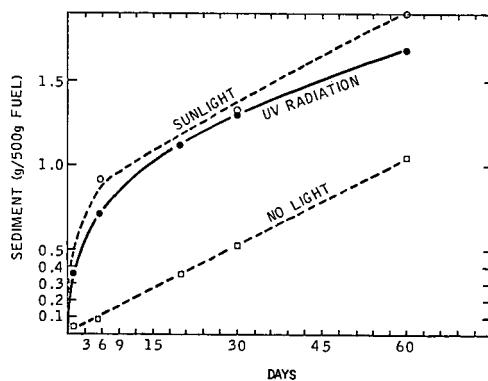


FIGURE 2

EFFECTS OF UV RADIATION  
ON SEDIMENT FORMATION BY  
2,5-DMP IN N-DECANE



Preliminary experiments in JP-5 indicated a significant effect. This was confirmed in experiments using n-decane as the diluent. The results are summarized in Table 2.

TABLE 2  
SEDIMENT FORMATION WITH 2,5-DIMETHYLPYRROLE (DMP)  
UNDER THE INFLUENCE OF ORGANIC ACIDS

Acid (1)	Storage Conditions (2)	Cumulative Sediment (g/500 g Decane)					Appearance
		1 Day	5 Days	15 Days	30 Days	60 Days	
None	Light	.213	.524	.869	1.12	1.52	Dark Red
	Dark	---	.060	.197	.394	.840	Dark Red
<u>n</u> -Decanoic	Light	.390	.821	1.25	1.49	1.84	Dark Red
	Dark	.057	.147	.497	.990	1.50	Dark Red
Cyclohexane Carboxylic	Light	.391	.821	1.26	1.56	1.83	Dark Red
	Dark	.083	.216	.621	1.08	1.84	Dark Red
Benzoic	Light	.259	.476	.858	---	---	Clear,
	Dark	.057	.165	.414	---	---	Colorless
<u>n</u> -Decanoic Alone (3)	Light	---	---	---	---	---	Clear,
	Dark	---	---	---	---	---	Colorless

(1) Nitrogen compounds added at 2,000 ppm N level; acids at 500 ppm O level.

(2) Light = UV radiation (366 nm; 1100  $\mu$ W/cm<sup>2</sup>).

(3) No DMP in these samples.

Both n-decanoic acid and cyclohexanecarboxylic acid significantly increased the rate of sedimentation. This was evident in both light and dark. The acids promoted a 20% increase in sediment in 60 days in the light and by 100% or more in the dark over samples containing DMP alone. Control samples containing the acidic compounds but no DMP gave no sediment nor was any darkening of the fuel observed. Benzoic, a typical aromatic acid, showed no effect under light storage, but did tend to increase deposit formation in the dark.

It would appear that the acid and light catalysts operate independently rather than in any sort of synergistic or antagonistic fashion. This was apparent from a 3x3 factorial analysis of the data from Table 2. In the case of DMP and decanoic acid, the "light effect" accounted for 0.674 g of sediment in 15 days and 0.683 g in 60 days. The corresponding values for the "acid effect" are .303 g and .663 g. The sums of the two acting independently would be .977 g for 15 days and 1.34 g for 60 days. These values are fairly close to the 1.06 g and 1.00 g obtained in the same time periods from the experiment when both light and acid were present. It would appear that the two catalysts do not interact. An analysis was made for cyclohexanecarboxylic acid with similar results.

A number of phenols were examined with respect to promoting sediment formation with DMP in n-decane. All had an inhibitory effect, although considerable variation was observed. Results of these studies are given in Table 3. One of the most effective inhibitors was 2,6-di-t-butylphenol. Plots of sediment formation with DMP both with and without added 2,6-di-t-butylphenol are shown in Figure 3. A 58% reduction in sediment formation was obtained under light storage at 60 days and 80% reduction after 15 days as compared to controls. Under dark storage conditions, the corresponding reductions were 45% and 82%. A 3x3 factorial analysis for these experiments was performed. The "light effect" in this case is .683 g

TABLE 3

EFFECTS OF PHENOLS ON DEPOSIT FORMATION<sup>(1)</sup> WITH 2,5-DIMETHYLPYRROLE

Phenol Added (2)	Cumulative Sediment (g/500 g/Decane)			
	15 Days		60 Days	
	Light	Dark	Light	Dark
None	.869	.197	1.52	.840
2,4,6-Trimethyl-	.681	.123	1.33	1.01
2,6-Di- <i>t</i> -Butyl-	.173	.035	.640	.496
2,4-Dimethyl-	.569	.213		
2,6-Di- <i>t</i> -Butyl-4-Methyl-	.270	.138		
2-Hydroxy-3-Isopropyl- (3-Isopropylpyrocatechol)	.154	.058		

(1) All samples contained 4,000 ppm N as 2,5 dimethylpyrrole.

(2) At levels of 500 ppm O.

(1.52 g - .837 for DMP alone) and the "phenol effect" is -.344 g. The net additive effect would be .339 g (.683 g - .344 g). However, the actual sediment obtained in the presence of both the phenol and light is .640 g, .20 g less than that observed under dark storage alone (60 day results). Apparently, this phenol is effective in combatting the effects of the light catalyzed reaction as well as the sedimentation under dark storage conditions.

The influence of other phenols on sediment formation varied considerably (Table 3). Those with *t*-butyl or isopropyl groups were most effective in retarding sedimentation. Substitution in position 4 with methyl groups tended to reduce effectiveness although the effect was not large. Work is continuing in this area to elucidate structural effects further.

Similar effects of acids and phenols were observed with indole as the nitrogen compound (Figure 4). Decanoic acid significantly increased sediment formation in the case of indole. A 6-fold increase in sediment was observed in the sample stored under UV light. Insufficient data is available for a factorial design analysis, but, in this case, light and acids may interact in some way to promote especially heavy sediment formation. Di-*t*-butylphenol appears to have a slight inhibitory effect on sediment formation with indole (Figure 4). The 2,4,6-trimethylphenol showed no detectable influence. These findings suggest that certain phenols may prove useful as sludge-preventing additives for future synfuels of the JP-5 type.

#### Characteristics and Chemical Structure of the Sediments

Determining the structure of the nitrogeous sediment is useful for elucidating the mechanism of formation and thereby finding methods of preventing it. Although storage conditions and the presence of acid may effect the rate of formation and quantity of sediment, they do not seem to alter the characteristics of the sediment. Elemental analyses of the sediments suggest that the deposits are made up largely of repeating units of the dimethylpyrrole. This is clear since the average C/N ratio in the sediments (6.3/1) is very close to the C/N ratio of dimethylpyrrole (6/1). Thus, no other carbon-containing species have been introduced into the polymer. On the other hand, considerable oxygen (about 1.5 atoms per N) has been incorporated, mostly at the expense of hydrogen. The approximate average molecular composition of 11 sediment samples, obtained under various storage conditions, was:

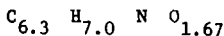


FIGURE 3

EFFECT OF DI-*t*-BUTYLPHENOL ON SEDIMENT  
FORMATION WITH 2,5-DIMETHYLPYRROLE IN DECANE

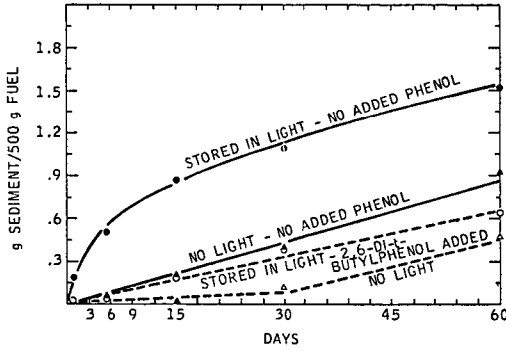
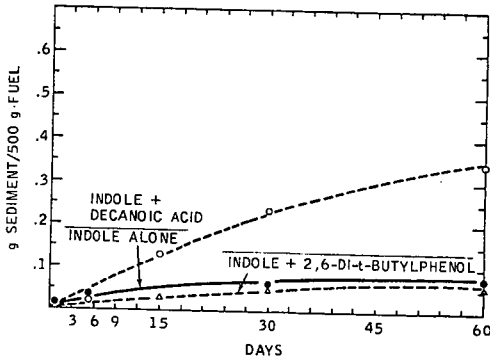
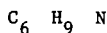


FIGURE 4

EFFECTS OF *n*-DECANOIC ACID AND  
2,6-DI-*t*-BUTYLPHENOL ON SEDIMENT  
FORMATION WITH INDOLE IN *n*-DECANE -  
STORAGE IN PRESENCE OF UV LIGHT



while that of dimethylpyrrole is:



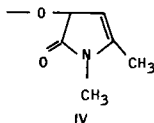
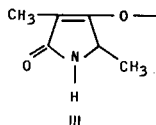
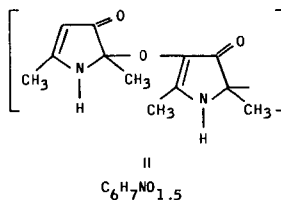
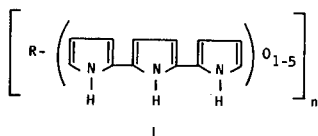
The major infrared bands from the sediments are shown in Table 4. The spectra were obtained as smears or mulls between salt plates since the extreme insolubility of the sediment precludes the measurement of solution spectra. The analysis confirms that the pyrrole ring is intact and suggests that oxygen has been introduced in the form of a carbonyl group. The strong  $-\text{CH}_3$  absorption relative to  $-\text{CH}_2$  indicates the methyl groups remain intact and that no long chain  $-\text{CH}_2-$  units (from other components of the media) have been introduced. Previous reports (5) have proposed structure I, the so-called "pyrrole black" for the sediment obtained from pyrrole added to various fuels. The present results do not support this structure since no "R" group is present and a carbonyl group clearly is. Instead, a structure such as II (7) is more likely. The partial structures, III and IV, cannot be ruled out although an unlikely methyl group migration is required (8).

TABLE 4

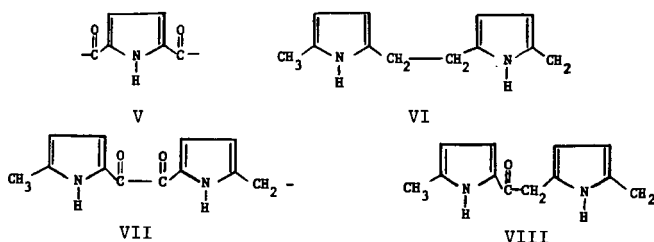
MAJOR IR BANDS IN SEDIMENT FROM 2,5-DIMETHYLPYRROLE (1)

$\text{Cm}^{-1}$	Significance
3300-3500 (s)	-NH or -OH
2970 (s) 1375 (s)	$-\text{CH}_3$
2925 (w) 1450 (w)	Lack of $-\text{CH}_2$
1640-1670 (vs)	Conj C O or Amide

- (1) Smear or mull between salt plates.  
 (2) s = strong; vs = very strong; w = weak.



The mass spectra of sediment samples are complicated because of the sediment's polymeric nature. However, some generalizations are possible. If a single structure is present, the representation best fitting all data is II, although partial structures III and IV cannot be ruled out. In addition, the mass spectra of some samples suggests the sediment may consist of several compound types of which four (V-VIII) are prevalent. The average properties of the sediment, as analyzed by elemental and infrared methods, therefore could readily be accounted for by such a mixture.



Surprisingly, the highest parent peaks observed (~400 mass units) correspond to no more than 3-4 pyrrolic units. This is consistent with reports on the autooxidation of 1-methylpyrrole (8). These workers found no more than five repeating pyrrole units in a short chain. Additional work is scheduled in this area to determine the character and mechanism of sediment formation.

#### CONCLUSIONS

- Nitrogen compounds can be seriously deleterious to the storage stability of synfuels.

- (a) Pyrrolic types and some amines are deleterious; many other nitrogen containing compounds are not.
- (b) The pyrrolic compounds vary in the magnitude of their influence on sediment formation. The rate is very high with 2,5-dimethylpyrrole.

- Storage conditions may play an important role; the effect of light is particularly noteworthy.

- Certain trace impurities are also important in their effects on promoting sediment formation.

- (a) Carboxylic acids accelerate the formation rate; the effect is most pronounced in the dark.
- (b) Some phenols inhibit sediment formation; structural effects are important.

- The sediments appear to have a definitive structure which may be amenable to analysis. With DMP this appears to be low to medium molecular weight oligomers consisting of partially oxidized repeating units of the nitrogen compound.

#### REFERENCES

1. Taylor, W. F. and Hall, H. J., "Future Synthetic Fuels", Scientific and Technical Application Forecast, Department of the Army, Contract No. DAAD05-73-C-0059 (1975).
2. Reynolds, T. W., "Thermal Stability of Some Aircraft Turbine Fuels Derived from Oil Shale and Coal", NASA TM X-3551 (1977).
3. Compounds of the Pyrrole Type Absorb Strongly in This Region (Friedel, R. A. and Orchin, M., "Ultraviolet Spectra of Aromatic Compounds", Wiley and Sons, Inc., New York, 1951).
4. See, for example, Paulson, R. E., Jensen, H. B., and Cook, G. L., Amer. Chem. Soc., Division of Petroleum Chem. Preprints 16 (1):A49 (1971); Dinneen, G. U. et al., "Composition of Shale-Oil Naphtha", U.S. Bureau of Mines Bulletin 593 (1961).
5. Oswald, A. A. and Noel, F., J. Chem. Eng. Data 6 (2) 294 (1961).
6. Structures such as II have been proposed for pyrrole oxidation products (see Seebach, D., Chem. Ber., 96, 2723, 1963 or Beer, R. J. S. et al., J. Chem. Soc. (1954) 4139).
7. Methyl migrations have been proposed by Seebach (Chem. Ber. 96, 2723, 1963) for certain pyrrols under rather severe oxidative conditions.
8. Smith, E. B. and Jensen, H. B., J. Org. Chem., 32, 3330 (1967).

The Thermodynamics of Coal Chars;  
Correlation of Free Energy of Formation with Reactivity

Leslie L. Isaacs

Department of Chemical Engineering  
The City College of The City University of New York  
New York, New York 10031

INTRODUCTION

A large number of existing and proposed coal conversion technologies yield a char as a by-product or as a process intermediate. These technologies may be classified into the following categories:

1. Coal carbonization procedures, yielding a char by-product.
2. Steam or steam-oxygen gasification. Char is either a gasification intermediate or a by-product.
3. Coal gasification with hydrogen or hydrogen rich gas. The char intermediate is gasified with steam and oxygen or further gasified with hydrogen.
4. Supercritical gas extraction. A char by-product might either be gasified or used as fuel.

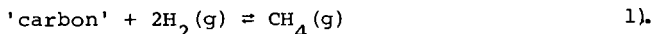
For the proper design of a given process and for the comparison of competing processes, both in the technical and economic sense, an understanding of the gasification reactivity (kinetics) and thermochemistry of the chars is essential.

Broadly speaking, the chemical reactivity of a char (in reference to gasification with steam or carbon dioxide, or hydrogen, or in combustion with oxygen) is its most important property in relation to its subsequent utilization. A traditional test for the measurement of the reactivity of a char is the rate of reaction of the char with carbon dioxide (1). The gasification process can be divided into two distinct stages (2); the first stage due to pyrolysis and the second stage due to the char-gas reaction. The pyrolysis reactivity can be related to volatile matter content of the solid, to the rate of heating and to the pyrolysis temperature. The reactivity of the char in the gasification stage seems to depend on the source of char (nature of the original coal) and the thermal history (heat treatment) of the char (3).

In spite of the efforts of many researchers, kineticists are far from able to make a priori prediction of reaction rates for the gasification of a given coal or char in various devices (processes). Consider the steam gasification process. The situation is highlighted by the fact that an oven coke - resembling blast furnace coke and having intrinsically a low chemical reactivity - gasifies poorly in a steam-oxygen blown gravitating bed gasifier, yet gasifies in a steam fluidized bed with much the same reactivity as an intrinsically reactive char made at low temperatures (4).

In an attempt to correlate the gasification data from steam fluidized beds, Squires (4) proposed that the data be explained by thermodynamic equilibrium considerations. The chemical reaction of

relevance is:



Squires hypothesized that the methane in the effluent stream from a steam fluidized bed stands in a quasi-equilibrium relationship to the hydrogen and carbon material present in the bed. He demonstrated that the calculated "equilibrium" constants for various processes and solid feeds correlated with temperature in the usual manner if the thermal history of the 'carbon' was taken into account. The data for fluidized beds with continuous feed of raw (or lightly pretreated) coals fell on a line indicating higher yields of methane at a given temperature than the data for chars and anthracite coals that had been kept for some time at elevated temperature under nitrogen atmosphere before they were fed to a steam fluidized bed. However, in all cases the methane yields obtained were substantially higher than one would have calculated from thermodynamic equilibrium assuming that the 'carbon' in the feed was graphite. The implications of this observation and hypothesis are that (a) the chars have an excess free energy of formation relative to graphite and (b) the amount of excess energy is a function of the thermal history of the char. Thus, one should be able to correlate the reactivity of a char with its thermodynamic properties. This conjecture is not made to place thermochemical data in competition with structural and kinetic information that has been developed. Indeed, all the information should be regarded as complementary.

To test Squires' hypothesis we may calculate the equilibrium constant,  $K$ , for the reaction given by Equation 1 using data for a selected 'carbon', at a given temperature and compare it to the equilibrium constant for the same reaction, at the same conditions, whereas for 'carbon' graphite is assumed to be used. From the standard thermodynamic relationship, the ratio of the equilibrium constants  $K^{\text{ch}}/K^{\text{gr}}$  is related to the free energy changes,  $\Delta G$ , for the reactions by:

$$\ln \frac{K^{\text{ch}}}{K^{\text{gr}}} = \frac{1}{RT} (\Delta G^{\text{gr}} - \Delta G^{\text{ch}}) \quad 2).$$

The symbols have their usual meaning. The superscripts  $\text{ch}$  and  $\text{gr}$  indicate that 'carbon' is in the form of char or graphite in the reaction considered (Eq. 1). It is obvious that in the present case

$$\Delta G^{\text{gr}} - \Delta G^{\text{ch}} = G_f^{\text{ch}} - G_f^{\text{gr}} \quad 3).$$

where  $G_f$  is the free energy of formation of the species at the reaction temperature. Thus, a test of the hypothesis reduces to the estimation of the free energy of formation of a char relative to that of graphite at a reaction temperature, and comparing the calculated ratio of equilibrium constants to that found experimentally.

The free energy of formation of a substance at a given temperature is usually calculated from the standard heat of formation, the absolute entropy of formation and heat capacity of the substance as a function of temperature. The heat of formation can be calculated

from a measured heat of combustion. Before we proceed to an actual calculation of the free energy formation of a char relative to graphite, a short review of the relevant available data is undertaken.

#### Standard Heat of Combustion of Chars and Graphite

The API Project 44's value for the heat of combustion of graphite is 7831 calories/gram. Dolch and Rank (5) inferred heats of combustion of chars, prepared from lignite, steam activated charcoal, cellulose and coke from peat as ranging from 8135 to 8277 cal/gram of fixed carbon. The hydrogen content of these materials ranged from 0.5 to 0.8% and carbon contents were above 96.7%. Recently, the heats of combustion of two well characterized chars have been measured (6). These chars were produced in experimental runs on a synthane process test unit and one corresponded to a char heat treated at 400°C and the other to a char heat treated at 900°C. They were produced from an Illinois No. 6 coal feed. The heat of combustion of the 400°C char is 8540 cal/gram carbon and of the 900°C char 8322 cal/gram carbon. The hydrogen-to-carbon ratios as determined from elemental analysis were: 0.73 for the 400°C and 0.20 for the 900°C. Thus the difference in the heats of combustion of chars and graphite ranges from 300 to 700 cal/gram of carbon. The larger heat of combustion of the chars relative to graphite reflects both the energy associated with the residual hydrogen in the chars and the excess heat of formation of the chars. Bronowski (7) reported measurements on the carbonization of bituminous coals. The carbonization process is exothermic and the heat involved is of the order of 500 cal/gram. This is of the same order of magnitude as the excess heat content of the chars as measured by the relative difference between the heats of combustion of chars and graphite on a fixed carbon basis. Thus, in subsequent calculations, the standard heat of formation of a char relative to graphite will be estimated as the difference between the respective heats of combustion on a per gram atom of carbon basis.

#### The Heat Capacity of Chars and Graphite

The heat capacity of graphite has been measured by numerous investigators. The data available covers the entire temperature range of interest and has been reviewed by Kelly and Taylor (8). It has been noted by many of the investigators that the heat capacity of graphite is dependent on the state of the structural perfection of the graphite specimen. Natural crystalline graphites have the lowest heat capacities at any given temperature. Synthetic graphites prepared by carbonization procedures have excess heat capacities. The amount of excess is mainly a function of the carbonization temperature. Attempts to eliminate the excess heat capacity of the synthetic graphites by heat treatments above 3000°C were unsuccessful. Thus, one should expect that the heat capacity of chars will be in excess of that of graphite.

Heat capacity data on coal chars are extremely scarce. An extensive literature search yielded only three sets of data relevant to the task at hand. The Bartlettville and Albany Laboratories (6) of ERDA measured the heat capacities of the same two synthane process chars for which they measured the heats of combustion. However,

the heat capacities were only measured above 300K. Data in the 50K to 300K region were reported by Kasatochkin, et al., (9) for chars prepared from a fossil carbon, Schungite, and from anthracite coals. These chars were prepared by "heat treatments" (pyrolysis) ranging from 600°C to 2800°C. The third set of data is from the Carbon Research Laboratories, SUNY, Buffalo (10) on chars prepared from resin C pitch by heat treatments ranging from 600°C up. The temperature range for heat capacity measurements was from 1K to 5K.

Some important generalizations can be deduced from the analysis of the above three data sets. First of all, as expected, the chars have an excess heat capacity relative to graphite at all experimental temperatures. The excess heat capacity of the chars is related to the heat treatment temperature. The lower the heat treatment temperatures for a given char the greater is its excess heat capacity relative to graphite.

One may quantify the relation between char heat capacity and heat treatment temperature by noting that the data on the resin-C chars and on Schungite chars can be expressed as:

$$C^{ch}(T) = C_0(T) \exp(a(T)/T_{HT}) \quad 4).$$

Here  $C^{ch}(T)$  is the heat capacity of the char at a given temperature (°K) per gram atom of carbon contained in the char, and  $C_0(T)$ ,  $a(T)$  are constants and  $T_{HT}$  is the heat treatment temperature (°K). We found that this relationship is useful for fitting heat capacity data on all chars as a function of arbitrary heat treatment temperature.

The magnitude of the excess heat capacity is not a function of heat treatment temperature alone. The 900°C synthane process char has more excess heat capacity than the 600°C Schungite char. This difference may be simply due to the structural differences in the coals from which the chars were made. Alternately, it is possible that this difference in excess heat capacities is related to the residual hydrogen content and ash content of the chars. These conjectures should be subjected to experimental verification.

In Table 1 the heat capacity of the 900°C synthane process char is compared to that of graphite as a function of temperature. Entries into this table were obtained as follows: The heat capacity of graphite was taken from literature (11). The heat capacity of the char above 300K is calculated from the Barlettsville data (6) directly. Below 300K entries for the char were calculated using the following procedure. We assume that below 300K the synthane char heat capacity has the same kind of functional dependence on temperature as the experimentally determined heat capacities for Schungite (9) and resin-C pitch chars (10). Therefore, if we have the heat capacity of one char as a function of temperature, the values for another may be calculated by assuming that the fractional change in heat capacity between two temperatures is the same. That is, we use a relation of the following form to calculate the heat capacity of the synthane char at a temperature  $T_2$ .

$$\frac{\text{Synthane } C(T_2) - \text{Synthane } C(T_1)}{\text{Synthane } C(T_1)} = \frac{\text{Ref } C(T_2) - \text{Ref } C(T_1)}{\text{Ref } C(T_1)}$$

where  $C^{\text{Ref}}$  is a reference char of known heat capacity at temperatures  $T_1$  and  $T_2$ , and the  $C^{\text{Synthane}}$  is known (or has been calculated) at temperature  $T_1$ . For reference char, a char of the same thermal history, i.e., heat treatment temperature is selected. Thus the  $C^{\text{Ref}}$  versus temperature curve between 50K and 300K was established using Equation 4 to calculate the heat capacities of a Schungite char, hypothetically heat treated at 900°C. The same procedure was used between 1K and 5K using for reference a hypothetical resin-C pitch char.

The reference heat capacity curve was completed between 5K and 50K by smoothly joining the two calculated curves. The accuracy of calculated heat capacities for the Synthane process char is probably of the order of 5 percent.

#### The Absolute Entropy of Formation of Chars and Graphite

The entropy of formation of carbon in the form of graphite is 1.35 (cal/gram atom-°K) at standard conditions. The entropy of formation of coals at standard conditions have been estimated as 4 to 12 (cal/mole-°K) with the preferred value around 5 (12). Chars are expected to have lower entropies of formation than coals. Since chars are not fully crystalline, structurally ordered materials, they do not follow the third law of thermodynamics. A residual entropy due to structural disorder must be added to the thermal entropy calculable from heat capacity data, in order to have a value of the absolute entropy of formation at a given temperature. Using the data given in Table 1, the standard entropy of formation,  $S_f^{\text{Std}}$ , for the 900°C synthane process char was calculated as  $S_f^{\text{Std}} = S_0 + 2.49$  (cal/gram-atom carbon-°K). Here  $S_0$  is the residual entropy of the char.

The residual entropy for the char could be estimated experimentally. For example, it could be done from the accurate determination of the equilibrium constant for a reaction involving the char. However, due to the lack of data we will arbitrarily assume that  $S_0$  for this char equals one cal/(gram-atom carbon-°K). We feel that this number is of the right order of magnitude.

#### Test of Squires' Hypothesis

The thermodynamic data assembled in the preceding sections on the 900°C synthane process char are sufficient to test Squires' hypothesis. We expect that the numbers we will get will only be correct to an order of magnitude due to the assumptions we make with regard to the residual entropy of the char, the low temperature heat capacities and heat of formation. The calculation is done considering that the gasification reaction as given by Equation 1 is carried out at 1200K.

As we have indicated, first we must calculate the Gibbs free energy of formation of the char relative to that of graphite at the selected temperature. Then we use Equation 2 to calculate the ratio of the equilibrium constants. The relative free energy of formation at temperature  $\tau$  may be written in the usual form:

$$G_f^{\text{ch}} - G_f^{\text{gr}} = (H_f - \tau S_f)^{\text{ch}} - (H_f - \tau S_f)^{\text{gr}} = H_f^{\text{ch}} - H_f^{\text{gr}} - \tau (S_f^{\text{ch}} - S_f^{\text{gr}}) \quad (6).$$

Here, all the symbols have their usual meaning, and the superscripts have been defined. All quantities must be evaluated at the reaction temperature  $\tau$ .

The relative heat of formation at the reaction temperature is given by the expression:

$$H_f^{\text{ch}} - H_f^{\text{gr}} = \Delta H_f^* + \int_{\tau^*}^{\tau} [C^{\text{ch}}(T) - C^{\text{gr}}(T)] dT \quad (7).$$

where  $\tau^*$  is the standard temperature, and  $\Delta H_f^*$  equals the difference in the standard heats of formation of the char and graphite. Experimentally determined heats of combustion data can be converted to yield heats of formation. In this case this is not done but  $\Delta H_f^*$  is estimated as the difference between the measured standard heats of combustion of the char and the graphite. Justification of this procedure has been made in a prior section of this paper. For the 900°C synthane process char  $\Delta H_f^*$  equals 5.9 Kcal/gr atom carbon.

The integral in Equation 7 is evaluated graphically. Data in Table 1 are used to prepare a smooth graph of the heat capacity difference between the char and graphite as a function of temperature. The numerical value of 1.7 Kcal/gr atom carbon is obtained by graphical integration for the increase in the relative heat of formation between the standard temperature and the assumed reaction temperature of 1200K. Therefore,  $H_f^{\text{ch}} - H_f^{\text{gr}}$  equals 7.6 Kcal/gram-atom carbon at 1200K.

The relative entropy of formation can be written as:

$$S_f^{\text{ch}} - S_f^{\text{gr}} = S_0 + \int_0^{\tau} \left[ \frac{C^{\text{ch}}(T) - C^{\text{gr}}(T)}{T} \right] dT \quad (8).$$

For  $S_0$  the value of 1 cal/gr-atom carbon-°K is assumed since all the residual entropy is associated with the char. The integral in Equation 8 is again evaluated graphically from a smooth graph of the ratio of the heat capacity difference to the temperature versus temperature. The value of this integral between the indicated limits is 3.82 (cal/gram atom carbon-°K). Thus the relative entropy of formation at 1200K is 4.82 (cal/gram atom carbon-°K).

Substituting the numerical values into Equation 6 we obtain 1.8 Kcal/gr atom carbon for the relative Gibbs free energy of formation,  $G_f^{\text{ch}} - G_f^{\text{gr}}$ , at 1200K. The ratio of the equilibrium constants  $K^{\text{ch}}/K^{\text{gr}}$  is calculated with use of Equation 2 and is found to be 2.14 at 1200K. From the experimental data compiled by Squires

(4) for the gasification of pretreated chars in steam fluidized beds the value of 3.5 at 1200K is estimated for  $K^{ch}/K^{gr}$ . Considering all the assumptions involved in this calculation the agreement between experimental data and calculation is significant. While this calculation does not provide a clearcut proof of Squires' hypothesis, it does strongly support it.

### Conclusions

From the available experimental data one may conclude that coal chars have larger heat capacities and heats of combustion than graphite when these quantities are compared on equivalent amount of carbon content basis. The magnitude of the thermodynamic quantities depends both on the thermal history of the char and on the source of the char. The magnitude of the excess quantities relative to graphite varies with the pyrolysis temperature of the char in an inverse fashion. In case of the heat capacity function a relationship was found (Equation 4) which enables one to estimate the heat capacities of a given char at some assumed pyrolysis (heat treatment) temperature. Chars obtained from a bituminous coal have larger excess heat capacities than chars originating from anthracite coals or fossil carbons. One may speculate that this difference could be related to the amount of residual hydrogen contained in a given char.

Since chars are not fully crystalline ordered solids, they must have some residual entropy of formation. There is no experimental data which allow one to estimate the magnitude of the residual entropy. A value for the residual entropy must be assumed. If one makes the reasonable assumption of one (1) (cal/gram atom carbon-°K) for the value of the residual entropy, then the calculated value of the Gibbs free energy of formation of chars is positive relative to that of graphite. Hence, one concludes that chars should be chemically more reactive than graphite. This conclusion of course is consistent with other experimental data on char reactivity.

In order of magnitude agreement between the numerical values of the equilibrium ratio  $K^{ch}/K^{gr}$  as calculated and as inferred from experimental data, tends to support Squires' hypothesis that the observed gasification yield in a steam fluidized bed process depends on equilibrium considerations. For a more quantitative test of the hypothesis more thermodynamic data than presently available are needed.

The available data show the importance of the pyrolysis temperature as a major factor in the thermal history, and consequently in the thermodynamics of the coal chars. However, the thermal history of a char should also depend on the rate of temperature rise to the pyrolysis temperature and on the length of time the char is kept at the pyrolysis temperature (soak time). The effect of these factors on the thermodynamics of the chars should be investigated. For example, one would expect that longer soaking times will reduce the residual entropy.

### Acknowledgements

Helpful discussions with Professor Arthur M. Squires of Virginia Polytechnic Institute and State University are gratefully acknowledged. This work was supported by NSF Grant #76-22970 (ENG.)

### References

1. S. Okstad and A. Moy, 2nd Conf. on Ind. Carbon and Graphite, Soc. of Chem. Ind., London, 1965; R.G. Jenkins, S.P. Nandi, and P.L. Walker, Jr., Fuel, 52, 288 (1973); T.A. Daly and C.F. Budge, Fuel, 53, 8 (1974); E. Hippo and P.L. Walker, Jr., Fuel, 54, 245 (1975).
2. S. Dutta, C.Y. Wen, and R.J. Bell, Ind. Eng. Chem. Process Des. Dev., 16, 20 (1977); S. Dutta and C.Y. Wen, *ibid* 16, 31 (1977).
3. J.T. Ashu and P.L. Walker, Jr., "Effects of Heat Treatment Conditions on Reactivity of Chars in Air," Technical Report (F.E. 2-30-TR3) to ERDA (Sept. 1977).
4. A.M. Squires, Trans. Inst. Chem. Engrs., 39, 3(1961); Science 191, 689 (1976).
5. M. Dolch and V. Rank, Brennsb. u. Warmew, 19, 72 (1937).
6. Internal Report of the Thermodynamics Research Group, Bartlesville Energy Research Center, ERDA, "Thermal Data on Gasifier Streams from Synthane Test" (1973).
7. J. Bronowski, Chemical Engineering in the Coal Industry, F.W. Sharpely (Ed.), pg. 93 (1956) (Pergamon Press).
8. B.T. Kelly and R. Taylor, Chem. and Phys. of Carbon, ed. by P.L. Walker, Jr. and P.A. Thrower, 10 1(1973) (Marcel Dekker, Inc.).
9. V.I. Kasatochkin, K. Usenbaev, V.M. Zhdanov, K. Sabyraliev, M. Rasalbaev and K. Zhumaliev, Dokl. Akad. Nauk, S.S.S.R. 216, 93 (1974).
10. P. Delhaes and Y. Hishiyama, Carbon 8 31(1970); K. Kamiya, S. Mrozowski, and A.S. Vagh, Carbon 10, 267 (1972).
11. W. DeSorbo, J. Amer. Chem. Soc. 77, 4713 (1955); P.H. Keeson and N. Perlman, Phys. Rev., 99, 1119 (1955); M.M. Spencer, Ind. Eng. Chem., 40, 2152 (1948).
12. O. Krikorian, Lawrence Livermore Laboratory, Internal Document CDTN 72-18 (1972).

Table 1

The Heat Capacities of a 900°C Synthane Process Char and of Graphite

<u>Temperature (°K)</u>	<u>c<sup>char</sup> (cal/gr-atom carbon-°K)</u>	<u>c<sup>graphite</sup> (cal/gram atom carbon-°K)</u>
1	0.23x10 <sup>-3</sup>	0.02x10 <sup>-3</sup>
3	1.1x10 <sup>-3</sup>	0.21x10 <sup>-3</sup>
5	4.1x10 <sup>-3</sup>	.67x10 <sup>-3</sup>
10	1.4x10 <sup>-2</sup>	3.0x10 <sup>-3</sup>
15	3.2x10 <sup>-2</sup>	1.0x10 <sup>-2</sup>
20	5.4x10 <sup>-2</sup>	1.8x10 <sup>-2</sup>
25	7.7x10 <sup>-2</sup>	2.6x10 <sup>-2</sup>
30	0.103	4.6x10 <sup>-2</sup>
40	0.172	8.3x10 <sup>-2</sup>
50	0.25	0.122
75	0.48	0.253
100	0.73	0.401
125	1.01	0.557
150	1.33	0.730
175	1.65	0.912
200	2.02	1.101
225	2.39	1.291
250	2.73	1.486
275	3.11	1.684
300	3.43	1.96
350	4.03	2.46
400	4.52	2.90
450	4.95	3.24
500	5.33	3.55
600	5.96	4.07
700	6.49	4.49
800	6.90	4.82
900	7.27	5.07
1000	7.57	5.26
1100	7.83	5.41
1200	8.08	5.54

## REACTION OF COAL WITH NITRONIUM TETRAFLUOROBORATE

S. K. Chakrabartty, H. O. Kretschmer and D. E. Ungarian

Alberta Research Council, Fuel Sciences Division  
11315-87th Avenue, Edmonton, Alberta, Canada, T6G 2C2

If, as is generally supposed, coal is comprised of predominantly aromatic carbon configurations, it should be open to attack by electrophilic agents. However, while sulphonation, halogenation and nitration of coal have been reported (1), interaction of coal with a selective electrophile - for example, interaction with the nitronium ion - have not yet been explored in detail. Some investigations of this reaction have been published by Brown (2) who employed cupric nitrate in acetic anhydride and by Lahiri et al (3) who used mixtures of nitric and sulphuric acids; and in these cases, it was presumed that the active agent was the nitronium ion which formed as an intermediate in the solvent system. With crystalline salts which contain the nitronium ion, e.g.  $\text{NO}_2^+\text{BF}_4^-$ ,  $\text{NO}_2^+\text{ClO}_3^-$  now readily available, it should, in principle, now be possible to achieve selective nitration more cleanly in non-aqueous, acid-free systems; and we have in fact used nitronium tetrafluoroborate for "activating" bituminous coal before subjecting it to hypochlorite oxidation (4). But recent studies, notably by Olah et al (5), indicate that such salts can also promote reactions other than nitration. They will, for example, oxidize benzyl alcohols to ketones, induce nitrolysis of alkanes, and cleave ethers. In the case of reactions between nitronium tetrafluoroborate and coal, it must therefore be expected that various oxygen-bearing functions as well as nitro-groups could be established in the coal. The work reported in this paper was undertaken in efforts to determine the validity of these expectations.

### EXPERIMENTAL

#### Reaction with nitronium salt

A mixture of 5 to 90 mmoles of the salt and 25 ml acetonitrile or methylene chloride was stirred at ice-bath temperature to produce a homogeneous suspension, and 1 g of dry coal was added. Reaction was allowed to continue for 16 hours at ice-bath temperature under a blanket of helium. The solvent was then evaporated under reduced pressure, the residue quenched with ice-water, and the product isolated by filtration and washed free of acid.

Similar reactions were performed with model compounds, e.g. polystyrene, adamantane, tetrahydronaphthalene and decahydronaphthalene.

For comparison, one coal sample was nitrated with 1:1 v/v concentrated with nitric-sulphuric acid at ice-bath temperature for 16 hours. The mixture was then poured into crushed ice, diluted to a large volume, the nitro-coal filtered off and finally washed free of acid.

#### Functional group analysis

The number of nitro groups introduced was estimated by titration with stannous chloride or titanous chloride, using a standard procedure (6).

The carboxylic acidity was estimated by ion-exchange with sodium acetate and distilling off the acetic acid, and the hydroxyl-content was determined by acetylation with acetic anhydride in pyridine, following the procedure developed by L. Blom (7).

### RESULTS AND DISCUSSION

Tetramethylene sulfone, acetonitrile and various other solvents have been used for nitration with nitronium salts. Initially, acetonitrile was used in this study. The nitration of polystyrene in this system introduced one nitro group per chain-length of four monomer units. The yield of mono-nitrotetralin was 78%. In con-

rest, adamantane and octahydronaphthalene could not be nitrated but varying yields (up to 85%) of some other nitrogen-containing product was obtained. The product derived from adamantane was identified as N-(1-adamantyl)acetamide by comparing melting point, infra-red and  $^1\text{H}$ -n.m.r. spectra of the sample with authentic compound. The spectral data indicated the formation of a similar product (in 3% yield) from octahydronaphthalene, whilst tetrahydronaphthalene only furnished the mono-nitro product.

It may be presumed that the nitronium ion, being an oxidant, oxidizes adamantane to the adamantyl radical or ion which, in turn, reacts with the solvent according to



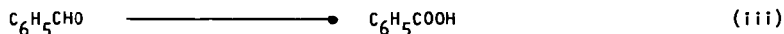
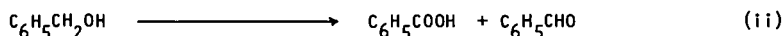
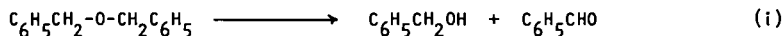
It is interesting to note that of the four model compounds studied, adamantane has the most easily oxidizable C-H bonds. From hypochlorite oxidation (4), it was demonstrated that coal has similar types of C-H bonds, and it is possible that reaction with nitronium salt in acetonitrile may produce an acetamide derivative of coal.

Nitro-coal prepared with nitric-sulfuric acid mixtures gave a titration profile which accounts for all added nitrogen in nitro groups, and similar results were obtained when coal was treated with nitronium salt in methylene chloride. However, in acetonitrile solvent, depending on the amount of nitronium salt used in each reaction, only 48-67% of the added nitrogen could be found in nitro groups (Table 1).

Material balances indicate that little, if any, carbon is lost when the coal is treated with  $\text{HNO}_3/\text{H}_2\text{SO}_4$  mixture or with a nitronium salt in methylene chloride. However, the reaction of coal with nitronium salt in acetonitrile yields products with more carbon and nitrogen content. Since the only extraneous source of carbon was the solvent, the added carbon must come from the reaction of acetonitrile with coal. Moreover, it was also found that for every nitrogen atom added other than as N in nitro groups two carbon atoms were added. And hydrolysis of the products in 1N phosphoric acid gave acetic acid. From these observations it is surmised that a nitronium salt in acetonitrile introduces acetamido as well as nitro groups. The results of reaction between nitronium salts and coal, based on material balances and titration data, are presented in Table 2.

Mazumdar et al (8) have reported that the major reactions during nitration of coal with  $\text{HNO}_3/\text{H}_2\text{SO}_4$  involve introduction of nitro groups and, even under very mild conditions, simultaneous oxidation of the carbon-structure. The oxidation creates carboxyl, hydroxyl and ketonic functions, with formation of carboxyl being the dominant process. But since no loss of carbon was observed, it was concluded that oxidation is limited to methyl groups. Reaction of coal with nitronium salt also induces some oxidation and 7-15% weight increase could be ascribed to newly created oxygen functions. The concentration of oxygen-bearing groups in variously treated coal samples are shown in Table 3.

It is interesting to note that whatever the nitrating system, almost identical oxygen-bearing groups are generated. Since nitronium salts can cleave ethers, the oxidation can be related to such cleavage reactions followed by further degradation depending on the oxidation potentials of the nitrating systems, e.g.



From the nitration studies, some inferences about coal structure can be drawn. Thus, reaction with nitronium salt introduces 3-7 nitro groups per 100 carbon atoms while  $\text{HNO}_3/\text{H}_2\text{SO}_4$  mixtures permit addition of 8-10 nitro groups. If it is assumed that isomerizations of condensed polycyclic aliphatic structures to aromatic structures does not occur during nitration at  $0^\circ\text{C}$ , the number of nitro groups per 100

carbon atoms may provide information about aromatic ring size. In Table 4, the average composition of coal sub-units with nitro group are calculated from published data (8). These sub-groups vary from  $C_{12}H_9$  to  $C_{10}H_6$  and consequently suggest that only benzene or naphthalene nuclei are present in them.

Some support for this deduction is afforded by data relating to reduction of coal with lithium in ethylene diamine. Reduction of aromatic compounds in such or similar systems yields dihydro- or tetrahydro-derivatives, and assuming benzene or naphthalene as the only aromatic structure in the unknown molecule, the hydrogen uptake by the sample can be calculated from the number of such ring per 100 carbon atoms of the samples (Table 5). A comparison of these data with experimental results indicates that the abundance of naphthalene rings increases with rank. It is hardly expected that the reduction of single benzene ring would stop at the tetrahydro-stage. From this discussion we conclude that the smallest hydrocarbon skeletal structure in coal may be in units of  $C_{12}H_9$  to  $C_{10}H_6$ , and that, depending on rank and geographical location, the nucleus of such unit is a benzene or naphthalene ring.

#### REFERENCES

1. Lowry, H. H. (Editor). Chemistry of Coal Utilization. Vol. I and II. Wiley, London, (1945), Suppl. Vol. p. 1091-92, Wiley, London, (1963).
2. Brown, J. K., Given, P. H., Lupton, V. and Wyss, W. F. Residential Conference on "Science in the Use of Coal", Sheffield, Preprints, A-43, April (1958).
3. Bhattacharyya, A. C., Chatterjee, A. K. and Lahiri, A., Fuel, London 46, 25 (1967).
4. Chakrabartty, S. K. and Kretschmer, H. O., Fuel 51, 160 (1972).
5. (a) Olah, G. A. and Ho-T-L, J. Org. Chem. 42 (18), 3097 (1977);  
(b) Olah G. A. and Lin, H. C., J. Amer. Chem. Soc. 93, 1259, (1971);  
(c) Olah, G. A. and Ho-T-L, Synthesis 609 (1976).
6. Becker, W. W., Anal. Chem. 22, pp. 185-8 (1950).
7. Blom, L., Analytical Methods in Coal Chemistry, Joh. Luuk C. V., Eindhoven, Netherland, (1960).
8. Mazumdar, B. K., Chatterjee, A. K. and Lahiri, A., Fuel 46 379 (1967).

Table 1. Nitro-groups in Reacted Coal and Model Compounds

Sample	N <sub>total</sub> mmole/g	N <sub>NO<sub>2</sub></sub> , mmole/g SnCl <sub>2</sub>	TiCl <sub>3</sub>	N <sub>NO<sub>2</sub></sub> /N <sub>total</sub> (added) %
a. 1 g coal reacted with				
(i) HNO <sub>3</sub> -H <sub>2</sub> SO <sub>4</sub> (10°C)	5.1	4.14	4.28	100
(ii) 90 mmole NO <sub>2</sub> BF <sub>4</sub> /MeCN	5.6	2.36	2.50	48
(iii) 45 " " " "	3.0	1.28	1.35	57
(iv) 5 " " " "	1.5	0.00	0.49	67
(v) 90 " " " CH <sub>2</sub> Cl <sub>2</sub>	2.9	2.32	2.35	100
b. Model compounds/NO <sub>2</sub> BF <sub>4</sub> /MeCN				
(i) Polystyrene	2.0	2.26	2.40	
(ii) Adamantane	7.2	0.00	0.00	
(iii) Aniline	14.5	7.28	6.98	
(iv) Benzoic acid	6.0	6.0	5.98	

Table 2. Reactions with Nitronium-Tetrafluoroborate

Substrate	% Weight Increase	Product	Analysis			
			%C	%H	%N	NO <sub>2</sub> meq/g
<u>Acetonitrile Solvent</u>						
1. Polystyrene (C <sub>8</sub> H <sub>8</sub> ) FW n x n <sub>104</sub>	10	(C <sub>8</sub> H <sub>8</sub> ) <sub>3.35</sub> C <sub>8</sub> H <sub>7</sub> NO <sub>2</sub> FW 498.2	a. 83.39 b. 84.2	6.8 7.0	2.8 2.8	2.0 2.4
2. Coal %C = 85.7  C <sub>100</sub> H <sub>78.3</sub> N <sub>0.93</sub> O <sub>6.76</sub> FW 1401	36	C <sub>100</sub> H <sub>68</sub> N <sub>0.93</sub> (NO <sub>2</sub> ) <sub>6.4</sub> (NHCOMe) FW 1904	a. 68.0 b. 69.0	3.9 4.4 4.1	6.3 8.2 7.9	3.4 3.2
3. Coal %C = 88.8  C <sub>100</sub> H <sub>65.9</sub> N <sub>0.43</sub> FW 1350	35	C <sub>100</sub> H <sub>59.1</sub> N(NO <sub>2</sub> ) <sub>5</sub> (NHCOMe) FW 1822	a. 68.2 b. 69.0	1.8 3.6 3.3	13.5 6.0 6.2	2.7 2.6
<u>Methylene Chloride Solvent</u>						
4. Coal %C = 88.8	21	C <sub>100</sub> H <sub>55.1</sub> N(NO <sub>2</sub> ) <sub>2</sub> FW 1623	a. 74.0 b. 74.0	3.4 3.4	4.1 4.0	2.3 2.3
a. calculated b. found						

Table 3. Oxygen-Bearing Functional Groups in Treated Coal

Sample	-OH meq/g	-COOH, meq/g
1. Coal %C = 88.8	0.9	nil
2. Sample 1/NO <sub>2</sub> BF <sub>4</sub> /CH <sub>3</sub> CN	2.3	3.0
3. Sample 1/NO <sub>2</sub> BF <sub>4</sub> /CH <sub>2</sub> Cl <sub>2</sub>	1.5	0.8
4. Sample 1/HNO <sub>3</sub> /H <sub>2</sub> SO <sub>4</sub>	2.2	2.8
5. NO <sub>2</sub> -Coal* from Coal %C = 89.8	2.8	3.5

\*See Reference (8)

Table 4. Nitration of Bituminous Coals\*

Coal %C	Nitro gr per 100 C-atoms	Average composition of subunit/NO <sub>2</sub> gr			
		Number of atoms			
		C	H	N	O
80.8	8.6	11.6	8.9	0.24	1.24
83.6	8.2	12.2	9.6	0.29	0.90
85.5	9.2	10.9	7.9	0.22	0.65
87.1	9.9	10.1	7.7	0.24	0.38
89.8	8.6	11.6	7.3	0.23	0.27
90.2**	9.3	10.8	6.6	0.15	0.31

\*Data recalculated from B. K. Mazumdar et al, Fuel 46, 380, 1967.

\*\*From the study by the author.

Table 5. Reduction of Coals by Alkali Metals in Basic Solvent  
H-uptake per 100 Carbon Atoms

Coal % C	Calculated value from nitration of Gondwana coal		Experimental value (10) American coal	
	dihydro	tetrahydro	%C	H-uptake
80.8	17.2	34.4		
83.6	16.4	32.8	83.1	17
85.5	18.4	36.8	85.1	19
87.1	19.8	39.6	88.7	27
89.8	17.2	34.4	89.3	29
90.2*	18.6	37.2	90.1	45
*Canadian coal				